VOLUME 33 MAY 1955 NUMBER 3

Canadian Journal of Technology

Editor: G. A. LEDINGHAM

Published by THE NATIONAL RESEARCH COUNCIL
OTTAWA CANADA

CANADIAN JOURNAL OF TECHNOLOGY

(Formerly Section F, Canadian Journal of Research)

Under the authority of the Chairman of the Committee of the Privy Council on Scientific and Industrial Research, the National Research Council issues THE CANADIAN JOURNAL OF TECHNOLOGY and six other journals devoted to the publication, in English or French, of the results of original scientific research. Matters of general policy concerning these journals are the responsibility of a joint Editorial Board consisting of: members representing the National Research Council of Canada; the Editors of the Journals; and members representing the Royal Society of Canada and four other scientific societies.

The Chemical Institute of Canada has chosen the Canadian Journal of Technology and the Canadian Journal of Chemistry as its medium of publication for scientific papers.

EDITORIAL BOARD

Manuscripts for publication should be submitted to Dr. Léo Marion, Editor-in-Chief, Canadian Journal of Technology, National Research Council, Ottawa 2, Canada.
(For instructions on preparation of copy, see **Notes to Contributors** (inside back cover).)

Proof, correspondence concerning proof, and orders for reprints should be sent to the Manager, Editorial Office (Research Journals), Division of Administration, National Research Council, Ottawa 2, Canada.

Subscriptions, renewals, requests for single or back numbers, and all remittances should be sent to Division of Administration, National Research Council, Ottawa 2, Canada. Remittances should be made payable to the Receiver General of Canada, credit National Research Council.

The journals published, frequency of publication, and prices are:

Canadian Journal of Biochemistry and Physiology	Bimonthly	$3.00 a year
Canadian Journal of Botany	Bimonthly	$4.00 a year
Canadian Journal of Chemistry	Monthly	$5.00 a year
Canadian Journal of Microbiology*	Bimonthly	$3.00 a year
Canadian Journal of Physics	Monthly	$4.00 a year
Canadian Journal of Technology	Bimonthly	$3.00 a year
Canadian Journal of Zoology	Bimonthly	$3.00 a year

The price of single numbers of all journals is 75 cents.

*Volume 1 will combine three numbers published in 1954 with six published in 1955 and will be available at the regular annual subscription rate of $3.00.

Contents

Printed in Canada *by* University of Toronto Press

CANADIAN JOURNAL OF TECHNOLOGY

Notes to Contributors

Manuscripts

(i) ***General.*** Manuscripts, in English or French, should be typewritten, double spaced, on paper 8½×11 in. **The original and one copy are to be submitted.** Tables and captions for the figures should be placed at the end of the manuscript. Every sheet of the manuscript should be numbered.

Style, arrangement, spelling, and abbreviations should conform to the usage of this journal. Names of all simple compounds, rather than their formulas, should be used in the text. Greek letters or unusual signs should be written plainly or explained by marginal notes. Superscripts and subscripts must be legible and carefully placed.

Manuscripts should be carefully checked before they are submitted; authors will be charged for changes made in the proof that are considered excessive.

(ii) ***Abstract.*** An abstract of not more than about 200 words, indicating the scope of the work and the principal findings, is required, except in Notes.

(iii) ***References.*** References should be listed **alphabetically by authors' names,** numbered, and typed after the text. The form of the citations should be that used in this journal; in references to papers in periodicals, inclusive page numbers should be given but titles should not. All citations should be checked with the original articles and each one referred to in the text by the key number.

(iv) ***Tables.*** Tables should be numbered in roman numerals and each table referred to in the text. Titles should always be given but should be brief; column headings should be brief and descriptive matter in the tables confined to a minimum. Vertical rules should be used only when they are essential. Numerous small tables should be avoided.

Illustrations

(i) ***General.*** All figures (including each figure of the plates) should be numbered consecutively from 1 up, in arabic numerals, and each figure referred to in the text. The author's name, title of the paper, and figure number should be written in the lower left corner of the sheets on which the illustrations appear. Captions should not be written on the illustrations (see Manuscripts (i)).

(ii) ***Line Drawings.*** Drawings should be carefully made with India ink on white drawing paper, blue tracing linen, or co-ordinate paper ruled in blue only; any co-ordinate lines that are to appear in the reproduction should be ruled in black ink. Paper ruled in green, yellow, or red should not be used unless it is desired to have all the co-ordinate lines show. All lines should be of sufficient thickness to reproduce well. Decimal points, periods, and stippled dots should be solid black circles large enough to be reduced if necessary. Letters and numerals should be neatly made, preferably with a stencil (**do NOT use typewriting**) and be of such size that the smallest lettering will be not less than 1 mm. high when reproduced in a cut 3 in. wide.

Many drawings are made too large; originals should not be more than 2 or 3 times the size of the desired reproduction. In large drawings or groups of drawings the ratio of height to width should conform to that of a journal page but the height should be adjusted to make allowance for the caption.

The original drawings and one set of clear copies (e.g. small photographs) are to be submitted.

(iii) ***Photographs.*** Prints should be made on glossy paper, with strong contrasts. They should be trimmed so that essential features only are shown and mounted carefully, with rubber cement, on white cardboard with no space or only a very small space (less than 1 mm.) between them. In mounting, full use of the space available should be made (to reduce the number of cuts required) and the ratio of height to width should correspond to that of a Journal page (4½×7½ in.); however, allowance must be made for the captions. Photographs or groups of photographs should not be more than 2 or 3 times the size of the desired reproduction.

Photographs are to be submitted in duplicate; if they are to be reproduced in groups one set should be mounted, the duplicate set unmounted.

Reprints

A total of 50 reprints of each paper, without covers, are supplied free. Additional reprints, with or without covers, may be purchased.

Charges for reprints are based on the number of printed pages, which may be calculated approximately by multiplying by 0.6 the number of manuscript pages (double-spaced typewritten sheets, 8½×11 in.) and including the space occupied by illustrations. An additional charge is made for illustrations that appear as coated inserts. The cost per page is given on the reprint requisition which accompanies the galley.

Any reprints required in addition to those requested on the author's reprint requisition form must be ordered officially as soon as the paper has been accepted for publication.

Canadian Journal of Technology

Issued by THE NATIONAL RESEARCH COUNCIL OF CANADA

VOLUME 33 MAY 1955 NUMBER 3

CHEMICAL STUDIES OF A GOITROGENIC FACTOR IN RAPESEED OILMEAL[1]

BY Z. M. RACISZEWSKI,[2] E. Y. SPENCER,[3] AND L. W. TREVOY

ABSTRACT

The presence of 2–4 mgm. of *l*-5-vinyl-2-thiooxazolidone per gram of oilmeal from rapeseed grown in Saskatchewan was indicated by ultraviolet absorption measurements. Isolation of the *l*-5-vinyl-2-thiooxazolidone from the oilmeal allowed positive identification of the compound to be made by comparison of infrared absorption curves of the isolated naturally occurring material and of synthetic *d,l*-5-vinyl-2-thiooxazolidone. Some observations regarding procedure and yields in the reactions involved in the synthesis of *d,l*-5-vinyl-2-thiooxazolidone are also included.

The goitrogenic activity of rape and cabbage seeds when fed to rats was demonstrated by Hercus and Purves (8) in 1936; Kennedy and Purves (11) in 1941 reported that the addition of rapeseed to the diet caused thyroid enlargement in rats. The only antithyroid compounds that had been definitely isolated from plants were 5,5-dimethyl-2-thiooxazolidone (9) and thiourea (12) until Astwood (1) in 1949 extracted *l*-5-vinyl-2-thiooxazolidone (I) from rapeseed as well as from other brassica plants including rutabaga, turnip,

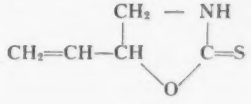

I

and cabbage. Bell (2) has recently studied growth depression in mice fed rapeseed oilmeal. The effect on thyroid size was not investigated and 0.1% iodinated casein was found to be of no value in counteracting the growth depressor(s) although this compound has been reported (13) to be effective in other species. These experiments therefore suggest either species differences in response to the rapeseed goitrogen or, more likely, the presence of more than one deleterious factor in rapeseed oilmeal. In view of the marked variation

[1]*Manuscript received November 22, 1954.*
Contribution from the Department of Chemistry, University of Saskatchewan, Saskatoon, Sask.

[2]*Graduate student; present address: Department of Chemistry, University of Notre Dame, Indiana.*
[3]*Present address: Science Service Laboratory, London, Ontario.*

in the quantities of chemical constituents present in plants with changes in geographical location and considering also the possibility of loss of *l*-5-vinyl-2-thiooxazolidone due to heating the oilmeal in the Anderson Expeller (operating temperature 260° F. or higher) used for removing the oil from the rapeseed, this work was undertaken with the object of determining whether or not *l*-5-vinyl-2-thiooxazolidone is present in oilmeal produced from Saskatchewan grown rapeseed. The information gained should be of value in the interpretation of the results of animal experiments where rapeseed oilmeal is used in the feed.

Water extraction of rapeseed oilmeal has been shown (1, 2) to remove one or more deleterious factor(s) from the oilmeal and by a determination of the ultraviolet absorption of these aqueous extracts in the region of 240 mμ an indication both qualitative and quantitative of the presence of *l*-5-vinyl-2-thiooxazolidone may be obtained. Preliminary experiments with rapeseed oilmeal in this laboratory (14) demonstrated, in agreement with Astwood's observations, that the precursor of a compound with an absorption maximum at 240 mμ is present in rapeseed oilmeal and that the absorbing compound may be generated from its precursor by acid catalyzed hydrolysis using a mineral acid such as hydrochloric acid, or by enzymatic hydrolysis using extracts from rape or cabbage leaves, and occasionally may result from production of enzymes by microorganisms contaminating the oilmeal.

Since the absorption at 240 mμ is characteristic of any compound possessing a thioncarbamate group it was necessary to establish the identity of the compound in rapeseed oilmeal having this absorption maximum. To this end a sample of rapeseed oilmeal was treated with an extract from fresh rape leaves and, as Astwood had observed for whole rapeseed, *l*-5-vinyl-2-thiooxazolidone was isolated and characterized by melting point and infrared absorption data. Having by this means established the presence of I in oilmeal prepared from Saskatchewan grown rapeseed, three different samples of rapeseed oilmeal were assayed using a spectrophotometric method (1) and the results are presented in Table I. These results may be compared with the values determined by Astwood for three varieties of rapeseed of 1.8 to 2.1 gm. of goitrogen per kilogram of whole rapeseed assayed.

Laboratory syntheses were required for the preparation of both the optically active and the racemic modification of the goitrogen and these were accomplished following the procedures of Ettlinger (4). Yields were improved when

TABLE I

DETERMINATION OF *l*-5-VINYL-2-THIOOXAZOLIDONE IN OILMEAL PREPARED FROM SASKATCHEWAN RAPESEED

Rapeseed oilmeal sample number	Year oilmeal produced	Quantity of *l*-5-vinyl-2-thiooxazolidone in the oilmeal in gm./kgm.
I[a]	1950	4.2
II[b]	1952	2.4
III[b]	1953	2.8

[a]*Courtesy of Prairie Vegetable Oil Company Ltd., Moose Jaw, Sask.*
[b]*Product of Saskatchewan Wheat Pool Vegetable Oil Plant, Saskatoon, Sask., and prepared from a mixture of Polish and Argentine rapeseed.*

inhibitors were added to prevent polymerization of unsaturated compounds. The butadiene monoxide required for the synthesis of the goitrogen was prepared using a procedure described by Freedman and Becker (6), which is a modification of the method of Kadesch (10).

The synthesis of *d,l*-5-vinyl-2-thiooxazolidone provided a supply of the compound for study of such chemical properties as its stability when heated with water at 100° C. and its stability in dilute acid medium. Compounds having a thione group give a green coloration with Grote's reagent (7) and this serves as the basis for another colorimetric method for the quantitative determination of the goitrogen. Using this method of analysis it was found that heating an aqueous solution of *d,l*-5-vinyl-2-thiooxazolidone at 100° C. for four hours resulted in a better than 90% recovery of the goitrogen. These results indicate that the steaming of rapeseed would have little effect on *l*-5-vinyl-2-thiooxazolidone but may have a quite different effect on the precursor of this compound in view of the findings of Hercus and Purves (8) who reported beneficial results from the steam treatment of rapeseed.

EXPERIMENTAL

Isolation of l-5-Vinyl-2-thiooxazolidone from Rapeseed Oilmeal

Seventy-five grams of fresh rape leaves, ground with clean Ottawa sand in a mortar, were added to 3 kgm. of rapeseed oilmeal (sample III in Table I) suspended in 12 liters of water and after stirring the mixture was allowed to stand for 20 hr. The solid material was then separated by straining the mixture through cloth and the extract after being heated to 60° C. was filtered through Super-cel. The yellow filtrate (volume, 5 liters) was concentrated to a thin sirup (volume, 1 liter) using a rotating flask evaporator (3). This concentrate was extracted three times with 2-liter portions of peroxide-free ether; the formation of stable emulsions caused some difficulty and loss in effecting these extractions but it was possible to break the emulsions by centrifugation and so to separate a clear yellow ether phase. The solvent, ether, was partially removed by distillation and the yellow solution was further purified (1) by washing with saturated sodium bicarbonate solution; after extracting the ether solution with 2 *N* sodium hydroxide the alkaline extract was neutralized by bubbling in carbon dioxide, the aqueous solution was extracted with ether, the ether was removed by evaporation, and the oil that remained was taken up in 50 ml. of water.

When the water was removed by evaporation from a portion of this solution and the oil remaining was seeded with a crystal of synthetic *l*-5-vinyl-2-thiooxazolidone, cooling at −10° C. for several hours caused a colorless solid to crystallize, m.p. 46–48° C., mixed m.p. with synthetic *l*-5-vinyl-2-thiooxazolidone, 46–48° C. (Lit. m.p. 50° C. (1).) The oil isolated from the rapeseed oilmeal showed a specific rotation $[\alpha]_D^{23}$ −50.1° (in methanol) which may be compared with $[\alpha]_D^{31}$ −70.5° (in methanol) (1) for pure *l*-5-vinyl-2-thiooxazolidone. The infrared absorption curve for the oil with maxima at 2.96, 3.07, 6.01, 6.54, 6.77, 7.68, 8.53, 10.10, and 10.81μ was in excellent agreement with the corresponding curve determined for synthetic *d,l*-5-vinyl-2-thio-

oxazolidone. (Astwood reports absorption bands at 2.92, 3.17, 6.63, 8.57, 10.17, and 10.88μ (1).) The aqueous solution of material extracted from the oilmeal had an absorption maximum at $\lambda = 240$ mμ and by a comparison of the intensity of absorption with data for solutions of pure racemic goitrogen the total recovery of *l*-5-vinyl-2-thiooxazolidone from the oilmeal was determined to be 0.45 gm. This large scale extraction procedure was inefficient, when compared with the assay data presented below, but it did serve to establish the presence of the goitrogen in the rapeseed oilmeal.

Assay of Rapeseed Oilmeal Samples

Ten grams of the oilmeal was mixed with 1 gm. of macerated fresh rape leaves* and was made up to a volume of 100 ml. with water; the mixture was allowed to stand for 24 hr.** The mixture was filtered, a 10 ml. aliquot of the filtrate was extracted with 10 ml. of ether, a 5 ml. aliquot of the ether extract was evaporated, and the residue was dissolved in 20 ml. distilled water. Optical densities for this solution were determined at 220, 240, and 260 mμ and the optical density at 240 mμ was corrected for nonspecific absorption (1) and then was compared with absorption data for solutions of pure racemic goitrogen.

Preparation of 3,4-Epoxy-1-butene

A mixture of 1-chloro-3-buten-2-ol and 2-chloro-3-buten-1-ol was prepared by the reaction of hypochlorous acid and butadiene according to the procedure described by Freedman and Becker (6). The mixture of chlorohydrins, b.p. 60–80° C. at 30 mm. Hg, was isolated in 37% yield based on calcium hypochlorite used and without further purification was converted to 3,4-epoxy-1-butene by reaction with 50% aqueous sodium hydroxide solution. Distillation through an efficient fractionating column gave 3,4-epoxy-1-butene, b.p. 64–65° C., in 74% yield.

Preparation of d,l-5-Vinyl-2-thiooxazolidone (*4*)

Ammonolysis of 3,4-epoxy-1-butene resulted in the formation of 1-amino-3-buten-2-ol and 2-amino-3-buten-1-ol. These amino alcohols were separated by means of the fractional crystallization of the corresponding acid oxalate salts. When Astwood's procedure was used for the decomposition of the 1-amino-3-buten-2-ol acid oxalate with barium hydroxide solution and for the recovery of the 1-amino-3-buten-2-ol by distillation, only a 52% yield was realized, the remainder of the product having formed a nonvolatile polymer. If, however, 0.5% of pyrogallol (5) was added to the crude 1-amino-3-buten-2-ol prior to distillation then the yield was increased to 84%. Similarly, in the digestion of the lead salt of 1-amino-3-buten-2-ol dithiocarbamate to form *d,l*-5-vinyl-2-thiooxazolidone and in the subsequent purification of the latter the addition of 0.5% *p*-benzoquinone (5) served to inhibit the polymerization reaction.

**Tests showed that l-5-vinyl-2-thiooxazolidone was not present in fresh rape leaves.*

***Tests showed that no additional release of l-5-vinyl-2-thiooxazolidone from its precursor occurred after 24 hr.*

Preparation of l-5-Vinyl-2-thiooxazolidone

The procedure used for the preparation of this compound was identical with that described by Ettlinger (4) and involved the resolution of 1-amino-3-buten-2-ol as the *d*-α-bromocamphor-π-sulphonate salt and then conversion of the *l*-1-amino-3-buten-2-ol *d*-α-bromocamphor-π-sulphonate into *l*-5-vinyl-2-thiooxazolidone.

Dependence of the Stability of d,l-5-Vinyl-2-thiooxazolidone on Temperature and pH

The Grote's reagent (7) used was two to five days old and light absorption was determined using a Coleman Universal Spectrophotometer Model 11. The procedure for the determination of the concentration of goitrogen in a given solution was as follows: an aliquot containing 0 to 20 mgm. of goitrogen was diluted with water to 100 ml., 35 ml. saturated sodium bicarbonate solution and 5 ml. Grote's reagent were added, and the mixture was allowed to stand for 25 to 30 min. after mixing; then a reading of optical density was taken at $\lambda_{max} = 620$ mμ and the thiooxazolidone concentration was read from a standardization curve prepared by plotting optical density against concentration of *d,l*-5-vinyl-2-thiooxazolidone.

Using this analytical procedure it was found that an aqueous solution of 1.16 gm. of racemic goitrogen per liter after being heated for four hours at 100° C. still contained 90% of the goitrogen originally present. However, when a similar solution of goitrogen was made 1 *N* with respect to hydrogen chloride and was heated under reflux for four hours only 30% of the goitrogen originally present remained undecomposed.

ACKNOWLEDGMENT

The authors express their gratitude to Dr. R. W. Freedman and Dr. E. I. Becker for details of their preparation of butadiene monoxide, to Miss A. Epp, Mr. L. Wiseblatt, Dr. H. Bauer, and Dr. R. U. Lemieux for determining the optical rotation and the infrared absorption curves of the goitrogen, and to Mr. E. C. W. Coxworth for technical aid in the preparation of the oilmeal extracts. We are also indebted to the National Research Council for financial assistance.

REFERENCES

1. Astwood, E. B., Greer, M. A., and Ettlinger, M. G. J. Biol. Chem. 181: 121–130. 1949.
2. Bell, J. M. and Williams, K. Can. J. Agr. Sci. 33: 201–209. 1953.
3. Craig, L. C., Gregory, J. D., and Hausmann, W. Anal. Chem. 22: 1462. 1950.
4. Ettlinger, M. G. J. Am. Chem. Soc. 72: 4792–4796. 1950.
5. Foord, S. G. J. Chem. Soc. 48–56. 1940.
6. Freedman, R. W. and Becker, E. I. Private communication.
7. Grote, I. W. J. Biol. Chem. 93: 25–30. 1931.
8. Hercus, C. E. and Purves, H. D. J. Hyg. 36: 183–203. 1936.
9. Hopkins, C. Y. Can. J. Research, B, 16: 341–344. 1938.
10. Kadesch, R. G. J. Am. Chem. Soc. 68: 41–45. 1946.
11. Kennedy, T. H. and Purves, H. D. Brit. J. Exptl. Pathol. 22: 241–244. 1941.
12. Klein, G. and Farkass, E. Oesterr. botan. Z. 79: 107–124. 1930.
13. Purves, H. D. Brit. J. Exptl. Pathol. 24: 171–173. 1943.
14. Raciszewski, Z. M. M.Sc. Thesis, University of Saskatchewan, Saskatoon. 1952.

THE DETERMINATION OF THE ORIGIN OF OPIUM

PART I. BY MEANS OF THE COMPOSITION OF THE ASH

By J. C. Bartlet and C. G. Farmilo

ABSTRACT

A procedure has been developed, based on composition of the ash, by which it is possible to determine the origin of opium found in the illicit traffic in narcotics. Methods are presented for the determination of the major and minor constituents of opium ash. Potassium, calcium, and sodium were determined flame photometrically; phosphate by a molybdenum-blue procedure; while silica, iron, aluminum, titanium, magnesium, boron, manganese, molybdenum, copper, tin, and lead were determined spectrographically. The application of these methods to 102 opium samples of known origin is described. The median percentages of the constituents for Yugoslav, Turkish (druggist), Turkish (soft), Iranian, Indian, and Far Eastern opium are given. The effects of accidental and deliberate contamination are taken into account by means of a correction factor. The major portion of the ash was found to be potassium sulphate and potassium phosphate but the composition showed geographical variations which permitted determination of the origin of the opium. It was found, for example, that Turkish (druggist) opium ash has a high calcium and a low potassium content. Iranian opium contains significant amounts of copper and tin, while opium from the Far East contains more phosphate relative to the potassium and calcium content than any other type. Opium from other producing areas can be distinguished by certain other characteristics.

INTRODUCTION

The basic raw material of the illicit narcotic trade of the world is opium. It is used directly for smoking, and is also the source of morphine and heroin. In order to control the international drug traffic, the geographical origin of opium in the illicit trade must be known so that supplies of the drug may be cut off at the source. To this end, the Economic and Social Council of the United Nations in 1948–49 authorized research into devising chemical methods of identifying opium, and invited member governments to participate in such a program and to provide authentic samples for opium research (14, 15).

Under the United Nations' program, investigations have been carried out in 15 countries and by the chemists of the United Nations Secretariat. The percentage of codeine, thebaine, papaverine, narcotine, meconic acid, cryptopine, and other alkaloids have been investigated (16). The porphyroxine–meconidine value and microscopic characteristics of opium under polarized light have been described showing the relationship of these values to the geographical origin of the opium (7, 8, 16). This laboratory also collaborated with the Secretariat's chemists on the determination of a number of the alkaloids in 50 samples of opium from the major producing areas.

The composition of opium ash as a means of determining the origin of opium has also been considered. Fulton has made reference to ash characterization

[1]*Manuscript received in original form July 26, 1954, and, as revised, January 12, 1955.*
Contribution from Food and Drug Laboratories, Department of National Health and Welfare, Ottawa, Canada. Work undertaken under U.N.E.S.C.O. Resolution 246F(IX). Also see E/CN. 7/278 for general summary of program.

in two United Nations' publications (7, 13) and Schnopper and Adler (12) in 1947 determined relative concentrations of 10 minor elements in five samples from different countries. Lucas and Burgener (10) carried out a preliminary spectrographic survey on the composition of opium ash. These workers determined spectrographic intensity ratios, but not actual concentrations, for a number of minor elements. Statistical treatment of these data by Dunnet (6) showed that this method had definite promise for the differentiation of opium samples from Turkey, Iran, and India. While the work reported in this paper was in progress, Jermstad and Waaler (9) published a report of a qualitative investigation of the trace constituents of the ash of 18 samples of opium from seven countries.

With respect to other plant materials a survey of the literature showed a large number of papers on the ash constituents, but the investigations were invariably carried out from the point of view of the plant or animal nutritionist. Differences in the content of elements such as potassium, calcium, and phosphorus which occur between species and varieties were often described, but were only incidental to the main information of the paper. For example, Brunstetter and Myers (5) described the variations in the percentages of K, P, Ca, Mg, Al, Fe, Mn, Cu, and B in the leaves of Concord, Ontario, and Delaware grapes. There were significant variations between varieties in the content of some of these elements. Magoon *et al.* (11) presented a more detailed analysis of the same data and showed that there is little variation in the leaf ash composition from vines of the same variety grown under different fertilizer treatment, while there is a very significant difference in ash constituents between varieties.

The over-all composition of opium ash has not been studied extensively. Annett and Bose (1) analyzed several samples of opium ash from "a pure race of poppy" grown in India. There was little variation in composition traceable to the wide variation in fertilizer treatment used in the experiments. No other strains of poppy were studied.

The available information indicated that quantitative analysis of opium ash for both major and minor constituents could bring to light differences in samples from the major producing areas. Although all opium comes from one species of poppy, *Papaver somniferum*, variations in opium ash composition might be expected from a number of causes:

(*a*) Local varieties of *Papaver somniferum*,
(*b*) Regional climatic conditions,
(*c*) Soil composition, pH, etc.,
(*d*) Methods of cultivation including fertilizer techniques, harvesting techniques, etc.,
(*e*) Methods of handling raw opium,
(*f*) Adulteration.

Since these factors may affect both major and minor constituents, it was felt desirable to determine as many of the ash components as were conveniently possible for as many samples as were available. This project was carried out

in order to establish the variations in opium ash composition in samples from within a single region and to establish the differences between samples from the various opium-producing regions.

ANALYTICAL METHODS

A Beckman Model DU spectrophotometer with an oxygen–acetylene flame attachment was used to determine potassium, calcium, and sodium; phosphate was determined by a molybdenum-blue procedure; silica, iron, magnesium, aluminum, titanium, boron, manganese, molybdenum, tin, copper, and lead were determined spectrographically using a Hilger large Littrow spectrograph and a Jarrell-Ash microphotometer.

Preparation of the Sample

If possible, the air-dried opium was finely ground and thoroughly mixed. A sample (2–10 gm.) was placed in a weighed platinum dish in a muffle, and ignited at 150–200°C. The temperature was gradually raised to 550°C., and maintained overnight to ensure complete ashing. The ash was then cooled, weighed, and mixed by grinding.

Flame Photometer Determination of Potassium, Calcium, and Sodium

A sample of ash (0.040 gm.) was dissolved in concentrated hydrochloric acid (five drops) followed by hot water (10 ml.). The mixture was filtered through a No. 40 Whatman filter paper and the acid-insoluble residue washed with hot water. The filtrate was diluted to 50 ml. with water in a volumetric flask. An aliquot (5.0 ml.) of this dilution was further diluted to 50 ml. to yield a solution containing 0.08 mgm. of acid-soluble ash per ml.

Potassium and calcium were determined with the flame photometer (4) at 767 and 554 mμ using the dilute sample solution. Sodium was determined at 589 mμ using the concentrated sample solution. Corrections for background and enhancement of emission due to the amount of potassium present were made for the sodium and calcium determinations (4).

Phosphate Procedure

Reagents

Ammonium molybdate solution.—Concentrated sulphuric acid (10 ml.) was added to water (40 ml.) and cooled. This solution was used to dissolve ammonium molybdate (1.0 gm.) and was then diluted to 100 ml.

Hydrazine sulphate solution.—Hydrazine sulphate (0.05 gm.) was dissolved in water (100 ml.).

Standard phosphate solution.—Disodium phosphate (0.159 gm.) was dissolved in water and diluted in 1 liter. This solution contains 0.1 mgm./ml. of phosphate. A solution containing 10 μgm./ml. was prepared by further dilution. A few drops of chloroform were added to the concentrated standard to inhibit mold formation.

Method

The phosphate content of an aliquot of the dilute sample solution used for flame photometry was determined by a colorimetric method similar to that

used for arsenate (3). An aliquot (2.0 ml.) was placed in a 25 ml. volumetric flask and *N* hydrochloric acid (4 ml.), hydrazine sulphate solution (2.0 ml.), and ammonium molybdate solution (2.0 ml.) were added. The sample was diluted to 25 ml. and heated in a boiling water bath for 10 min. and then cooled. The absorbance was measured in a 1.0 cm. cell at 820 mμ and the amount of phosphate determined from a standard curve drawn up from known phosphate solutions. The phosphate was reported as % PO_4^{-3}.

Spectrographic Determination of Other Constituents

Three parts of ash were ground with one part of a 1:1 mixture of spectrographic grade graphite and bismuth trioxide, in an agate mortar. A 10.0 mgm. portion of the mixture was placed in a lower electrode (Fig. 1).

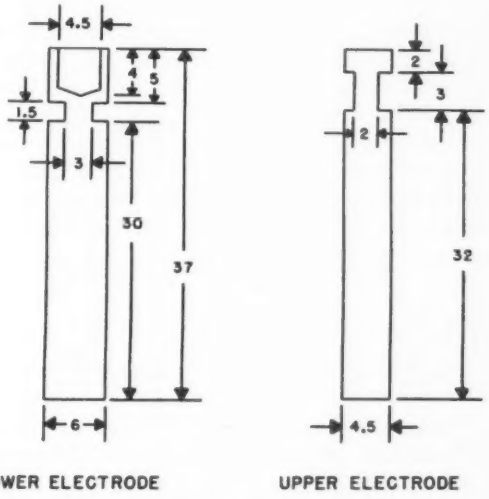

FIG. 1. Electrodes for opium ash analysis. (Measurements in mm.)

The arcing conditions were as follows:
Electrodes: see Fig. 1
Lower electrode: positive
Current: 12 amp. d-c.
Gap: 4 mm. (not adjusted during burning)
Time: to completion (90–130 sec.)
Plate: Eastman Kodak Spectrum Analysis No. 1
Water-cooled electrode holders and a step sector were used.
The following photographic developing conditions were used:
Developer: Kodak D-19 for 3.5 min. at 20°C.
Stop bath: Kodak SB-1(a) for 10 sec. at 20°C.
Fixer: Kodak Acid Fixer for one minute at 20°C.

TABLE I

ANALYSIS LINES FOR SPECTROGRAPHIC ANALYSIS OF OPIUM ASH

Element	Line wavelength, Å	Range, %	Internal standard line, Å	Standard error, %
B	2496.8 2497.7	0.003–0.1 0.020–0.1	Bi 2809.6 Bi 2809.6	5
Sn	2840.0 2661.2	0.003–0.1 >0.1	Bi 2809.6 Bi 2809.6	4
Pb	2833.1 2873.3	0.002–0.1 >0.1	Bi 2809.6 Bi 2809.6	5
Cu	2824.4	0.03–0.8	Bi 2809.6	9
Si	2532.4	1–32	None	7.5
Fe	2874.2	0.1–12	None	10
Al	2652.5 2660.4	0.8–3 0.05–0.8	None None	10
Mg	2781.4	0.1–5	None	8
Ti	3088.0	0.002–0.8	None	17
Mo	3132.6	0.0005–0.01	None	10
Mn	2949.2	0.003–0.1	None	13

TABLE II

MEDIAN VALUES OF ASH CONSTITUENTS

Country	No. of samples	% K		% Ca		% PO_4^{-3}		% SiO_2	% Fe	% Al	% Ti	Total mixed oxides	% Mg	% Na	% B	% Mn	% Mo	% Sn	% Cu	% Pb	Ratio 1	Ratio 2
		Uncorr.	Corr.	Uncorr.	Corr.	Uncorr.	Corr.															
Yugoslavia	5	32.6	35.9	4.7	5.1	11.6	12.7	5.7	1.4	0.75	0.04	8.7	1.2	0.41	0.018	0.025	0.0017	0.14	<0.03	0.034	3.08	2.79
Turkey (druggist)	24	20.5	25.0	9.8	12.8	10.6	12.9	10.6	0.6	1.0	0.10	15.8	1.4	0.36	0.036	0.045	0.0021	0.020	<0.03	0.008	3.02	1.90
Turkey (soft)	7	35.0	36.9	4.6	4.8	12.4	13.1	2.0	0.4	0.4	0.06	2.9	1.2	0.25	0.012	0.014	0.0020	0.08	<0.03	0.026	2.77	2.95
Iran	16	30.5	35.2	3.7	4.4	11.3	13.6	5.0	0.6	0.9	0.06	6.9	1.2	0.70	0.022	0.021	0.0020	0.95	0.11	0.021	2.56	2.50
India	33	35.1	39.7	2.8	3.1	11.8	13.0	5.3	0.95	0.85	0.08	10.9	1.0	0.39	0.017	0.022	0.0033	0.027	<0.03	0.018	2.84	3.00
Far East	11	24.2	33.3	3.6	4.8	18.0	23.8	13.5	1.0	3.0	0.10	24.1	1.8	0.46	0.025	0.050	0.0017	0.18	<0.03	0.094	1.60	1.57

The per cent transmission of analysis lines was determined by the microphotometer. The lines used are given in Table I for B, Sn, Pb, Cu, Si, Fe, Al, Mg, Ti, Mo, and Mn. The intensity ratios for the first four elements relative to bismuth 2809Å were calculated using a plate calibration (gamma) curve on an Applied Research Laboratories calculating board. The intensity in arbitrary units was calculated for the last seven elements using 10% transmission as unit intensity. The concentrations of the individual elements were then calculated from working curves prepared from chemically analyzed opium ash samples, and synthetic ash standards. The standard errors of the spectrographic results for the individual elements are included in Table I.

In order to determine the molecular constitution of the opium ash, so that similarly constituted synthetic standards could be prepared, the ash of 14 samples was analyzed by the X-ray powder diffraction method. Potassium sulphate was found to be the main constituent of the ash. Quartz was present in a few samples. The remaining minor components were not identified.

Synthetic standards were prepared by mixing and grinding reagent grade potassium phosphate (K_3PO_4) and sulphate, calcium sulphate, magnesium sulphate, sodium sulphate, and silica in amounts corresponding to the composition of chemically analyzed samples. Small amounts of the trace elements were added to form a "concentrated" standard and further "diluted" standards were prepared by adding a "blank" standard. The working curves for silica and iron were prepared from chemically analyzed samples.

RESULTS AND DISCUSSION

No attempt has been made to give the complete composition of all the individual samples.* However the median values for the various constituents of the ash are given in Table II. The table includes the "corrected" potassium, calcium, and phosphate values, the total of oxides of Fe, Al, Ti, and Si, and cation phosphate Ratios 1 and 2. The significances of these values in relation to origin are discussed in subsequent paragraphs. The percentages quoted are per cent of the ash, not per cent of the original opium. The median, rather than the arithmetic average, is discussed, since the median represents the value about which the samples are grouped.

Complete analysis carried out on four samples of the opium ash indicates that the difference between the sum of the percentages given in Table II and 100 was found to be almost entirely sulphate. A small portion of this difference may be acid-insoluble potassium, calcium, and phosphate. Carbonate was not detected in any of the samples when they were dissolved in acid.

It was noted during the survey that the amounts of silica, iron, aluminum, and titanium in the ash varied widely between samples from the same producing regions. In order to place all samples on a common basis, a "correction" factor was devised, and was based on the assumption that the major portion of these constituents was contributed by accidental contamination with soil and, in the case of iron, by storage in metal containers. The "corrections" were

*The complete data may be found in United Nations Document ST/SOA/SER.K/30. 1954.

obtained by the following calculations:

$$\% SiO_2 + \% Fe_2O_3 + \% Al_2O_3 + \% TiO_2 = A$$
$$\text{Corrected } \% K = \% K \times 100/(100-A)$$
$$\text{Corrected } \% Ca = \% Ca \times 100/(100-A)$$
$$\text{Corrected } \% PO_4^{-3} = \% PO_4^{-3} \times 100/(100-A).$$

We realize that the correction is imperfect since it does not take into account the amounts of calcium and magnesium contributed by contamination. These two elements are present as normal constituents of the plant latex as well as in contaminating soil, and it would be impossible to distinguish between normally occurring amounts and those contributed by contamination. Tin and lead, which are also present in amounts up to 6%, are not taken into account by the correction. However, the validity of the correction factor is indicated by the reduction of the spread of values of samples of a producing area as shown by the data in Figs. 8 and 9. The correction was not applied to the minor elements.

In general it was found that opium ash with a high potassium content had low calcium, while high calcium ashes were low in potassium. Calcium appears to replace potassium in the ash of some types on an equivalent basis. Some Chinese and Korean samples were either adulterated, or magnesium and sodium had replaced potassium and calcium to an appreciable extent.

The only anions detected in the ash were sulphate and phosphate. Since all the major cations and silica were determined, a determination of phosphate would allow approximate calculation of sulphate by difference. However it was found that phosphate was the only anion which yields information useful for origin determination. Comparison of per cent phosphate with the per cent potassium reveals differences between samples from various producing regions. Further, if equivalent per cent (equivalents/100 gm.) of phosphate is compared to the sum of equivalent per cents of potassium, calcium, and sodium, other differences in origin become apparent. These calculations give rise to Ratio 1 and Ratio 2 which are included in the criteria for identification of samples. These ratios are defined as follows:

$$\text{Ratio 1} = \text{equivalent per cent } (K+Ca+Na)/\text{equivalent per cent } PO_4^{-3}$$
$$\text{Ratio 2} = \% K/\% PO_4^{-3}.$$

Other elements detected spectrographically were: silver in nearly all samples; nickel in most samples; chromium, vanadium, and beryllium in a few. Other elements were sought, but were not detected or were present in such small amounts that positive identification could not be made in the wavelength region used. These include As, Sb, Cd, Cs, Co, Ga, Ge, Au, In, Li, Hg, Rb, Sr, Tl, W, and Zn. The elements detected such as Ag, Ni, and V did not seem to bear any significant relationship to origin, with the possible exception of silver, which was much higher in three Iranian samples than in any other sample. The silver line used for identification is very sensitive and even the highest silver concentration would not be more than a few parts per million. Zinc is probably present in all the samples, but the sensitive zinc lines in the wavelength region used are all coincident with lines of other elements such as iron or sodium.

IDENTIFICATION OF THE ORIGIN OF OPIUM SAMPLES

The ash composition of unknown samples may be compared to the ranges of composition found for samples from each of the producing areas in order to establish the origin. To facilitate this comparison, the composition data for the known samples have been reduced to composition profiles (Figs. 2 to 7), scatter diagrams (Figs. 8 to 11), and histograms (Figs. 12 to 14).

KEY TO FIGS. 2 TO 7

Constituent or other value	Factor by which values are multiplied for graph	Constituent or other value	Factor by which values are multiplied for graph
K	1	Mo	2000
Ratio 1 = Equiv. (K+Ca+Na)/ Equiv. PO_4^{-3}	10	Sn	10
		Cu	50
Ratio 2 = % K/% PO_4^{-3}	10	Na	10
PO_4^{-3}	1	Fe	4
Ca	2	Al	1
Total *A* (SiO_2+Fe_2O_3, etc.)	0.5	Mg	1
SiO_2	1	Ti	10
B	400	Pb	10
Mn	200		

Arrows on graphs indicate points of criteria for identification of samples.

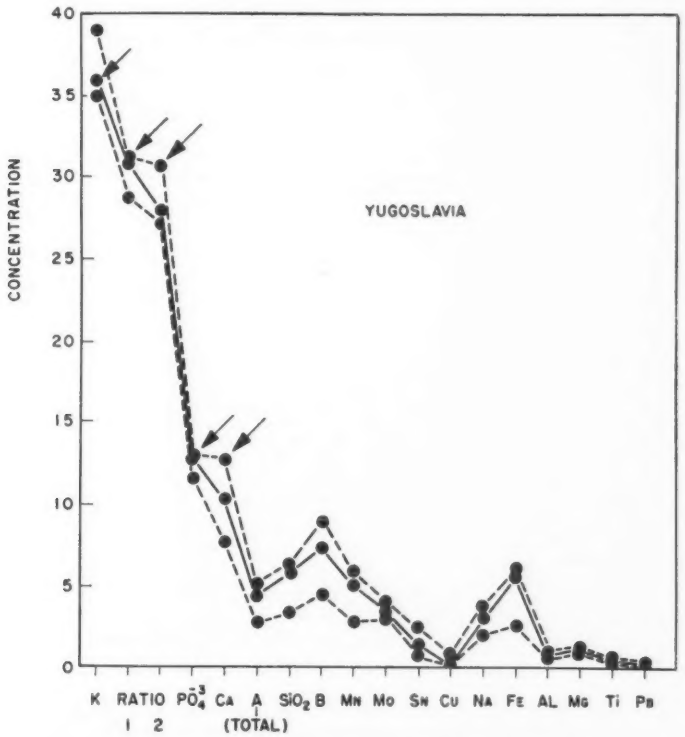

FIG. 2. Composition profile for Yugoslav opium ash.

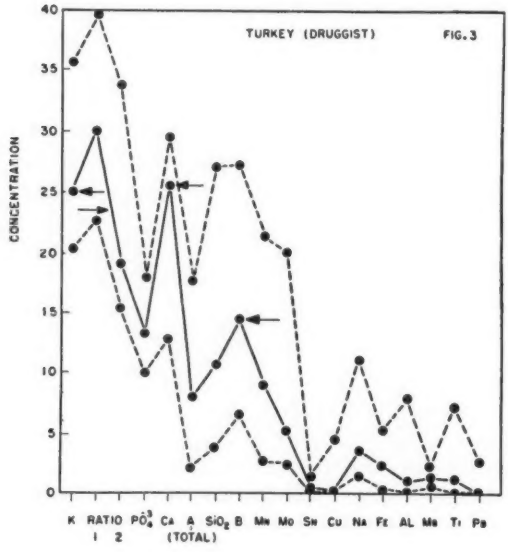

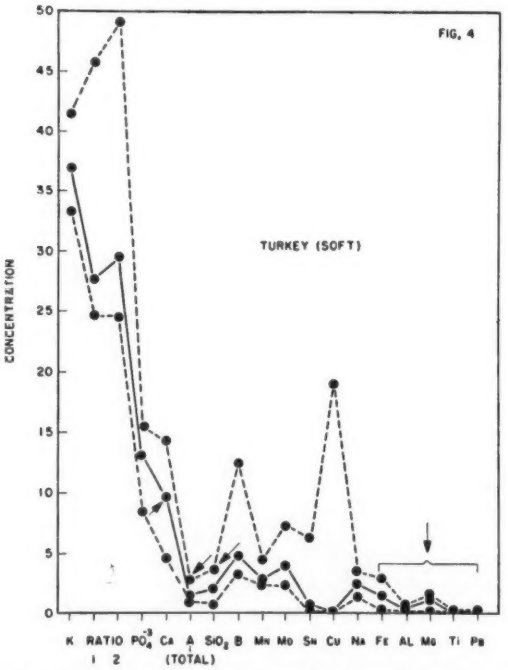

FIG. 3. Composition profile for Turkish (druggist) opium ash.
FIG. 4. Composition profile for Turkish (soft) opium ash.

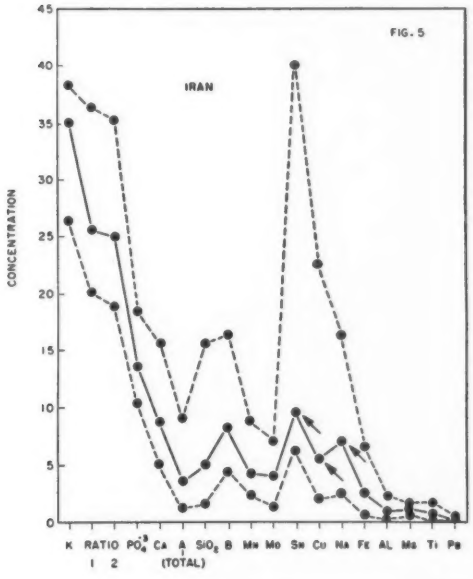

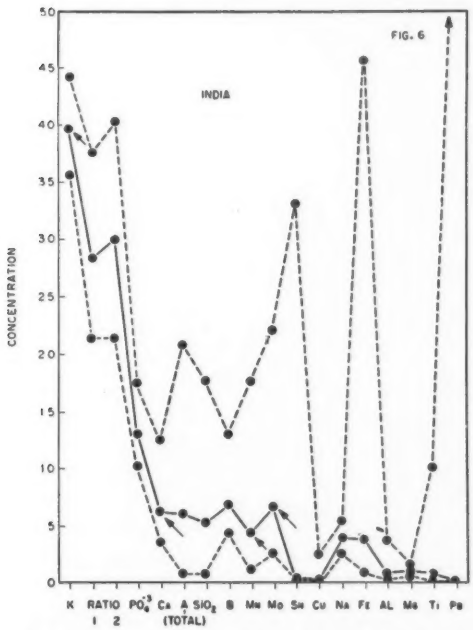

FIG. 5. Composition profile for Iranian opium ash.
FIG. 6. Composition profile for Indian opium ash.

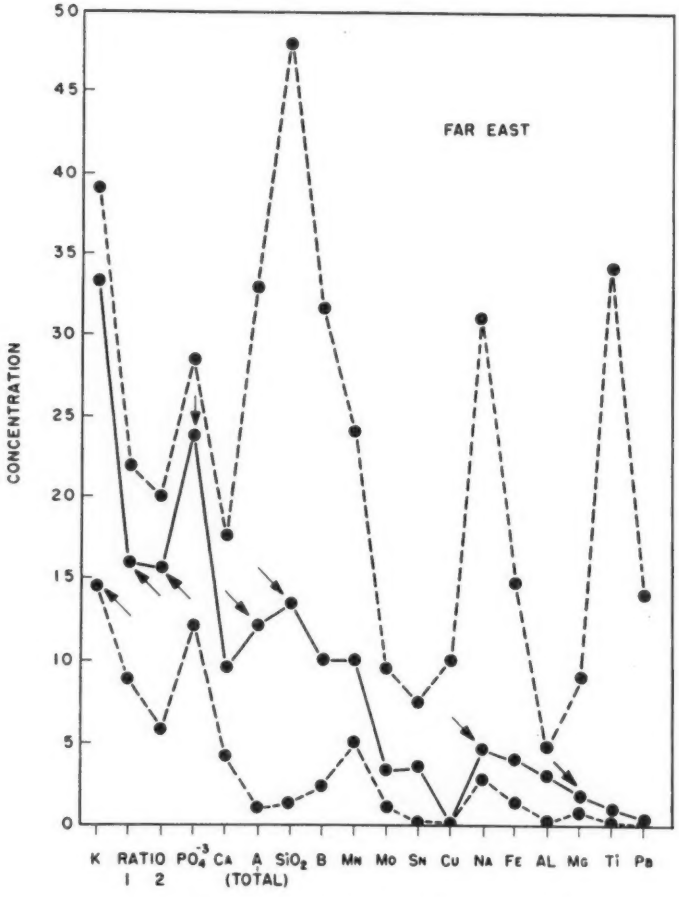

FIG. 7. Composition profile for Far Eastern opium ash.

Composition Profiles

Figs. 2 to 7 show composition "profiles" for the samples from Yugoslavia, Turkey (druggist), Turkey (soft), Iran, India, and the Far East. Individual elements, the sum of the contaminating oxides (the Total *A*), and two cation to phosphate ratios are spaced along the ordinate. The numbers along the concentration ordinate are based on the percentage of potassium in the ash. For convenience in graphing, the other values are multiplied by the factors shown in the key to the figures. The ranges are given on the charts by the top and bottom points for each element, and are joined by dotted lines. The median values are the middle points joined by the solid lines. The charts do not represent any one sample, as an individual ash may contain the maximum percentage

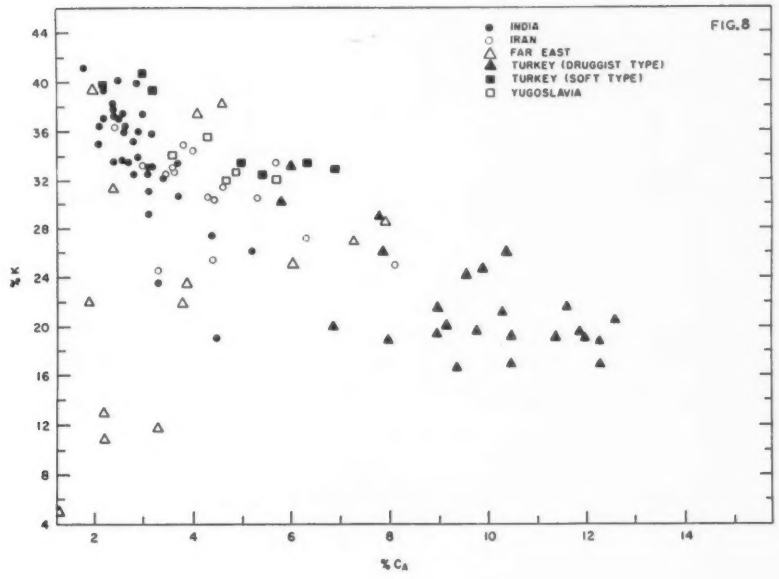

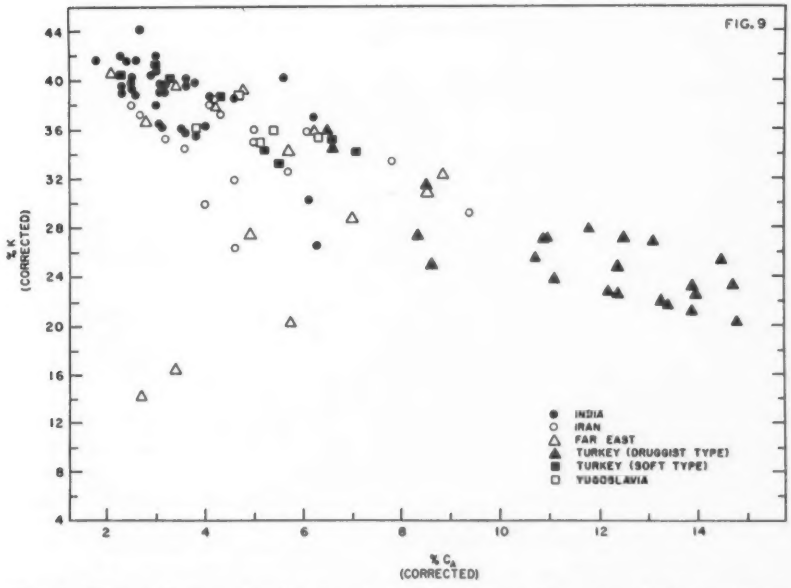

FIG. 8. Scatter diagram showing the relationship between the uncorrected potassium and calcium content of opium ash.

FIG. 9. Scatter diagram showing the relationship between the corrected potassium and calcium content of opium ash.

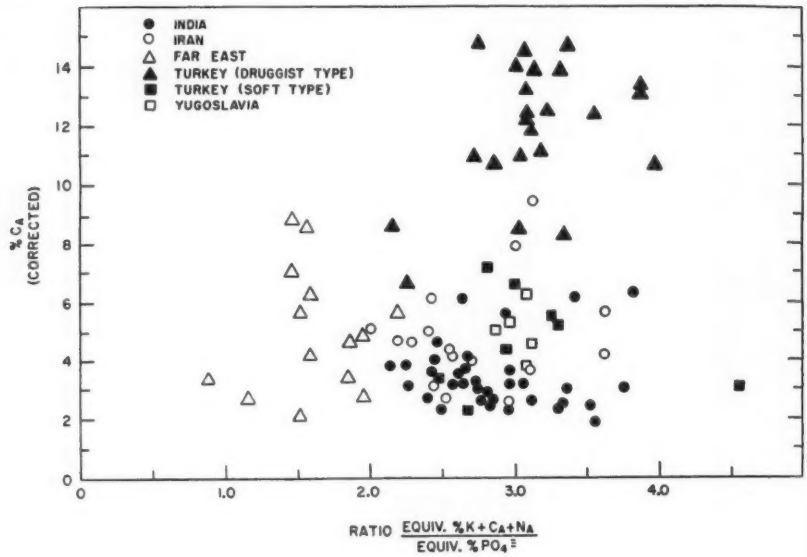

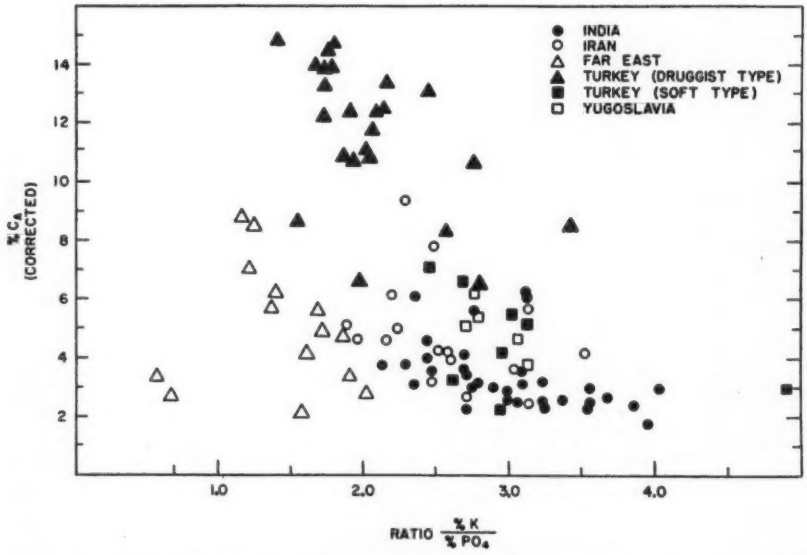

FIG. 10. (Top) Scatter diagram showing the relationship between ratio of total major cations to phosphate (Ratio 1) to per cent calcium of opium ash.

FIG. 11. (Bottom) Scatter diagram showing relationship between ratio of potassium to phosphate (Ratio 2) to per cent calcium of opium ash.

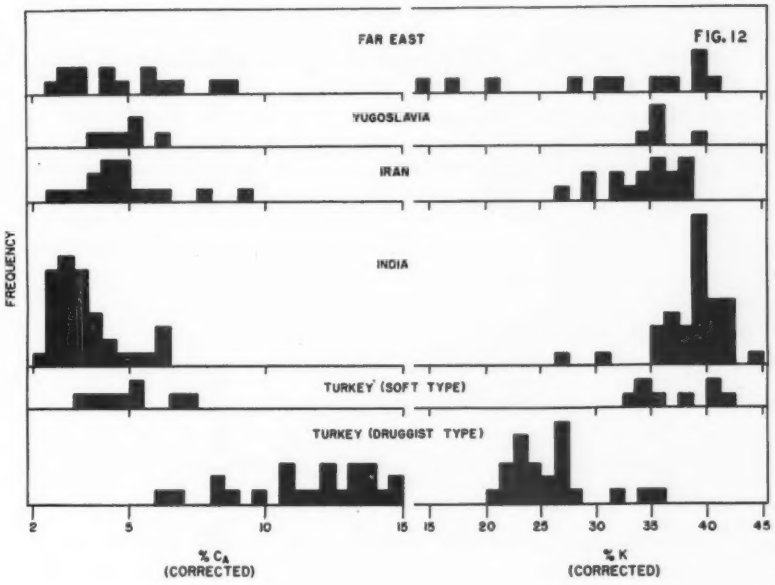

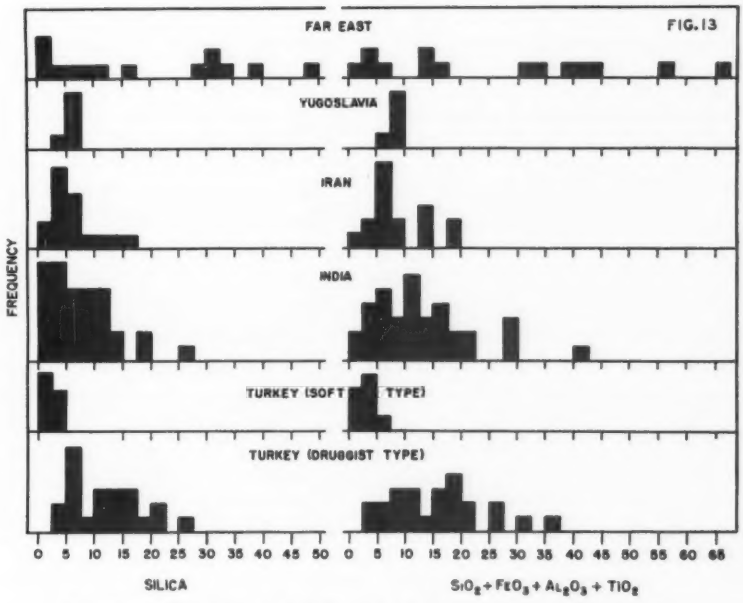

FIG. 12. Histograms of calcium and potassium content of opium ash.
FIG. 13. Histograms of silica and mixed oxide content of opium ash.

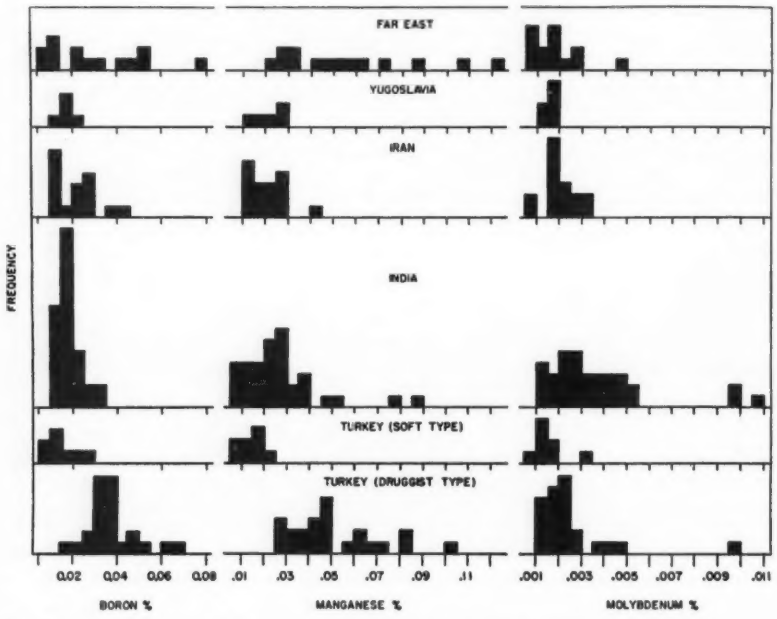

FIG. 14. Histograms of boron, manganese, and molybdenum content of opium ash.

of one element and the minimum of another. A hypothetical typical sample, however, would have a profile shown by the solid median line. The points used as criteria of the different regions are indicated by small arrows on the charts. These criteria points are more fully explained in the following sections.

Scatter Diagrams and Histograms

Fig. 8 shows the distribution of the uncorrected potassium percentages plotted against the calcium percentages, and Fig. 9 illustrates the same relationship using the corrected values. In Figs. 10 and 11 Ratios 1 and 2 are plotted against the corrected calcium percentage. The frequency distributions of some of the elements most useful for origin identification are given in Figs. 12 to 14.

Characteristics of Opium Ashes of Producing Regions

In the following sections the opium ash composition for samples from each of the major producing regions is discussed with a view to demonstrating the characteristics most useful for origin identification.

Yugoslavia

The ash composition of Yugoslav opium is very uniform. Samples from this region have approximately the following composition: K, 35%; Ca, 5%; PO_4^{-3}, 12.5%; and SiO_2, 5%. This composition is similar to that of some

Turkish (soft) and Indian samples. However, the ash has less phosphate and hence higher Ratios 1 and 2 than similar Indian samples. The iron, silica, and total mixed oxides are higher for Yugoslav samples than for the Turkish (soft) opium ashes. (See Fig. 2.)

Turkey (Druggist Type)

The majority of the ashes of druggist-type opium from Western Turkey contain less potassium and more calcium than the ashes of any other region. It is usually possible to identify a druggist opium on the basis of these two elements alone. Other characteristics usually found are the low value of Ratio 2 compared to Ratio 1, and a high silica, boron, manganese, and molybdenum content. A typical druggist opium is one of the easiest samples to identify, but some samples from the druggist-producing area differ in one or more of these characteristics and may resemble the soft type from eastern Turkey. (See Fig. 3.)

Turkey (Soft Type)

The soft opium from Eastern Turkey gives an ash which may easily be confused with Yugoslav or Indian samples. However, the samples usually contain more calcium than Indian samples, and less iron, silica, and aluminum than ashes from these two countries. (See Fig. 4.)

Iran

The amounts of the major constituents in Iranian opium ash may vary from about those in Turkish (druggist) to those in Indian opium ash. However the major distinguishing feature of all Iranian ashes studied is the high tin content (above 0.3%) and the high copper content (above 0.03%). On the basis of these two elements, only one Turkish (soft) and one Afghan sample would have been placed in the Iranian group, while none of the Iranian samples would have been excluded. Annett *et al.* (2) reported, with respect to Persian (Iranian) opium, that "the juice is collected and conveyed to the market in copper vessels". If these vessels were brass rather than copper, contamination from this source could account for the high tin and copper content of Iranian opium. Iranian opium often contains more sodium than most of the other samples. (See Fig. 5.)

India

The main distinguishing features of Indian opium ash are the high potassium content (about 40%) and the relatively low calcium content (about 3%). Some of the Turkish (soft) samples are similar in ash composition but Indian samples may generally be distinguished by higher silica and iron values. The Yugoslav samples may be differentiated by means of the lower phosphate content. Indian samples may also contain more manganese and molybdenum than most other opiums. (See Fig. 6.)

Far East

Far Eastern opium samples may easily be distinguished from any of the other types of opium studied, since the phosphate content of the ash is unusually

high compared to the potassium and calcium content and Ratios 1 and 2 are low in every case. The remainder of the ash composition of these samples varied over a much wider range than any of the other groups. Some of the Korean and Chinese samples studied were apparently adulterated, since they contained much more silica and magnesium than any other samples. However, Japanese, Indo-Chinese, and other Korean samples approximated closely the samples from other areas. The calcium content of the Indo-Chinese samples tends to be higher than that of the more northern sources. (See Fig. 7.)

Miscellaneous

Several samples received from other producing areas have been analyzed but have not been included in the identification criteria since there were insufficient data available for establishing the variation of ash composition. However, the results of analysis of the samples are discussed individually.

The only sample of opium available from Greece was highly contaminated with iron, tin, and copper and is probably not representative of that country.

One sample seized in the illicit traffic in Lebanon resembled Turkish (soft) samples closely and has been included in that group on the charts.

Only two samples of Afghan opium were available. One of these was very similar to Iranian opium while the other fell within the Indian range. These samples have been plotted as Indian on the charts.

A sample of experimental production from Pakistan appears to resemble the strain of Indian opium studied by Annett and Bose in 1918 to 1922 (1). These samples resemble the Far Eastern samples more closely than the Indian group that we have studied.

CONCLUSIONS

The composition of opium ash shows regional variations which can aid in the identification of origin of illicit samples from Yugoslavia, Turkey, Iran, India, and the Far East. We have found that the ash constituents most useful for origin determination are potassium, calcium, and phosphate. Among the minor constituents, copper, tin, boron, manganese, molybdenum, silica, and iron are useful in special cases, while lead is of little value. Combined with the established methods for determining origin such as the microscopic test (7), porphyroxine–meconidine value (8), codeine percentage (7), and combinations of these and other alkaloid percentages (16), the ash analysis will permit positive origin identification of most samples of opium.

The methods described here have been applied to 20 authentic samples whose origins were unknown to us at the time of analysis. The conclusions that were reached as to origin—based on the ash analysis alone; on the microscopic test, codeine, and porphyroxine–meconidine alone; and on the combined data—will be reported in a subsequent paper.

ACKNOWLEDGMENTS

We wish to thank Mr. G. Savary of this laboratory for much of the sample preparation, Dr. W. H. Barnes of the National Research Laboratories of Canada

for the X-ray diffraction analysis, and Dr. L. I. Pugsley and Dr. R. A. Chapman of the Food and Drug Laboratories for advice and assistance during the course of the study. We would also like to thank Mr. K. C. Hossick, Chief, Narcotic Control Division, for his continued support of the work. Mr. C. C. Fulton through the United Nations Secretariat supplied the samples of opium used in this study, and his generous help is gratefully acknowledged.

REFERENCES

1. ANNETT, H. E. and BOSE, M. N. Mem. Dept. Agr. India, Chem. Ser. 8: 45–51. 1925.
2. ANNETT, H. E., SEN, H. D., and SINGH, N. D. Mem. Dept. Agr. India, Chem. Ser. 6: 1–60. 1921.
3. BARTLET, J. C., WOOD, M., and CHAPMAN, R. A. Anal. Chem. 24: 1821–1824. 1952.
4. Beckman Bulletin No. 259. 1951.
5. BRUNSTETTER, B. C. and MYERS, A. T. J. Opt. Soc. Amer. 31: 163–166. 1941.
6. DUNNET, C. W. Private communication. 1951.
7. FULTON, C. C. Bull. Narcotics, U.N. Dept. Social Affairs, 1: 14–19. 1949.
8. FULTON, C. C. Bull. Narcotics, U.N. Dept. Social Affairs, 4: 15–25. 1952.
9. JERMSTAD, A. and WAALER, T. United Nations Document ST/SOA/SER.K/23. 1954.
10. LUCAS, G. H. W. and BURGENER, J. E. University of Toronto, Toronto, Ont. Private communication. 1951.
11. MAGOON, C. A., MYERS, A. T., DIX, F. W., and BRUNSTETTER, B. C. Proc. Am. Soc. Hort. Sci. 36: 485–491. 1938.
12. SCHNOPPER, I. and ADLER, I. U.S. Customs Laboratory, New York. Private communication. 1947.
13. United Nations Note by the Secretary General. Document E/CN 7/117/Add. 2. 22 Sept. 1948.
14. United Nations Economic and Social Council Resolution 159(VII) IIc. 3 August, 1948.
15. United Nations Economic and Social Council Resolution 246F(IX). 6 July, 1949.
16. United Nations Documents ST/SOA/SER.K/No. 1 to 34. 1950–1955.

THE EFFECT OF CHLORINATION AND SUBSEQUENT DECHLORINATION ON THE TANNING PROPERTIES OF LIGNINSULPHONATES[1]

By Alan G. Newcombe and H. Borden Marshall

ABSTRACT

Attempts have been made to increase the phenolic hydroxyl content of lignin-sulphonates by chlorination, and by chlorination followed by alkaline hydrolysis. The materials investigated were crude waste sulphite liquor and a high molecular weight fraction of waste sulphite liquor obtained by dialysis. Chlorination of the high molecular weight fraction caused extensive demethoxylation and a slight increase in phenolic hydroxyl content. Subsequent alkaline hydrolysis caused a further increase in phenolic hydroxyl content. The result of the two processes was to triple the number of phenolic hydroxyl groups/C_9 unit. The tanning properties of the ligninsulphonates, particularly their effect on shrinkage temperature, were improved by chlorination. Subsequent alkaline hydrolysis further improved the tanning properties with the exception of shrinkage temperature. All products, however, were inferior to quebracho.

INTRODUCTION

Recent investigations (17, 19) on the mechanism of tanning have indicated that collagen combines with the natural tannins by the formation of hydrogen bonds between the protein and the phenolic hydroxyl groups of the tannin. The tanning properties of ligninsulphonates are attributed to the presence of sulphonic acid and phenolic hydroxyl groups, although ligninsulphonic acid possesses a smaller percentage of the latter than do the natural tanning agents (7). It has, therefore, been suggested by workers in this field that the problem of converting the ligninsulphonic acid component of waste sulphite liquor into a useful tanning agent may be viewed as a problem of introducing phenolic hydroxyl groups (8).

As part of a project in this laboratory to develop a satisfactory tanning agent from waste sulphite liquor (12), the effect of chlorination, and of subsequent dechlorination, on the phenolic hydroxyl content and on the tanning properties of waste sulphite liquor have been investigated. Previous investigations on the chlorination of waste sulphite liquor have been studied both from the point of view of bleaching and from the point of view of producing a tanning agent, but opinions as to the efficacy of the latter are at variance. No evidence was available as to the effect of chlorination in aqueous solution on the hydroxyl content of the ligninsulphonates.

In earlier work, it was claimed (5, 10, 16) that chlorinated waste sulphite liquor produced a good leather, but Hägglund (9) stated that such leathers gradually decomposed, owing to the formation of hydrochloric acid from the chlorinated material. For this reason, later workers (13, 15) treated their chlorinated waste sulphite liquor with base in order to remove these reactive chlorine atoms before use of the liquor as a tanning material. No analytical data on these products were given.

[1]*Manuscript received January 3, 1955.*
Contribution from the Department of Chemistry, Ontario Research Foundation, Toronto, Ont.

Swartz (18) has compared the effects of chlorinating ligninsulphonic acid at pH values of 2, 6, and 10 and has found that the loss of methoxyl groups and the increase in chlorine content were greatest at pH 2.

Since there was a possibility that the loss of methoxyl groups might be accompanied by the formation of phenolic hydroxyl groups, the chlorinations described in the present investigation were carried out at low pH values, in order to achieve maximum demethoxylation. The solutions chlorinated had an initial pH value of approximately 1.0 and during the chlorination the formation of hydrochloric acid lowered this value still more. In order to favor substitution, rather than addition, so that in subsequent hydrolysis phenols rather than cyclohexenols would be formed, the chlorinations were carried out in the absence of light and in the presence of a halogen carrier.

EXPERIMENTAL

Analytical Methods

Sulphur was determined by the procedure of Yorston (21) and chlorine by the sodium peroxide fusion method. The acetylation method of Erdtman, Lindgren, and Pettersson (6) was used for the determination of hydroxyl groups but the sulphur dioxide which distilled over simultaneously was determined by titration with standard (0.01 *N*) iodine solution. Total solids determinations were carried out on the free acids by allowing their solutions to evaporate at room temperature and then drying to constant weight *in vacuo* over phosphorous pentoxide (14).

The tannin contents were estimated by the Official Method of the American Leather Chemists' Association (2) except that the solutions were shaken with the hide powder for 48 hr. Previous experience (11) has indicated that this modification is necessary for ligninsulphonates.

Chlorination of Waste Sulphite Liquor

Chlorinations were carried out on portions of the same large batch of commercial waste sulphite liquor (WSL) resulting from a soft cook of mixed spruce and balsam. In order to lower the pH, without the addition of mineral acid, the ligninsulphonates were converted to the free ligninsulphonic acids by the use of a cation exchange resin (Amberlite IR-120). The sulphurous acid formed on decationization, together with other low molecular weight acids, was removed by the use of an anion exchange resin (Amberlite IRA-400).

The chlorination apparatus consisted of a three-necked 3 liter flask equipped with a sintered glass inlet tube, a glycerol-sealed stirrer, and a stirrer-equipped foam breaking flask; to the latter were connected in series four gas washing bottles containing sodium hydroxide solution. The reaction vessel was immersed in a bath of ice and water during the chlorinations.

A weighed amount (209 gm.) of liquid chlorine in a graduate was allowed to vaporize and the gaseous chlorine was passed into a reaction mixture consisting of 2000 ml. (224.8 gm. of solids) of deionized WSL, 5.6 gm. of ferric chloride, 5.6 gm. of iron filings, and 5.0 ml. of a 1% solution of DC Antifoam A

(a chemically inert silicone compound) in carbon tetrachloride. Vaporization of the chlorine was complete in about 2.5 hr. and carbon dioxide was passed through the apparatus to carry over residual chlorine. A beige colored precipitate appeared during the reaction and was removed by centrifugation on the following day. The decantate (pH $\leqq$ 0) was passed through columns of Amberlite IRA-400 to remove free hydrochloric acid and the columns subsequently regenerated with a known volume of standard base to determine the amount of hydrochloric acid removed (148.2 gm.). The solution was then passed through Amberlite IR-120 and IRA-400 to remove Fe^{+3} and Cl^{-} respectively. The effluent was then concentrated to a small volume (500 ml.) of "soluble" chlorinated WSL solution containing 121.8 gm. of solids.

The precipitate from the reaction mixture was freed from metallic iron by dissolving the organic material in ethanol. The alcoholic solution was concentrated to dryness *in vacuo* and 96.0 gm. of "insoluble" chlorinated WSL obtained. The analytical values, shown in Table I, for the soluble and insoluble fractions are typical of those obtained in several chlorinations.

TABLE I

ANALYSES OF WSL AND CHLORINATED DERIVATIVES

	WSL	Insoluble chlorinated WSL	Soluble chlorinated WSL	Soluble chlorinated WSL after dechlorination
% S	5.9	3.5	4.2	4.9
% OCH_3	7.9	5.0	0.3	0.7
% Cl	0.0	22.4	14.7	5.48
% OH	9.0	—	9.5	3.8
% Fe	—	0.6	0.1	0.0
% Tannin	46	—	47	65

The chlorine (6.5 gm.) and hydrochloric acid (7.1 gm.) present in the caustic traps at the end of the reaction were determined by iodometric and potentiometric titrations, respectively.

Chlorination of High Molecular Weight Ligninsulphonic Acid

Fermented waste sulphite liquor was extensively dialyzed until free of sugars as determined by paper chromatography. The non-dialyzable high molecular weight fraction was then decalcified, using Amberlite IR-120 resin on the hydrogen cycle, and concentrated *in vacuo* to a concentration of 11.2 gm./100 ml. The dialyzed ligninsulphonic acid (LSA) solution, containing 227 gm. of solids, was chlorinated as above, using 191 gm. of chlorine. After standing for nine hours, the precipitate of "insoluble" chlorinated LSA which formed was dissolved by the addition of 4300 ml. of water. The solution was freed of hydrochloric acid as before and concentrated *in vacuo*. The yield of solids (227.7 gm.), calculated on the basis of the reacting weights shown in Table III, was 86.6%. The analyses of the LSA and the chlorinated LSA are shown in Table II. A chlorine recovery of 189 gm. (99% of that used) was

obtained; the chlorinated LSA contained 38.9 gm., the Amberlite IRA-400 removed 154.1 of hydrochloric acid (150.0 gm. of chlorine), and neither chlorine nor hydrochloric acid were found in the caustic traps.

Dechlorination of Soluble Chlorinated Waste Sulphite Liquor

A solution (363 ml.) containing 55.2 gm. of soluble chlorinated WSL was neutralized with 4.750 *N* sodium hydroxide solution to a reference pH of 2.00 by the addition of 22.0 ml. and to a pH of 12.80 by the further addition of 92.80 ml. The resulting solution was then heated at 100° C. in a sealed flask in the absence of air for 22 hr. The alkali consumed (0.080 moles) was determined by back-titration* of an aliquot. The solution was restored to a pH of 12 and then heated at 100° C. for another 18 hr. The alkali consumed, as determined by titration of an aliquot as before, amounted to 0.041 moles. Since the solution was still strongly basic, no additional alkali was added prior to heating for a further 18 hr. at 100° C. No alkali was consumed by this treatment and it was therefore concluded that all labile chlorine atoms had been removed. The solution of the dechlorinated material, after removal of sodium chloride and sodium hydroxide by passage through columns containing Amberlite IR-120 and Amberlite IRA-400, had a pH of 2.1 and contained 28.0 gm. of solids. The low yield obtained (50.7%) was due to absorption of organic material by the strongly basic Amberlite IRA-400. The analyses are shown in Table I.

Dechlorination of Chlorinated Ligninsulphonic Acid

A solution (170 ml.) containing 55.2 gm. of chlorinated LSA was brought to a pH of 2 and then dechlorinated in three steps as above by heating with 88.0, 34.3, and 24.5 ml. of 4.75 *N* sodium hydroxide solution for 29, 35, and 21 hr., respectively. The total amount of base consumed was constant after the second treatment and amounted to 0.133 moles. The resulting solution was passed through a column of Amberlite IR-120 and then through the weakly basic Amberlite IR-4B, rather than Amberlite IRA-400, since the latter had been found in the previous experiment to absorb a high proportion of organic material. The yield of solids was 40.3 gm. (73%), the analyses of which are shown in Table II.

The formulas for LSA, chlorinated LSA, and chlorinated LSA after dechlorination, calculated on a C_9 basis, are shown in Table III.

Tanning Evaluation

Pieces of acetone-dehydrated cowhide grain split, each 4 in. square, were rehydrated in 10 times their weight of acetate buffer (pH 5.0), and washed for 30 min. in running water. They were tanned by gentle agitation for 16 hr. in 125 ml. of a 2% tan solution, adjusted to a pH of 5.0, followed by four hours agitation in 100 ml. of a 3% tan solution, adjusted to a pH of 3.5.

**Since chlorinated WSL is not stable at pH values greater than 3.0 the initial pH value of 2.0 was used as a reference point; the titration curve is steep enough at this pH value that this may be done.*

TABLE II

ANALYSES OF LSA AND CHLORINATED DERIVATIVES

	LSA	Chlorinated LSA	Chlorinated LSA after dechlorination
% C	54.4	44.3	44.8
% H	5.6	4.1	3.5
% S	6.3	4.5	3.7
% Cl	—	17.1	8.0
% OH (total)	3.2	9.6	7.8
% OH (phenolic)*	1.1	1.7	3.0
% OCH_3	13.2	3.8	5.7
% Fe	—	0.1	0.0
% Tannin	58	70	83

**Determined by the hydrazineolysis of the tosyl esters according to the method of Freudenberg, K. and Walch, H. Ber. 76:305. 1943.*

TABLE III

FORMULAS FOR LSA AND CHLORINATED DERIVATIVES

Material	C	H	O	SO_3H	OCH_3	Cl	Phenolic OH	Non-phenolic OH	Reacting wt.
LSA	9	8.6	2.0	0.43	0.93	0.00	0.14	0.27	219
Chlorinated LSA	9	7.6	1.9	0.36	0.31	1.22	0.26	1.17	253
Chlorinated LSA after dechlorination	9	6.1	3.8	0.29	0.46	0.57	0.44	0.73	253

TABLE IV

EVALUATION OF LEATHER SAMPLES

Tannage	Weight yield	Shrinkage temp., ° C.	Color	Softness of grain*	Smoothness of grain*
LSA	123	68.5	Medium brown	Hard (5)	Fairly smooth (5)
Chlorinated LSA	135	75.5	Medium brown	Rather hard (4)	Smooth (4)
Chlorinated LSA after dechlorination	140	76.0	Dark brown	Fairly soft (2)	Smooth (2)
Chlorinated WSL after dechlorination	141	74.3	Brownish-black	Fairly soft (3)	Smooth (3)
Quebracho	170	84.5	Light reddish-brown	Very soft (1)	Very smooth (1)

**The numbers given are subjective and indicate decreasing order of softness and smoothness relative to quebracho.*

After being tanned, the pieces were soaked for one hour in water at 40° C. The quebracho leather was given an additional treatment with 0.3% sodium carbonate solution at 40° C. for one minute to clear the grain of insolubles, then washed with water, bleached in 1% sulphuric acid solution at 40° C. for one minute, and washed again with water.

The excess water was removed and 0.2 gm. of neatsfoot oil (5% based on the weight of hide substance) was applied uniformly to each piece of damp leather to replace the natural oils removed by acetone dehydration. The leathers were then tacked out and dried in a cool room. To further improve their softness, all samples were subjected to a staking operation, i.e., stretching and bending at a moisture content of 34%, which separates the fibers without breaking them. Finally, they were tacked out and dried in a conditioned room (65% R.H., 70° F.). The analysis and properties of the resulting leathers are given in Table IV.

DISCUSSION OF RESULTS

It has been suggested that the demethoxylation which occurs during chlorination of waste sulphite liquor results in the formation of methyl chloride. Since methyl chloride is volatile and resistant to hydrolysis, it would escape to the atmosphere and would therefore result in an incomplete chlorine recovery. In the chlorination of ligninsulphonic acid, 99% of the chlorine has been accounted for; if the 0.69 moles of methoxyl groups which were lost during the reaction were converted to methyl chloride, the net loss of chlorine would be 0.69 gm.-atoms or 12.8% of the total chlorine used. This result therefore suggests that methyl chloride is not formed during chlorination of ligninsulphonates.

The reactions which occurred during the chlorination of the dialyzed ligninsulphonic acid may be quantitatively expressed by the reactions shown in Table V which are based on the C_9 formulas given in Table III. This mechanism explains the results obtained but may not be the true explanation.

TABLE V

POSTULATED MECHANISM FOR CHLORINATION OF LIGNINSULPHONIC ACID

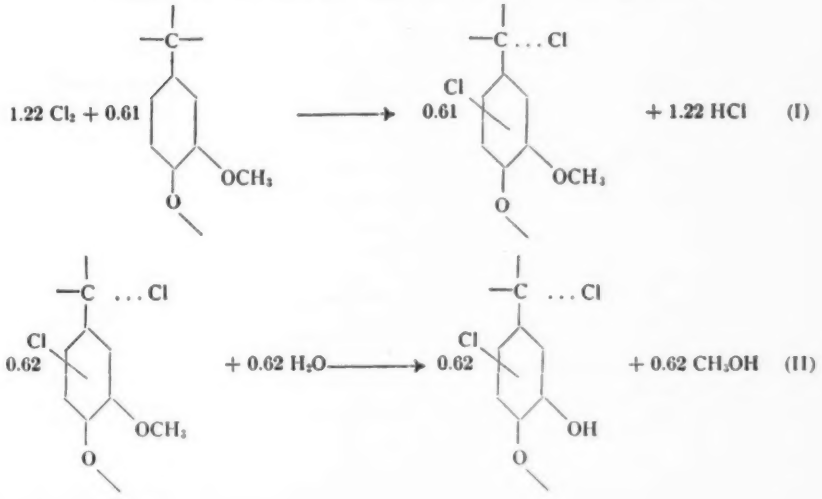

TABLE V—*Continued*

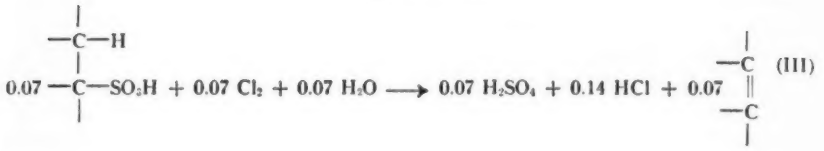

(III)

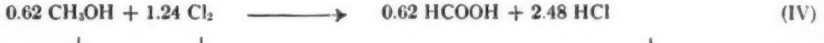

(IV)

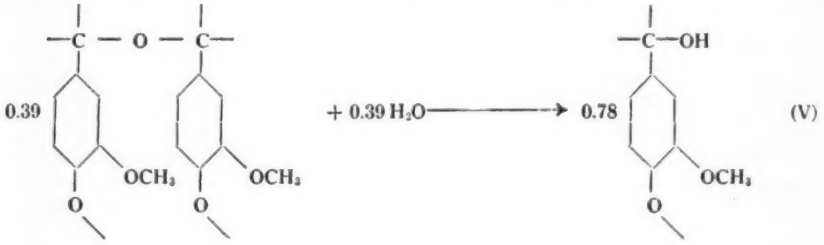

(V)

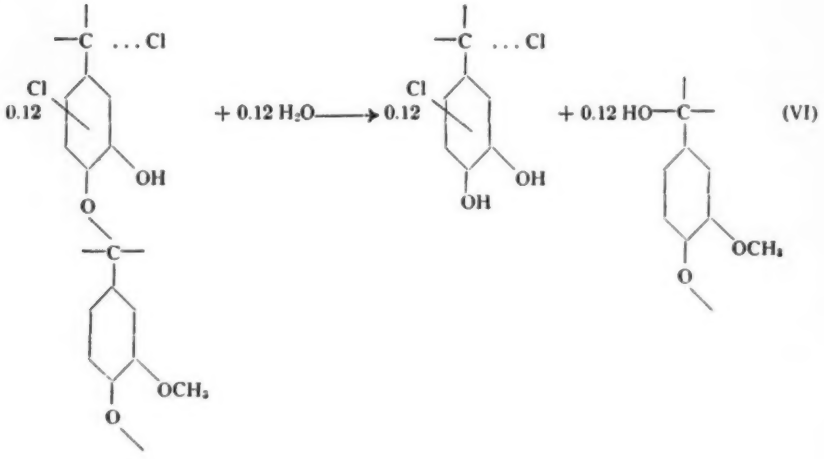

(VI)

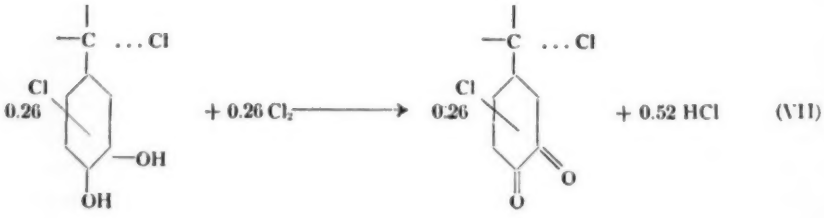

(VII)

In equation I, it is assumed that half of the organically bound chlorine (0.61 gm.-atoms) is attached to the aliphatic side chain and the other half to the aromatic ring. This assumption is supported by the fact that 0.62 moles of methoxyl were lost during the reaction and it is probable that the loss of methoxyl is associated with the entrance of a chlorine atom into the ring (equation II). Moreover, 0.65 gm.-atoms of chlorine are removed by alkaline hydrolysis and these are presumed to be mainly aliphatically bound labile chlorine atoms.

The sulphur split off during chlorination (0.07 gm.-atoms) would undoubtedly form sulphurous acid which would then be oxidized by chlorine to sulphuric acid (equation III). Likewise, it is presumed that methoxyl groups are hydrolyzed to methyl alcohol which in turn is oxidized to formic acid (equations II and IV).

Brochet (4) has shown that aqueous methanol is easily oxidized by chlorine to give formaldehyde and decomposition products of formic acid. For purposes of calculation, it has been assumed that only formic acid, which is unstable in acid solutions (3), would be produced.

The increase of 0.90 moles of aliphatic hydroxyl may be explained by the hydrolysis of 0.78 moles of benzyl ethers, a reaction which is known to occur readily in acid solutions (1) (equation V) and by the hydrolysis of 0.12 moles of alkyl aryl ethers (equation VI). The latter reaction is required to create 0.12 moles of para phenolic groups, which together with the 0.14 moles present in the original lignin are required for equation VII.

The actual increase in phenolic hydroxyl content (0.12 moles) is considerably less than that resulting from demethoxylation (0.62 moles) and it is therefore assumed that vicinal phenolic hydroxyl groups are destroyed by oxidation to quinones (equation VII), a reaction which has previously been suggested by other workers (20).

The changes in the amounts of functional groups per C_9 unit of lignin-sulphonic acid actually found and those calculated from the above equations are summarized in Table VI. The amount of chlorine actually used was 2.55 moles, and the amount of hydrochloric acid actually produced was 4.08 moles, per C_9 unit of ligninsulphonic acid. Correction has been made for the chlorine consumed in oxidizing metallic iron catalyst to ferric chloride and for the hydrochloric acid produced during ion exchange treatment by the

TABLE VI

CHANGES IN THE AMOUNTS OF FUNCTIONAL GROUPS PER C_9 UNIT OF LIGNINSULPHONIC ACID AFTER CHLORINATION

	H	O	SO_3H	OCH_3	Cl	OH	
						Phenolic	Aliphatic
Calculated	−1.22	+0.01	−0.07	−0.62	+1.22	+0.22	+0.90
Found	−1.00	−0.1	−0.07	−0.62	+1.22	+0.12	+0.90

ferric chloride originally added. In the equations in Table V, 2.79 moles of chlorine were used and 4.36 moles of hydrochloric acid were produced.

No attempt has been made to postulate the changes which take place on dechlorination due to the extensive oxidation which occurred.

The tanning properties of ligninsulphonic acid were improved by chlorination and further improved by subsequent dechlorination. The increase in weight yield of leather is probably due to the increase in the equivalent weight of the ligninsulphonic acid due to the loss of sulphonic acid groups. The increase in the shrinkage temperature on chlorination and dechlorination parallels the increase in phenolic hydroxyl content. Previous results obtained in this laboratory (12) have shown that increasing the phenolic hydroxyl content of lignin by condensation with phenol improved the tanning properties. In this investigation the phenolic hydroxyl content of the lignin molecule has been increased by chemical alteration of the basic lignin structure, rather than by condensation with phenolic nuclei, and a similar improvement in tanning properties has resulted. This is further confirmation of the hypothesis that the tanning properties of lignin can be improved by increasing its phenolic hydroxyl content.

ACKNOWLEDGMENTS

Grateful acknowledgment is made to Mr. W. R. Kenzie for evaluating the leather samples and to the Micro-Tech Laboratories for C, H, and S analyses. The waste sulphite liquor used in this investigation was kindly supplied by the Ontario Paper Company, Thorold, Ontario. We are also indebted to the Research Council of Ontario for financial support and permission to publish this paper.

REFERENCES

1. Adler, E. and Lindgren, B. O. Svensk Papperstidn. 55: 563. 1952.
2. American Leather Chemists' Association. Methods of sampling and analysis. American Leather Chemists' Assoc., Easton, Pa. 1946. p. A.-13.
3. Branch, G. E. K. Chem. Abstr. 9: 2832. 1915.
4. Brochet, A. Ann. chim. et phys. (7), 10: 289. 1897.
5. Caminneci, A. Ger. Patent No. 479,909. Jan. 21, 1925. Chem. Abstr. 23: 5059. 1929.
6. Erdtman, H., Lindgren, B. O., and Pettersson, T. Acta Chem. Scand. 4: 228. 1950.
7. Freudenberg, K. Collegium, 19: 3. 1937.
8. Gustavson, K. H. Tek. Tidskr. Uppl. C. Kemi och Bergsvetenskap, 73: 59. 1943. Ing. Vetenskaps Akad. Handl. No. 177: 82 pp. 1944.
9. Hägglund, E. Chemistry of wood. Academic Press, Inc., New York. 1951. p. 226.
10. Hilpert, S. Chem. Abstr. 20: 2747. 1926.
11. Marshall, H. B., Krizsan, M., and Henry, W. C. J. Am. Leather Chemists' Assoc. 49: 505. 1954.
12. Marshall, H. B. and Krizsan, M. J. Am. Leather Chemists' Assoc. In press.
13. Müller, O. A. Brit. Patent No. 571,916. Sept. 14, 1945. Chem. Abstr. 41: 4327. 1947.
14. Newcombe, A. G. Can. J. Chem. 32: 1047. 1954.
15. Osakeyhtio, A. A. Norwegian Patent No. 74,547, Jan. 31, 1949. Chem. Abstr. 44: 3714. 1950.
16. Schmidt, A. Brit. Patent No. 178,104. March 31, 1922. Chem. Abstr. 16: 3208. 1922. U.S. Patent No. 1,567,395. Dec. 29, 1925. Chem. Abstr. 20: 666. 1926.
17. Shuttleworth, S. G. and Cunningham, G. E. J. Intern. Soc. Leather Trades' Chemists, 32: 183. 1948.
18. Swartz, J. N. Ph.D. Thesis, McGill University, Montreal, Que. 1939. pp. 59–60.
19. Tu, S. and Lollar, R. M. J. Am. Leather Chemists' Assoc. 45: 324. 1950.
20. White, E. V., Swartz, J. N., Peniston, Q. P., Schwartz, H., McCarthy, J. L., and Hibbert, H. Tappi, 24: 179. 1941.
21. Yorston, F. H. Pulp & Paper Mag. Can. 48 (No. 13): 74. 1947.

THE EXPLOSIBILITY OF WET AMMONIA–AIR MIXTURES[1]

By R. M. Clarke and George F Wright

ABSTRACT

A study has been made of an industrial plant explosion in which flammable ammonia–air mixtures over aqua ammonia were ignited inside storage tanks and piping where flame or spark could not have been present. It has been found that the temperature of 800°C. inside a pipe which is being arc-welded is insufficient to ignite the flammable mixture unless this hot metal is brought into contact with liquids such as aqua ammonia or very dilute hydrogen peroxide. A detailed description of the accident indicates that this combination of circumstances is sufficient to explain the occurrence. The flammable properties of wet ammonia–air mixtures are summarized here for the first time, in the hope that further accidents of this type may be prevented.

This report is based upon an explosion of the atmosphere above aqua ammonia in tanks that occurred at the Canadian Industries Ltd. plant in Toronto during March, 1953. Publication seems justified because of the peculiar circumstances attending this explosion and, in general, because of the paucity of information concerning the ignition of ammonia mixed with air.

Few accidents of the type have been reported adequately. Most have involved explosions of dry mixtures in ammonia compressor rooms (9, 1), and one was complicated by the presence of other inflammable gases in the mixture (8). The only public report of an explosion occurring in a tank containing aqua ammonia occurs in a daily newspaper (2). In this instance initiation of explosion seemed to be due to a spark from an arc-welding operation.

The information included in these reports, together with that available in International Critical Tables (6), may be summarized briefly as follows:

1. Mixtures with air containing 14.5–29.5% ammonia at 100°C. will ignite with suitable initiation.

2. The limits are decreased to 16.5–26.8% at ambient temperatures and are further decreased by presence of water vapor.

3. Initiation of explosion is possible with an open flame or a spark, but not with a glowing wire of platinum, iron, or chromium–nickel alloy unless it is coated with a catalyst of the dehydrogenation type.

4. The explosion is mild by comparison with mixtures of air with hydrogen, water gas, or producer gas.

This summary of properties is insufficient to explain the recent explosion in Toronto. In this instance three clean storage tanks (Nos. 1 and 2 of 18,000 gal. capacity and No. 3 of 22,000 gal. capacity) had been interconnected with 2-in. I.P.S. service lines by means of arc-welded joints, and 90–100 gal. of concentrated aqua ammonia (29.4%, sp. gr. 0.9) had been added from barrels to each tank in order to prevent rusting. During the next morning, which was

[1]*Manuscript received October 12, 1954.*
Contribution from the Department of Chemistry and the Department of Chemical Engineering, University of Toronto, Toronto 5, Ontario.

rainy with a temperature of 43–40°F., a welder, standing on the top of tank No. 1, was engaged with a mild steel Fleetweld No. 5 rod in making the last half of a third "pass" over that one (A, Fig. 1) of the already-closed joints on the far side of the ell which was attached to a 3-ft. length of vertical pipe (B, Fig. 1) leading into the top of the tank. Since this line, which vented to the atmosphere about 40 ft. away, was entirely closed it is impossible that sparks from the welding operation could have ignited the ammonia–air mixture within the tank.

FIG. 1.

While the welder was completing this joint he felt vibration underfoot which increased in several seconds to such an amplitude (about six inches) that he jumped to the ground just before the top C of the tank blew off and apart. The deflagration was then transmitted through the interconnecting 2-in. piping to tanks 2 and 3. Tank 2 appeared to have suffered the same effects as tank 1 save that the top and sides were separated as a unit from the bottom. Damage to tank 3 was not extensive. At the beginning of the incident a loud hissing sound was heard which, presumably, issued from the distant end of the vent pipe. The possibility that hydrogen or methane was present in sufficient quantity to sensitize the ammonia–air mixture is remote since

the aqua ammonia used to cover the bottoms of the tanks was poured in from drums that had been standing for many days at atmospheric pressure.

Inspection of the interior of the new pipe section that was being welded at the time of the accident revealed no abnormality such as the presence of iron sulphides which are often pyrophoric (4). Indeed this pipe interior was clean and free from rust, as one might expect of new material. Thus only the temperature inside the weld could have caused ignition of the ammonia–air mixture. This temperature was ascertained from a comparable weld of two steel plates by observation with an optical pyrometer to be 960°C. during the first pass and 780°C. during the second pass.

Although the flammability limits of dry ammonia–air mixtures are known with reasonable accuracy (8), the limits for mixtures which included water vapor are less well-defined, and no data seem to be available respecting the flammability limits of the atmosphere over aqua ammonia (7). Information available in the literature (3) together with a vapor pressure determination of 30 mole % (concentrated) aqua ammonia shows that the ammonia content above the solution at temperatures of −4°C. to about +10°C. will fall within the flammability range for dry mixtures. In order to ascertain whether wet mixtures within this temperature range are also flammable, an apparatus (Fig. 2) has been constructed in which the equilibrated atmosphere above

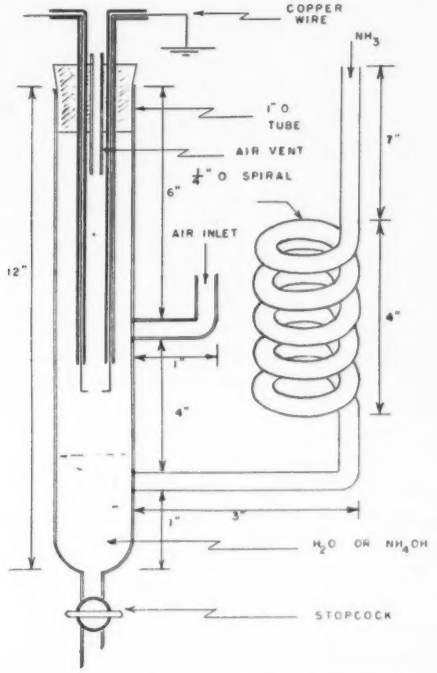

FIG. 2. Apparatus to determine the wet ammonia–air combustion limits.

ammonia-saturated water is subjected to a spark discharge. It has been found that 30 sec. of sparking will not produce a flame at +6°C. nor at −5°C. However flames are produced within the temperature range −4°C. to +5°C. with maximum ignitibility and propagation at −1°C. to 0°C. Thus it is apparent that the atmosphere in the storage tank No. 1 (at +5°C. at the time of the accident) was just within the flammability range with respect to spark ignition.

However ignition was not initiated in tank No. 1 but, rather, at the far side of the ell which is 3 ft. removed by a section of 2-in. pipe. Therefore it has seemed worth while to ascertain the probability that a low-energy flame such as that of ammonia–water–air will propagate through narrow tubes. The apparatus shown in Fig. 3 has been assembled partly for this purpose. After

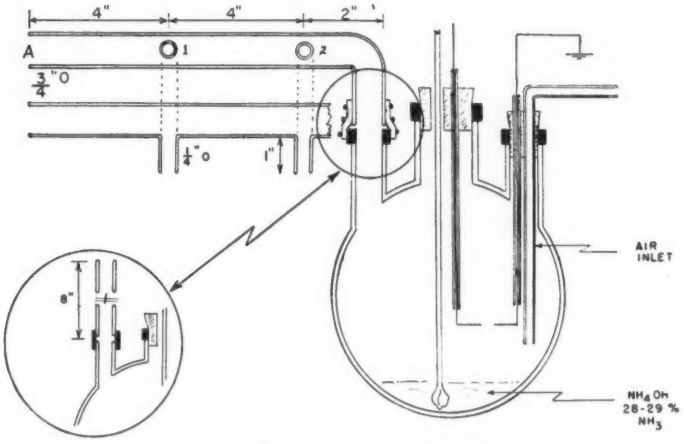

FIG. 3. Flame propagation in tubing.

100 ml. of 30 mole % aqua ammonia is placed in the 5 liter flask, the stirrer is operated for five minutes with the system at 20°C. Equilibrium with respect to the 30 mole % solution is not attained, as is shown by Orsat analyses of the gas phase, but the mixture is flammable as may be shown by use of the spark discharge. Furthermore the flammability may be judged qualitatively by the sparking time (sometimes 20–30 sec.) which is necessary before inflammation. In these circumstances the flame is yellow in color and it usually travels slowly through the flask during one to two seconds. When the composition of the gas phase is closer to the lower limit rather than to the upper limit of flammability an explosion usually occurs which forces the stopper from the flask. This rapid deflagration is much less yellow in color than is the slow flame. It is evident from these experiments that the gas phase above aqua ammonia at 20°C. may be dangerously explosive when it is not equilibrated with respect to the liquid phase.

When the ammonia–air mixture in the side-tube (A, wetted with aqua ammonia) is ignited by a bunsen flame either at the open end or at ports 1 and 2 the yellow flame cannot traverse the bend so as to ignite the atmosphere in the flask. If the side-tube A is replaced by a vertical tube 8 in. long by $\frac{3}{4}$ in. O.D., then ignition by bunsen flame at the upper end will produce a flame which travels down and sometimes inflames the atmosphere in the flask; more often the flame dies out just before it reaches the flask. However the occasional, though erratic, propagation of flame through the $\frac{3}{4}$ in. tube indicates a high probability that the flame will survive in a 2-in. pipe.

The type of slow (one to two second) deflagration described above is reproducible if ignition is effected by a bunsen flame directly at the side-neck of the 5 liter flask (Fig. 3). The progress of this deflagration is shown diagrammatically in Fig. 4. The initial flame is characteristically yellow, about one to two inches high, and may burn at the neck-opening for several seconds (Fig. 4, step 1), evidently until the composition of the gas in the flask becomes optimum. Then the flame is pinched off as shown in step 2 and travels down

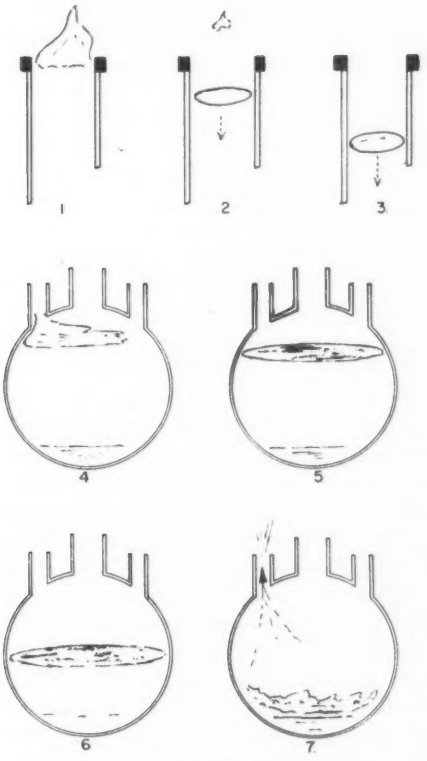

FIG. 4. Typical flame propagation.

the neck (step 3) in the shape of a thin yellow disk. Upon reaching the spherical space it loses its shape for an instant, then flashes sidewise (step 4) and re-establishes a large thin yellow disk which travels downward (steps 5 and 6). When the liquid level is reached the shape and color disappear. The hissing sound of gas escaping from the side-neck is then observed.

These studies of ignition by spark or flame are of interest in evaluation of the limits and types of wet ammonia–air inflammation. However they do not provide an explanation for the occurrence of the explosion in the Canadian Industries Ltd. plant because neither spark nor flame could have reached the atmosphere inside of the tank system. Consequently other methods of ignition have been studied in the apparatus shown in Fig. 3. Instead of a spark across the gap terminals a platinum coil (8 in. of No. 32 wire coiled 1 in. long by $\frac{1}{4}$ in. in diameter) is attached and heated electrically to a maximum temperature of 1120°C. as evaluated by an optical pyrometer. Despite a report to the contrary (8) a flame appears during the heating of this coil. This flame, about two inches high at the critical temperature when it appears, increases in size with increase in temperature. The base of the flame is confined to the length of the coil and its blue-yellow to colorless appearance designates it as a hydrogen flame induced by cracking of the ammonia. If the electrical power is shut off the flame continues to burn above the coil for several seconds and then is extinguished. In these circumstances it will be observed that the flame does not cause general deflagration in the flask although under certain conditions an explosion will occur. This occurrence is not related to the position of the heater in the flask, but it is reproducible either if air is admitted at the side-neck or if the hot coil is splashed with aqua ammonia. Either of these modifications seems to make the hydrogen flame capable of igniting the air–ammonia mixture. However it is noteworthy that a quiescent hydrogen flame will not induce ignition.

A nichrome coil of the same dimension behaves like the platinum coil although its behavior is less pronounced, probably because it operates at a lower maximum temperature (1060°C.). However an iron coil operating at the temperature of the weld which caused the accident will not induce a flame of any kind. Since the iron coil is not very durable under the series of repetitive tests that are necessary for reliability, a modified apparatus, shown in Fig. 5, has been assembled. This comprises a tube, A, terminating in a nozzle which will impinge a fine liquid spray on the bottom of B, a heater. This heater is constructed from mild steel, the lower end being machined to 0.25 in. O.D. by 0.20 in. I.D. Inside is placed a nichrome coil (54 in. of No. 28 wire) wrapped around a quartz or alundum tube and surrounded by thin mica. This 110 v. 1 amp. heater raises the external temperature to 800–850°C. or slightly above that observed during the second pass of the arc-weld. The stirrer (C, Fig. 5) is sufficiently loose-fitting that pressure can escape from the flask. The spark gap used for standardizing the flammability of the gas mixture is shown at D, while E is a tube through which air, gaseous ammonia, or aqua ammonia can be introduced.

Among 100 trials with flammable ammonia–air mixtures the iron heater at

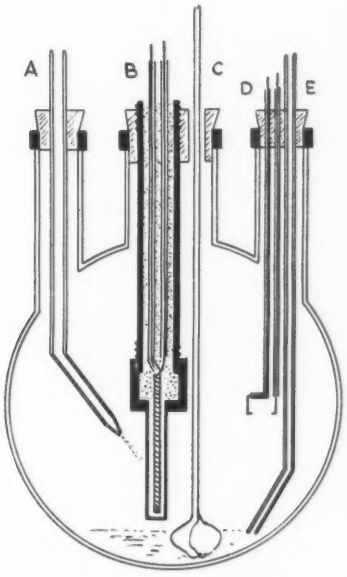

FIG. 5. Red-hot iron surface.

800–850°C. failed to produce a flame. Likewise no flame was observed when the hot surface was sprayed with water. However a spray of aqua ammonia on the hot surface produced a small flame in about 15–20% of 50 trials, and in one trial the entire atmosphere in the 5 liter flask deflagrated. The same effect could be produced by splash from the stirrer but with lesser frequency, probably because too much water vapor was generated by this means. In a modification of this test, 200 ml. of aqua ammonia was placed in a 4 liter beaker covered except for a $\frac{3}{4}$ in. hole in the center of the cover, and chilled to 5–10°C. after approximate equilibration was attained by swirling the liquid. A welding rod heated to cherry-redness was quickly immersed 100 times into the gas phase inside without sign of ignition. Yet in 25 subsequent experiments wherein the tip of the immersed cherry-red welding rod just touched the surface of the aqua ammonia a flame of varying size was repeatedly obtained.

Since the fine water spray which is ineffective in causing ignition at the hot iron surface must certainly absorb much ammonia from the gas phase in the 5 liter flask (Fig. 5), it is evident that the aqua ammonia spray, which does cause inflammation, must contain a substance not present in the gaseous ammonia–air mixture. Because of the possibility that the factor may have been an oxidation product a spray of 0.5% aqueous hydrogen peroxide has been impinged upon the hot iron surface. This treatment causes ignition at about the same frequency as is observed with the aqua ammonia spray but the color of the flame is much deeper yellow with local intense regions. Also

the frequency with which the flame propagates to complete deflagration is greater than is observed with the aqua ammonia spray.

The strongly-yellow color of the flames observed in ammonia–oxygen mixtures has been thought by Herzberg and Ramsay (5) to be due to $NH_2^{\cdot}$ radicals. This yellow color is also characteristic of the relatively cool flame encountered in the slow deflagration described above. The mode of ignition at the hot iron surface suggests that in this flame reaction NH_2 radicals may be formed and decomposed by a self-sustaining chain reaction involving atomic oxygen or hydroxyl radicals as expressed below

$$NH_3 + OH^{\cdot} \rightarrow NH_2^{\cdot} + H_2O$$
$$NH_2^{\cdot} + O_2 \rightarrow NH + HO_2^{\cdot}$$
$$NH_3 + HO_2^{\cdot} \rightarrow NH + H_2O + OH^{\cdot}$$

where the fate of imide will depend on the amount of available oxygen (10). Indeed the propagation of such a flame should depend on the reactions of imide because the postulated chain would not be expected to be self-sustaining for very long unless it received support from a subsequent reaction or series of reactions.

Whether or not this mechanism describing the initiation of deflagration in ammonia–air mixtures is valid, a reasonable explanation for the explosion at the Canadian Industries Ltd. plant is now at hand. One may presume that water accumulated in the horizontal section (D, Fig. 1) of the vent pipe interconnecting the storage tanks. This undoubtedly occurred during rains while the system was tack-welded and before the first pass on the several welds was completed. When aqua ammonia was added to the tanks a distribution of ammonia *via* the gas phase occurred. The aqua ammonia thus formed in pipe section D may have suffered slight oxidation. If now the welder, standing on the top of tank No. 1 while he commenced the third pass at A (Fig. 1), may have shifted his weight slightly, the buckling of the top of the storage tank would incline the horizontal portion, D, of the vent pipe. The aqua ammonia in D would then flow onto the red-hot metal underneath the weld. According to the experimental results outlined above this contact would be sufficient to initiate a flame that eventually would propagate into tank No. 1.

The authors wish to thank Canadian Industries Ltd. for permission to publish this report and for generous support of the work.

REFERENCES

1. Assoc. British Chemical Mfrs., Safety Summary, 14 (No. 56): 1943.
2. Chronicle, The. Northwich, England. Nov. 12, 1949.
3. Friend, J. N. Textbook of inorganic chemistry. Vol. VI. Part I. Charles Griffin & Co., Ltd., London. 1928. p. 84.
4. Griffith, R. H. and Morcom, A. R. J. Chem. Soc. 787. 1945.
5. Herzberg, G. and Ramsay, D. A. J. Chem. Phys. 20: 347. 1952.
6. International Critical Tables. Vol. II. McGraw-Hill Book Company, Inc., New York. 1927. pp. 173, 176.
7. Schaphorst, W. F. Natl. Engr. 53 (No. 12): 36. 1949. Chem. Abstr. 44: 8108. 1949.
8. Schliephake, O., Nagel, A., and Schemel, J. Z. angew. Chem. 43: 302. 1930.
9. Schlumberger, E. and Piotrowski, W. Z. kompr. flüss. Gase, 17: 49. 1915. J. Gasbeleucht. 57: 941. 1914.
10. Zawadski, J. Discussions Faraday Soc. No. 8: 140. 1950.

PHYSICOCHEMICAL STUDIES ON ALBERTA COALS

I. SURFACE AREA MEASUREMENTS[1]

By N. Berkowitz[2]

ABSTRACT

As a precursor to kinetic studies of reactions between coals and selected organic solvents in ultrasonic fields, measurements have been made of the accessible surface areas of typical Alberta coals by a heat-of-wetting technique. The experimental results show a well-defined catenary-type variation of surface areas with coal rank (carbon contents); surface areas vary from about 15 to 300 sq. m. per gm., with minimum values being reached among medium-volatile bituminous coals containing between 85 and 90% carbon. Some data are also reported for the effect of compression and of mild oxidation on surface area.

INTRODUCTION

The recognition that coal resembles a two-phase (air–solid) colloidal system (1) leads theoretically to an important, if not perhaps always fully appreciated, corollary. Regardless of the various structural forms currently assigned to coal (2, 10, 16), it suggests that many properties of coal may be governed not so much by elementary composition (or 'rank') or by molecular structure as by the extent of available surface (S). More specifically, it suggests that reactions between coal and oxygen (as in combustion or gasification) or between coal and liquids (as in solvent extraction) may, in a large measure, be determined by kinetic factors. And since there is as yet no compelling evidence for supposing that the degree of compaction of a coal—the result of tectonic forces and the principal determinant of S—must *necessarily* be covariant with chemical maturity, there are moreover grounds for thinking that such kinetic factors may be only loosely connected with coal rank.

But whilst elucidation of these factors thus becomes an integral part of modern coal utilization research and a necessary precursor to any fundamental study, it is important to bear in mind that a classical kinetic approach to reactions involving coal presents several unique problems. Not only are most coals petrographically extremely heterogeneous, but the coal 'series' is (even if genetically perhaps discontinuous) unquestionably continuous in terms of carbon, hydrogen, and oxygen contents, and the role of elementary composition (and of the still unknown molecular combinations into which these elements enter) cannot be unequivocally established. For the sake of simplicity, it is therefore more convenient to approach the general problem empirically by determining the surface area S and then comparing S with observed behavior. Such a reformulation has the further advantage that S provides, in itself, a useful classification parameter (15) and valuable evidence relating to the ultrafine structure of coal (2).

[1]*Manuscript received November 8, 1954.*
Contribution No. 43 from the Research Council of Alberta, Edmonton, Alberta.
[2]*Senior Research Chemist, Research Council of Alberta, University of Alberta, Edmonton.*

With this in mind, measurements have been made of the surface areas of a range of typical Alberta coals which form the subject of detailed study in these laboratories. The method for evaluating S was based upon a heat-of-wetting (or heat of immersion) principle (15), and the results generally reveal the same pattern as that established for British coals (15). But before reporting these results and the further information that has emerged from the present study, it will be helpful to consider briefly some aspects of the experimental method employed in these investigations.

HEAT OF WETTING AS A MEASURE OF SURFACE AREA

In principle, surface areas of porous solids can be determined by recourse to any one of several volumetric methods or to direct weighing of the adsorbent at several adsorbate pressures (as with the McBain sorption balance). In all cases, an isotherm is obtained from which monolayer capacities can be computed with only few assumptions; and whilst different methods of computation may occasionally lead to rather divergent results (7), agreement is generally very good. However, under certain conditions, adsorption methods suffer from an important inherent disadvantage: if the adsorbent is (like coal or coke) a solid whose pore system contains local constrictions of molecular dimensions, adsorbent–adsorbate equilibria are established only very slowly, and in the extreme case, equilibrium may require as much as three to six weeks for each isothermal point. In a survey in which the information gained is primarily of a statistical nature, it is therefore frequently convenient to adopt a different approach, even if this incurs some sacrifice of accuracy.

One such approach, and incidentally one that does *not* necessarily sacrifice accuracy, involves a phenomenon known as heat of wetting (or heat of immersion). It has long been known that immersion of a dry solid in a wetting liquid is accompanied by a heat release (ΔH) and, if the surface under examination is assumed to be energetically more or less uniform, that ΔH is proportional to the *extent* of wetted surface (14). If the heat release per unit surface is known from other measurements, the surface area S can hence be calculated directly from ΔH.

Theoretically, the calorimetric measurement of S via the heat of wetting would seem to be attended by several difficulties. Whilst the actual determination of ΔH is straightforward and subject only to the usual precautions involved in calorimetry, its numerical value must *prima facie* critically depend upon the previous history of the adsorbent, upon the state of the adsorbent surface, and upon the purity of the wetting fluid used. Moreover, interpretation of ΔH in terms of a surface area requires assumptions as to surface uniformity that are often not justified. But there are reasons for supposing that these theoretically anticipated difficulties either do not always appear in practice, or that they tend to cancel each other.

In the case of coal and related carbonaceous solids (such as cokes), attempts have been made to determine the heat release per unit surface by splitting individual samples into two fractions and comparing the results of a heat of

wetting determination (carried out on one) with that of a volumetric adsorption (carried out on the other). Using methanol[3] for both series of experiments, it has been shown that a heat release of 1 cal. corresponds to very nearly 10 sq. meters, and that this equivalent appears, for all practical purposes, to be independent of coal rank (or 'type'). The data reproduced in Table I

TABLE I

COMPARISON OF HEATS OF WETTING AND SURFACE AREAS

Coal	Rank	Carbon, %*	Heat of wetting in MeOH, cal./gm.*	Surface area by MeOH ads., sq. m./gm.*	Cal./sq. m.	Ref.
Bacchus Marsh, Victoria, Australia	Lignite	65.2	38.5	357	1.078	*a*
Koeflach, Austria	Lignite	68.4	33.4	332	1.006	*a*
Yallourn, Victoria, Australia	Lignite	71.8	38.8	348	1.115	*a*
Salt Range, Pakistan	Sub-bit.	74.6	19.8	197	1.005	*a*
Warwickshire, England	High-vol. bit.	81.1	17.7	176	1.006	*b*
Northumberland, England	High-vol. bit.	82.2	16.5	167	0.990	*b*
Ireland	Anthracite	92.4	4.8	50	0.960	*c*
Willow Charcoal	—	?	15.9	155	1.026	*d*

*Calculated on dry, ash-free basis.

References: a. Berkowitz, N. and Schein, H. G. Fuel, 31: 19. 1952.
b. Maggs, F. A. P. BCURA Conf., London, 1944. p. 95 et seq.
c. Berkowitz, N. Unpublished work.
d. Bangham, D. H. and Razouk, R. I. Proc. Roy. Soc. (London), A, 166: 572. 1938.

illustrate this point. Contrary to expectation, moreover, it is found that the measured values of ΔH are highly reproducible and that reproducibility essentially demands only one precaution, namely that the individual samples of a single coal shall correspond to each other in terms of petrographic composition. If this condition is satisfied by careful sampling and quartering of the bulk material, it appears that other factors become relatively unimportant. For example, it can readily be demonstrated that traces of moisture in the wetting fluid (methanol) do *not* significantly affect the observed value of ΔH; and in view of the constancy of the equivalent 1 cal. = 10 sq. m. (cf. Table I), it

[3]*The choice of methanol was based on the fact that MeOH provides the smallest molecule existing in the liquid phase at ordinary temperatures. Because of this, MeOH may be expected to penetrate into pore spaces from which larger molecules might be partially excluded. It has, moreover, been shown that MeOH is capable of* displacing *adsorbed methane and water from a coal surface and wetting by MeOH can hence be relied upon to take place on a substantially 'clean' surface.*

must also be concluded that possible differences in 'polarity' of various coals (as evidenced by different oxygen contents) lie equally within the limits of experimental error involved in the heat of wetting measurement.

It is of course clear that any measurement of S with as heterogeneous a solid as coal can yield no more than an average datum. However, this only introduces interpretational difficulties. Thus, neither the form nor the nature of the surface can at present be defined unless recourse is made to a micellar model such as has been developed by Bangham *et al.* (3); and since this model can at best apply only to so-called 'structureless vitrains', the assignment of a surface area measured with the *coal substance as a whole* involves speculations that may be as unsound as they would currently be unconfirmable. But subject to the proviso that S can at present offer no more than a correlation parameter, and subject also to the further recognition that *any* measurement of surface area involves considerable uncertainty, a direct conversion of ΔH into S would seem to be justified by the available evidence.

Reference should perhaps here be made to the fact that heat of wetting measurements with coal (using MeOH as wetting fluid) have recently come under criticism on other grounds. Determining surface areas of coals by volumetric adsorption of nitrogen (or argon) at *ca.* 83°K. and finding values of between 1 and 5 sq. m. per gm., Lecky *et al.* (19), Malherbe (20), and Zwietering *et al.* (21) have concluded that the very much higher values obtained from heat of wetting measurements at 25° or 30°C. (which vary, depending upon the rank of coal, between *ca.* 15 and 380 sq. m. per gm.) are due to some form of chemical interaction between coal and methanol. But it is not necessary here to deal with these criticisms *in extenso*: theoretical considerations and experimental evidence for regarding them as fundamentally untenable have already been given elsewhere (9), and still more recent evidence (by some of the original critics themselves) upholds this view (11). Krevelen (18) has himself shown that the observed discrepancies between low-temperature adsorption measurements and heat of wetting determinations are due solely to the nature of the pore system in coal; and earlier postulates of chemisorption, 'polar' adsorption, imbibition of methanol, and partial dissolution (or dispersal) of coal in MeOH, brought forward to account for the discrepancies, need thus not be considered further.

APPARATUS AND EXPERIMENTAL TECHNIQUE

In the present investigations, the heat of wetting apparatus used for the measurement of S was closely similar to the assembly described by Griffith and Hirst (15) and later by Berkowitz and Schein (8). The calorimeter consisted essentially of a 100 cc. capacity unsilvered Dewar flask set into a constant temperature water bath (at 30°C.) and clamped against an aluminum plate through which a stirrer and sample holder were fitted as shown in Fig. 1. Two modifications, however, were introduced in order to secure greater operational safety and flexibility of the apparatus and to increase its sensitivity. To break sample bulbs located in the small cage A (cf. Fig. 1), a spring-loaded tube fitted with two sharp steel needles was used; and the special long-stem

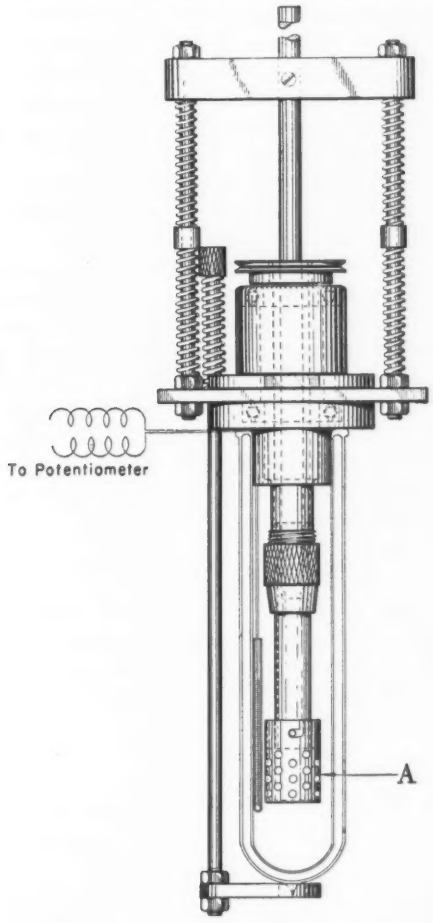

FIG. 1. Diagrammatic view of calorimeter.

thermometer previously employed for temperature measurements was replaced by a platinum resistance-thermometer which was mounted against the inner wall of the Dewar vessel and connected to a suitable Wheatstone bridge and galvanometer. ΔH was thus measurable in terms of a galvanometer deflection.[4]

The experimental procedure was as follows: The carefully quartered coal sample, ground to pass a 65 mesh Tyler screen and weighing between 2 and 3 gm., was dried *in vacuo* at about 105°C. for two hours, weighed into a tared, thin-walled glass bulb, and outgassed for two or three days at between 90° and

[4]*By first determining the heat capacity of the assembled calorimeter by means of the heat of neutralization of an acid and base, it proved possible to so adjust the Wheatstone bridge that a galvanometer shift of 1 mm. corresponded to 1 cal. Accurate readings could be made down to 0.1 mm.*

100°C. and at a final pressure of approximately 10^{-5} mm. Hg. Outgassing was considered complete when there was no appreciable tendency for the pressure to build up again after pumping was discontinued. The sealed-off bulb was then placed into the cage connected to the lower end of the stirrer (cf. Fig. 1), 40 cc. of pure dry methanol (reagent grade) added to the calorimeter vessel, and the whole assembly placed in the water bath. After a warming-up period of about two hours, galvanometer readings were taken at regular one-minute intervals, the sample bulb broken when there was a constant rate of galvanometer shift with time, and readings continued until steady temperature conditions obtained once more. ΔH was then determined from a plot of galvanometer readings against time, corrected for heat losses by the usual graphical methods, and (subject to the proviso that S may provide a relative rather than an absolute datum) converted into surface areas by means of the equivalent 1 cal. = 10 sq. m.

All determinations of S were made in duplicate and finally recalculated to the dry, ash-free coal basis on the assumption that mineral matter in coal makes no significant contribution to ΔH. This assumption receives partial justification from the fact that heat of wetting of coal *ash* in methanol does not exceed about 0.6 cal. per gm.

RESULTS AND DISCUSSION

Table II summarizes the results thus obtained: columns 2 and 3 give the carbon and hydrogen contents of the coals (also calculated on the dry, ash-free basis); columns 4 and 5 show the heats of wetting on the dry and dry ash-free basis respectively; and column 6 gives the percentage deviations from the

TABLE II

HEATS OF WETTING

Description of coal	% carbon, dry, ash-free	% hydrogen, dry, ash-free	Heat of wetting, cal./gm. Dry coal	Heat of wetting, cal./gm. Dry, ash-free coal	% deviation from mean (on dry coal)
Roselyn, Sheerness, Alta.	73.55	4.90	20.29±0.54	22.27	±2.66
Taylerton, Sask.	73.86	4.85	28.18±0.18	30.69	±0.64
Wabamun main seam, Alta.	75.22	4.58	25.49±0.37	27.47	±1.45
Lethbridge Galt Mine (top), Alta.	76.95	4.97	7.76±0.07	9.03	±0.90
Lethbridge Galt Mine (bottom), Alta.	77.83	5.29	7.03±0.13	7.54	±1.85
Lethbridge Fed. Mine #1581, Alta.	78.18	5.12	7.07±0.07	7.57	±0.99
Springhill #2 (top), N.S.	85.27	5.39	1.75±0.08	1.84	±4.57
International #2, Alta.	86.53	4.95	2.30±0.03	2.92	±1.30
Springhill #2 (bottom), N.S.	86.72	5.45	1.18±0.02	1.23	±1.69
International #4, Alta.	87.26	4.87	2.02±0.05	2.43	±2.48
Luscar, #4, Alta.	88.52	5.08	2.13±0.06	2.35	±2.82
Elk River #3 (middle), B.C.	89.95	4.70	2.18±0.01	2.32	±0.46
Elk River #3 (top), B.C.	90.43	4.44	2.35±0.05	2.58	±2.13
Canmore #5, Alta.	90.82	4.45	3.07±0.06	3.32	±1.95
Canmore #3, Alta.	90.84	4.15	3.29±0.06	3.61	±1.82
Canmore #4, Alta.	91.04	4.18	3.03±0.04	3.19	±1.32

arithmetic means, computed on the *dry* coal. S can be obtained from the data listed in column 5 by multiplying by 10.

A graphic representation of the variation of S with coal rank is reproduced in Fig. 2, in which surface areas have been plotted as a function of the carbon contents. For comparative purposes (and in order to emphasize trends) the diagram includes data for two British Columbia coals, two Nova Scotia coals, and a Saskatchewan lignite examined in this laboratory, and for a few Southern Hemisphere coals previously studied by the writer and Schein (8).

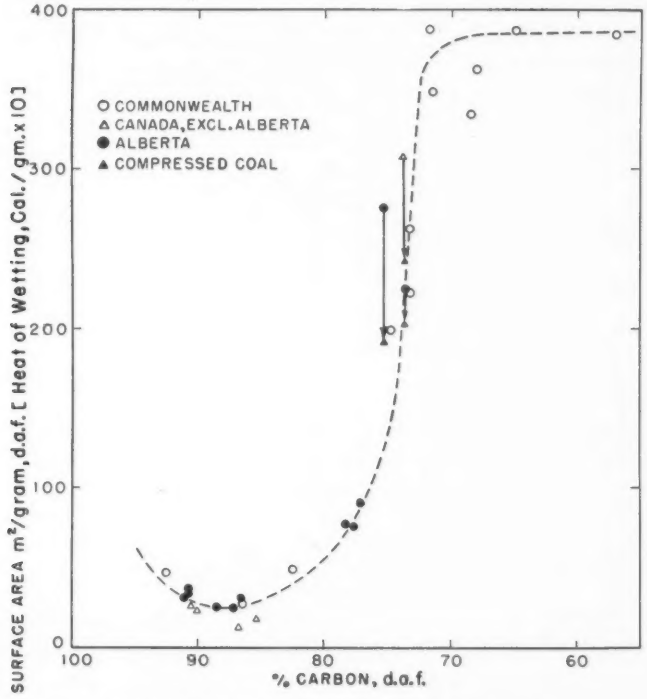

FIG. 2. Variation of heat of wetting with coal rank.

The most obvious feature of Fig. 2 is the statistically highly significant correlation between S and coal rank and the fact that this relation assumes the same form as that established for British coals (15) and for coals from several Commonwealth countries (8): there is the same rapid decrease in S among sub-bituminous and high-volatile bituminous coals ($C < 80\%$); S again tends towards minimum values among medium-volatile bituminous coals ($C = 85$–90%); and there is once more a clear trend for S to increase among low-volatile bituminous coals and anthracites ($C > 90\%$). Since this catenary-type variation of S with carbon contents has now been shown to apply to coals from

Canada as well as from Britain, Pakistan, Australia, and Africa, it may be assumed to reflect general behavior—provided that such generalization is not taken to exclude the possibility of occasionally very pronounced departures from the 'type-relation'. There is strong reason to think that such departures will, in fact, be found wherever tectonic forces acting on the *in situ* coal were either particularly light or particularly intense (see below).

Equally general validity can also be claimed for a direct, if rather less well-defined, proportionality between S and moisture contents. Such a proportionality, which is implicit in the view that the heat of wetting measures a surface area and hence is a function of the porosity of the coal, is clearly discernible in Table III in which column 3 lists the so-called 'capacity moisture contents'.[5] Broadly speaking, then, moisture contents and porosities can, as a first approximation, be regarded as functions that are interchangeable with S (or the heat of wetting) if they are numerically corrected by means of the appropriate proportionality constant.

TABLE III

COMPARISON OF HEATS OF WETTING AND CAPACITY MOISTURE CONTENTS

Coal	Heat of wetting in MeOH, cal./gm., dry, ash-free	Capacity moisture,* %
Springhill #2, N.S.	1.84	2.0
Elk River #3 (middle), B.C.	2.32	2.0
Luscar #4, Alta.	2.35	1.9
Elk River #3 (top), B.C.	2.58	1.8
International #4, Alta.	2.43	2.0
International #2, Alta.	2.92	1.9
Canmore #5, Alta.	3.32	1.9
Canmore #3, Alta.	3.61	2.3
Lethbridge #1, Alta.	7.54	10.3
Lethbridge Fed. Mine #1581, Alta.	7.57	11.3
Lethbridge #2, Alta.	9.03	11.1
Roselyn, Sheerness, Alta.	22.27	26.5
Wabamun main, Alta.	27.47	23.9
Taylerton, Sask.	30.69	34.7

**I am indebted to Mr. J. Fryer, Research Council of Alberta, for these determinations.*

Some further comment, however, is required in connection with Fig. 2. Quite generally, there are reasons for thinking that values of S as measured by adsorption or heats of wetting do not reflect the 'true' surface areas and that the extreme variability of S among the more immature coals ($C < 85\%$), which leads to a ratio of almost 20:1 as between lignites and medium-volatile bituminous coals, is due to progressively greater inaccessibility rather than to an actual collapse of inner surface during maturation. One finds, for example, that whilst ultrafine grinding increases the surface area of every coal, the increments (which always exceed those due to the fresh external surface

[5]*According to Report No. 35 of the Research Council of Alberta (1944), the capacity moisture content is defined as the least moisture in coal that will give a relative humidity of 100%. As such, it is a direct measure of the bed-moisture content of a coal.*

created by grinding) are far larger among medium-volatile bituminous coals than among coals of lower rank. Some typical values, recorded by Dresel and Griffith (12), are reproduced in Table IV in order to illustrate this. The decrease in S with increasing rank over the range $C \rightarrow 85\%$ must, in other words, be attributed to a progressive *in situ* compaction of the coal material under tectonic stresses that arise from its natural overburden and that may be locally intensified by shearing forces associated with orogenic movements.

TABLE IV

EFFECT OF ULTRAFINE GRINDING ON HEAT OF WETTING

Coal	Degree of comminution	Heat of wetting in MeOH, cal./gm., dry, ash-free	% increase in heat of wetting
Yorkshire sub-bituminous coal	(*a*) 100% 0.21 mm.	17.1	
	(*b*) "μ-coal"	27.4	60.2
Derbyshire high-volatile bituminous coal	(*a*) 100% 0.21 mm.	9.7	
	(*b*) "μ-coal"	23.3	150.5
South Wales medium-volatile bituminous coal	(*a*) 100% 0.21 mm.	2.7	
	(*b*) "μ-coal"	14.1	422.2

NOTE: *"μ-coal" is the product obtained by ball-milling the coal in an atmosphere of pure, dry nitrogen for 72 hr.*

If this interpretation is accepted, an interesting corollary suggests itself: since the measured value of S (at any particular size consist) can be considered a function of the degree of compaction of the coal, and hence an index of its physical maturity, one may conclude that physical maturity is itself an 'accidental' result of the geological history of the coal and that *the processes of physical maturation can be reversed by swelling or intensified by compression of the coal.*[6]

Owing to the fact that significant swelling can only be induced by solvents that may also cause chemical alteration of the coal and/or extract substantial portions of coal material, the reversibility of physical maturation rests, at present, on qualitative and largely circumstantial evidence: the fact that treatment of a bituminous coal with such solvents as pyridine, quinoline, or chloroform results in pronounced swelling and softening is sufficiently well known to obviate the need for comment here.

But it is possible to prove intensification of physical maturity by direct experiment. Table V shows what happens when comparatively immature coals (i.e. coals with low carbon contents and high initial surface areas) are compressed under conditions not dissimilar to those prevailing in a deep seam. The data were obtained by grinding three coals to pass a 65 mesh Tyler screen

[6]*The possibility of such reversibility suggests that physical maturation phenomena ought to be sharply separated from chemical maturation processes and that some more explicit definition of 'rank' may become essential.*

TABLE V

EFFECTS OF COMPRESSION ON HEAT OF WETTING

Coal	Heat of wetting, cal./gm., dry, ash-free	
	Before compression	After compression
Roselyn, Sheerness, Alta.	22.27	20.16
Taylerton, Sask.	30.69	24.17
Wabamun, Alta.	27.47	19.11

and, prior to outgassing and submission to a heat of wetting determination, compressing them at 140°C. for 24 hr. under 10 tons per sq. in. In every instance, the coal responded to the applied pressure with a very pronounced reduction in the measured surface area and, in every case, this effect appeared to be induced very quickly and more or less irreversibly. There was no observable tendency of the coals to revert to the original, more open structure on prolonged standing in an inert atmosphere, and compression for periods in excess of 24 hr. did not lead to measurable further decreases of S. We have here evidence that the coal substance can assume a new equilibrium configuration within a very short period of time and that 'readjustment' under external stress leads to a material whose physical properties correspond to those of a more mature coal.

In a general sense, the present results confirm observations previously made by Dulhunty (13) during a study of the effect of compression upon the capacity moisture content of Australian coals. But they draw attention to two other points. First, since the surface areas of the compressed coals are still high and since the conditions employed in the compression tests are certainly the most intense that can occur in tectonically undisturbed areas, they suggest that extreme compaction (such as would lead to the compression found among medium-volatile bituminous coals) may require shearing forces possibly coupled with locally rather higher temperatures. Compression in a direction normal to a seam would appear incapable of reducing accessible surface areas much below about 150 sq. m. per gm. Secondly, it is apparent that if an immature coal is, at some stage during its development, exposed to abnormally intense *in situ* compression, it will yield a material that is physically much more mature than other coals of equivalent rank and that may, for this reason, depart markedly from the type-relation provided by Fig. 2. It is undoubtedly to phenomena of this nature that we must look for an explanation of 'abnormal' coals such as occur in certain areas of Pakistan (8) and Borneo (4).

In connection with Table V it is, incidentally, noteworthy that the quantitative effects of compression stand in a very definite relationship to the surface areas measured with the raw coals. Thus, of the three coals tested, two were of the same rank (containing 73.5 and 73.8% carbon) but differed with respect to accessible surface: one gave $S = 223$ and the other $S = 307$ sq. m. per gm. Assuming the former to have suffered a greater degree of *in situ* compression, one would expect it to show a smaller response to compaction

in the laboratory, and this expectation is fully borne out: the respective percentage reductions in S amounted to 9.5 and 21.2%. The third coal, with C = 75.3%, gave S = 275 sq. m. per gm.; it may, because of this,[7] be considered physically less mature than 'normal' and significantly responded to compression with a 30.5% reduction in S.

One feature of Fig. 2, however, remains still obscure: this is the trend towards higher surface areas among low-volatile bituminous coals and anthracites. Qualitatively, this trend has been associated with loss of volatile matter by mild partial pyrolysis,[8] and in this connection, attention has been drawn to the fact that concurrently with an increase in S, there are also progressively more rapid increases in instrinsic strength, electrical conductivity, and elastic moduli. Viewed in their entirety, these changes are not inconsistent with the suggestion that maturation beyond C = 90% involves transformation of a colloidal assemblage into a progressively more rigidly cross-linked 'lattice structure'; and it is tempting to associate the increased accessibility of these solids (i.e. a greater measured surface area) with the inability of such solids to draw closer together under the influence of surface forces or external stresses.

Direct proof for this thesis is difficult, if not impossible, to adduce, but some support for it can perhaps be found in the relationship between carbon and hydrogen contents of coal (cf. Fig. 3). Whilst the hydrogen content remains

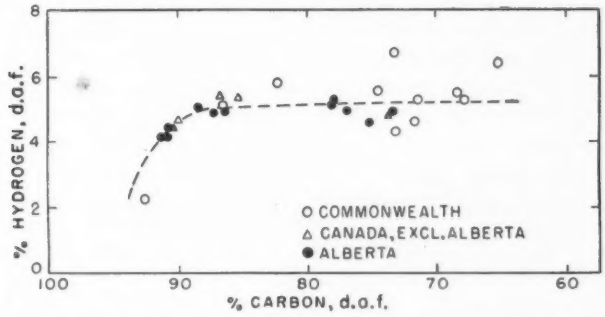

FIG. 3. Variation of hydrogen contents with carbon contents of coals.

approximately constant at a mean of *ca.* 5.4% below C = 90%, it decreases very rapidly with increases in carbon content beyond that point; and if it is borne in mind that the principal decomposition products obtained from high rank coals are elemental hydrogen and methane (both undoubtedly formed during disproportionation reactions), postulates of a lattice structure formation are quite plausible. But it is worth noting that the physical presence of hydrogen (perhaps in the form of aliphatic side-chains) appears in itself

[7] *Reference to Fig. 2 will serve to show that a 'normal' coal with C = 75% should have a surface area of approx. 160 sq. m./gm.*

[8] *Some investigators give formation temperatures for anthracites ranging as high as 700°C., but a temperature of ca. 400–450°C. would be more in keeping with the known decomposition temperatures of anthracites.*

capable of offering steric opposition to penetration. This point is illustrated by three coals of equal rank (*ca.* 86.5%) shown in Fig. 2 and, for convenience, listed in Table VI. The recorded values of S are here inversely proportional to the hydrogen contents.

Attempts to explore this point further (and to test the corollary that higher surface areas among anthracites may be partly due to the simple removal of

TABLE VI

Coal	% carbon, dry, ash-free	% hydrogen, dry, ash-free	Heat of wetting, cal./gm., dry, ash-free
International #2, Alta.	86.53	4.95	2.92
Wankie, S. Rhodesia	86.50	5.0	2.70
Springhill #2, N.S.	86.72	5.45	1.23

hydrogen) have so far proved unsuccessful. The abstraction of a definite small amount of hydrogen by mild oxidation of a coal at 30°C. actually caused a very significant decrease in S and current work in these laboratories is therefore endeavoring to reverse the procedure and to investigate the effect on S of mild hydrogenation of coal with nascent hydrogen. But measurements with the oxidized coal served, in the meantime, to establish another important point. Whilst mild oxidation will generally lead to a progressive deterioration and eventual loss of coking properties and to a steady increase in the capacity moisture content and related properties of a coal, the present results suggest that in certain instances, initial oxidation may induce reverse changes (cf. Fig. 4.) This finding is all the more significant as a direct relationship has been empirically found to exist between S (or moisture contents) and coking properties (5) and since Kreulen (17) has observed that slight oxidation can occasionally ***enhance*** coking properties. Since Fig. 4 forms a virtual mirror

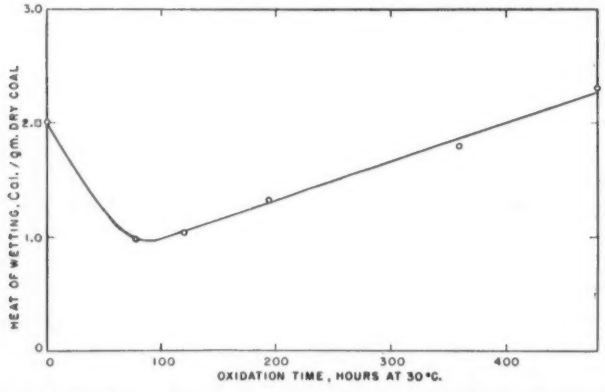

FIG. 4. Variation of heat of wetting with oxidation time (oxidation by means of moist oxygen at 30°C.).

image to the curves shown in Kreulen's paper, it would thus appear that a proportionality between S and coking properties may be as valid for mildly oxidized as for fresh coals. The theoretical implications of this relationship have already been discussed (5, 6).

ACKNOWLEDGMENTS

I am indebted to Mr. J. Fryer for the analyses of Canadian coals cited in this communication, and to Dr. N. H. Grace, Director of the Research Council of Alberta, for permission to publish.

REFERENCES

1. BANGHAM, D. H. Introductory Lecture, Brit. Coal Utilisation Research Assoc. Conf., London. 1944.
2. BANGHAM, D. H. Brit. Coal Utilisation Research Assoc. Conf., London. p. 32. 1944.
3. BANGHAM, D. H., FRANKLIN, R. E., HIRST, W., and MAGGS, F. A. P. Coal Research, Dec. 1948.
4. BERKOWITZ, N. Unpublished work.
5. BERKOWITZ, N. Fuel, 28: 97. 1949.
6. BERKOWITZ, N. Fuel, 29: 138. 1950.
7. BERKOWITZ, N. and SCHEIN, H. G. Nature, 169: 373. 1952.
8. BERKOWITZ, N. and SCHEIN, H. G. Fuel, 31: 19. 1952.
9. BERKOWITZ, N. and SCHEIN, H. G. Fuel, 31: 130. 1952.
10. BLAYDEN, H. E., GIBSON, J., and RILEY, H. L. Brit. Coal Utilisation Research Assoc. Conf., London. 1944.
11. BOYER, A. and FOUCAULT, G. Compt. rend. 237: 893. 1953.
12. DRESEL, E. and GRIFFITH, M. Private communication.
13. DULHUNTY, J. A. J. Proc. Roy. Soc. N. S. Wales, 82: 265. 1949.
14. GREGG, S. J. The surface chemistry of solids. Chapman & Hall, Ltd., London. 1951. p. 228 *et seq.*
15. GRIFFITH, M. and HIRST, W. Brit. Coal Utilisation Research Assoc. Conf., London. 1944.
16. KING, J. G. and WILKINS, E. T. Brit. Coal Utilisation Research Assoc. Conf., London. pp. 46–56. 1944.
17. KREULEN, D. J. W. Fuel, 29: 112. 1950.
18. KREVELEN, D. W. VAN. J. Inst. Fuel, 27: 626. 1954.
19. LECKY, J. A., HALL, W. K., and ANDERSON, R. B. Nature, 168: 124. 1951.
20. MALHERBE, P. le R. Fuel, 30: 97. 1951.
21. ZWIETERING, P., OELE, A. P., and KREVELEN, D. W. VAN. Fuel, 30: 203. 1951.

AN APPARATUS FOR THE DETERMINATION OF DIPOLE MOMENTS[1]

By C. C. Meredith and George F Wright

ABSTRACT

The machine described here will determine precisely the dielectric constant of either 15 ml. of liquid or 0.5 gm. of solid.

INTRODUCTION

The evaluation of the dipole moment of an organic chemical by the determination of its dielectric constant in a solvent requires a quantity of the substance which is frequently not conveniently available. We have therefore devised an apparatus with which a complete series of determinations at different concentrations can be made with a total of 0.5 gm. of material. This limitation requires that measurement be made in a capacitive cell of low liquid (14 ml.) and high electrical (220 $\mu\mu$f.) capacity. The cell is connected to a measuring device of high resolution and stability. The precision of which the apparatus is capable is necessary also to determine the dielectric constant of small pellets of the organic compound before it is dissolved for the measurement of orientation polarization. The dielectric constant of the solid phase provides an accurate evaluation of the "atomic polarization" of the substance. The value so obtained is more realistic than that taken as an arbitrary fraction of the "electronic polarization".

THE HETERODYNE OSCILLATOR

This instrument (Fig. 1) utilizes two identical oscillators designed to have a high order of frequency stability. After the initial warm-up period, stabilities of the order of one part in 10^6 have been realized. In construction of the apparatus, a previous design (1) has been elaborated in order to minimize residual inductance which has been shown to lead to error (3). The circuitry used (Fig. 2), derived from that of Franklin (2), consists essentially of a two-stage amplifier having aperiodic coupling elements and providing zero phase-shift between input and output terminals. By coupling input and output terminals to a suitable resonant circuit, oscillation will be maintained in the tuned circuit provided that the amplifier has sufficient gain to overbalance the voltage drop across the equivalent resistance representing the losses in the circuit. This tuned circuit may consist either of an inductance and a capacitance in parallel, or of a piezoelectric crystal which can be shown to be the electrical equivalent of such a tuned circuit having very low losses.

The Franklin circuit (2) has been used, since with a suitably designed amplifier it has been found to possess excellent frequency stability. Also this

[1] *Manuscript received December 28, 1954.*
Contribution from the Laboratory of C. C. Meredith and the Department of Chemistry, University of Toronto, Toronto, Ontario.

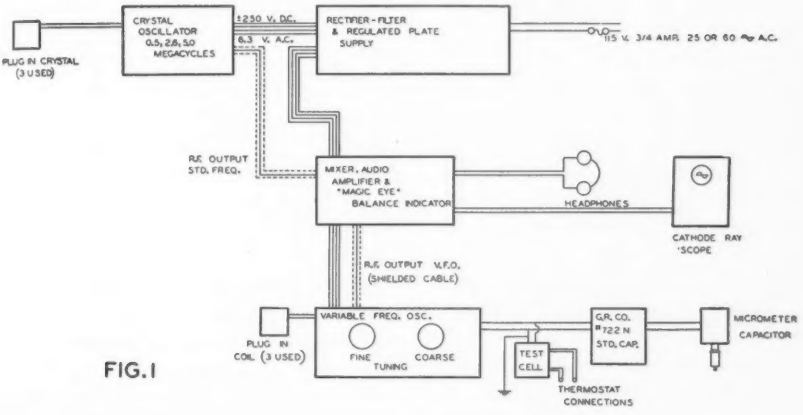

FIG. 1

circuit will oscillate reliably over a wide range of frequencies with large values of tuning capacitance (*ca.* 1000 $\mu\mu$f.) and with shunt conductances as high as 10^{-4} mho. The cathode-coupled amplifier (4, 6) utilized, which has been found to give adequate amplification over a wide range of frequencies, provides the necessary zero phase-shift between input and output; it has the added advantage of having a very high input impedance, due to its cathode-follower input stage. Using triodes designed for grounded-grid operation (6AB4's), stable operation can be obtained at frequencies as high as 18 to 20 Mc./sec. The high input impedance of this amplifier makes possible the use of very small coupling capacitors between the electronic circuit and the frequency determining element, thus minimizing frequency variations due to variations in tube parameters.

The standard-frequency oscillator (SFO) is provided with jacks to accommodate any one of three AT-cut crystals, offering a selection of three operating frequencies 0.5, 2.6, and 5.0 Mc. The other, the variable-frequency oscillator (VFO), is provided with jacks to accept the appropriate inductor of 120, 4.5, or 4.0 microhenrys. It was found impracticable to use inductances of less than 4 μh. and hence this value is used for the 5 Mc. range, compensation being made by the use of a fixed capacitor in series with the tuning capacitors. This series capacitor, when not required, is short-circuited by using a three-pin arrangement on the coil bases. For the two lower-frequency coils, two of these pins are connected together in such a way as to short-circuit the series condenser, while for the 5 Mc. range this connector is omitted in the 4 μh. coil assembly. This series condenser in the 5 Mc. tuned circuit has the effect of reducing the value of tuning capacity while at the same time leaving the full value of the tuning capacitors available for purposes of measurement.

The inductor jacks are connected to the two balancing capacitors internally, coarse adjustment being provided by C_4 and fine adjustment by C_5. External terminals are provided for connection to the General Radio Type 722-N standard capacitor, C_2, to the micrometer standard, C_3, and the test cell, C_1.

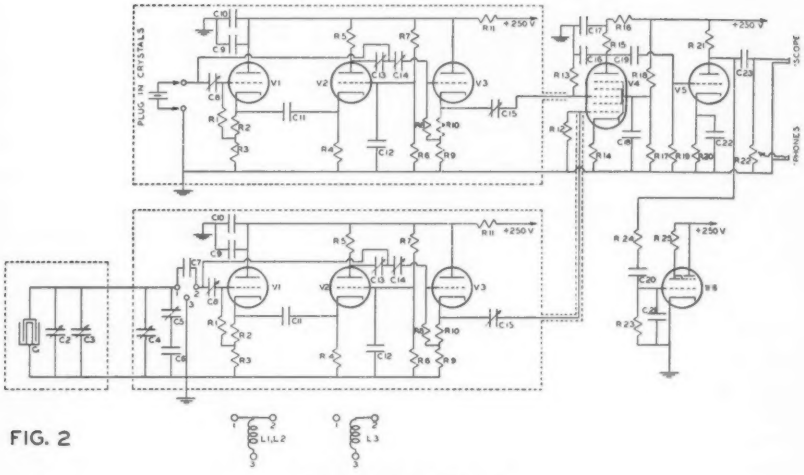

FIG. 2

PARTS LIST FOR FIG. 2

C_1	Test cell
C_2	#722-N G.R. Co. 1100 $\mu\mu$f. standard
C_3	Micrometer capacitor, $\Delta C = 2.5$ $\mu\mu$f.
C_4	#1428 G.R.Co. 1100 $\mu\mu$f. variable
C_5	#1427 G.R.Co. reduced to 6 $\mu\mu$f.
C_6	6 $\mu\mu$f. fixed
C_7	300 $\mu\mu$f. silver mica fixed
C_8, C_{13} / C_{14}, C_{15}	3 to 10 $\mu\mu$f. variable air or silver-ceramic adjustable caps
C_9, C_{11}, C_{12}	0.01 μf. mica or ceramic capacitors
C_{10}, C_{17}	40 μf. 450 v. electrolytic capacitors
C_{16}	500 $\mu\mu$f. mica capacitors
C_{18}, C_{20}	0.1 μf. 600 v. paper capacitors
C_{19}, C_{23}	0.25 μf. 600 v. paper capacitors
C_{21}	300 $\mu\mu$f. mica capacitors
C_{22}	150 μf. 150 v. electrolytic capacitors
L_1	120 μh. powder metal core R-F. inductance
L_2	*ca.* 4.5 μh. powder metal core R-F. inductance
L_3	*ca.* 4.0 μh. powder metal core R-F. inductance
R_1, R_8	2.5 meg $\frac{1}{2}$ w. carbon resistor
R_2, R_{10}	270 ohm $\frac{1}{2}$ w. carbon resistor
R_3, R_9	2700 ohm 1 w. carbon resistor
R_4	1500 ohm 1 w. carbon resistor
R_5	27 K 1 w. carbon resistor
R_6	10 K $\frac{1}{2}$ w. carbon resistor
R_7, R_{25}	1 meg 1 w. carbon resistor
R_{11}	25 K 10 w. wire wound resistor
R_{12}, R_{13}, R_{19}, R_{24}	470 K $\frac{1}{2}$ w. carbon resistor
R_{14}	150 ohm 1 w. carbon resistor
R_{15}, R_{21}	47 K 1 w. carbon resistor
R_{16}	22 K 1 w. carbon resistor
R_{17}	15 K 1 w. carbon resistor
R_{18}	82 K carbon resistor
R_{20}	2.2 K carbon resistor
R_{22}	100 K potentiometer, carbon
R_{23}	4.7 meg carbon resistor
V_1, V_2, V_3	6AB4 grounded-grid type triode
V_4	6BE6 penta-grid mixer
V_5	6C4 triode
V_6	6E5 "Magic Eye" indicator

The micrometer standard consists of the barrel and stem of a 25 mm. micrometer depth gauge secured by a brass sleeve to a polystyrene cylinder inside of which is pressed a brass tube 1.375 in. in length and with an inside diameter of 0.218 in., the 0.125 in. diameter micrometer stem entering this cylinder axially. The brass tube thus forms the outer, insulated electrode of a coaxial cylindrical capacitor, the micrometer stem acting as the axial, grounded electrode. The change in capacity as the micrometer head (and stem) is moved from its zero to maximum reading is 2.5 $\mu\mu$f., thus providing readings to 0.001 $\mu\mu$f. of capacity increment. The mounting of this micrometer standard may be observed in Fig. 8.

Each frequency-determining element is coupled through very small capacitors (*ca.* 3 $\mu\mu$f.) of the adjustable type to the input and output terminals of the cathode-coupled amplifier, and also through a similar adjustable capacitor to the grid of a cathode-follower output amplifier, V_3. The two first-mentioned small capacitors are adjusted to the minimum value necessary to obtain stable oscillation under the conditions of operation, while the third is adjusted to provide a voltage of *ca.* 0.5 v. r.m.s. at the control grid of the mixer tube, to which the cathode of the output stage is connected through an additional small capacitor of *ca.* 20 $\mu\mu$f. The mixer tube employed, V_4, is a standard, broadcast-receiver type of pentagrid mixer (6BE6), one of its control grids being connected as mentioned above to the SFO and the other similarly to the VFO. In practice, the voltage so derived from the SFO is applied to the mixer grid normally used for the local oscillator in the broadcast-receiver, and the magnitude of this signal is adjusted to a somewhat higher value than that derived from the cathode of the output amplifier associated with the VFO, the latter signal being applied to the other control grid of the mixer tube. This tends to maintain the beat-frequency output of the mixer tube relatively constant, even though the output from the VFO may vary somewhat with changes in the conductivity of the specimen being investigated.

The beat-frequency appearing in the output of the mixer tube is amplified with a single triode (V5) functioning as an audio-frequency amplifier. The time-constant of the audio coupling circuits is made sufficiently long to obtain adequate indication at signal frequencies of fractional cycles per second. This can readily be accomplished by the use of large coupling condensers and high values of grid resistors, since frequencies above one or two thousand cycles are of no interest and may be sacrificed to obtain sensitivity at very low frequencies, thus ensuring true indication of zero-beat conditions.

The output from the audio stage is available at either of two signal jacks, one of which is provided with a volume control and may be used with headphones, the other being used for connection to a cathode-ray oscilloscope. In addition, the audio signal is applied to the control grid of a 6E5 electron-ray indicator, which has been found to provide a very sensitive indication of zero-beat condition.

The electronically-regulated plate supply, with an output voltage of 250 at any current up to *ca.* 0.1 amp., is adapted from one previously published

(5). Additionally, it is desirable to utilize a stabilized line voltage source when the utmost in stability is desired, since changes in line voltage directly affect the cathode temperature and can thus produce frequency changes in the order of parts in 10^7 over a period of several seconds. A worth-while improvement would be the incorporation of an electronically-regulated heater supply.

THE TEST CAPACITOR FOR LIQUIDS

This cell has been constructed with the aim of attaining high electrostatic capacity with lowest possible liquid capacity and with electrical stability of the same order as that of the heterodyne oscillator. In order to obtain the shortest possible electrical connections, the thermostatting arrangement has been brought to the cell, which is shown in cross-section in Fig. 3. The cell consists of three coaxial cylinders of 18-8 stainless steel, mounted very rigidly to enable the spacing to be as close as possible. The outer and inner cylinders are electrically common and are at ground potential. The intermediate one is carefully insulated from the other two, and forms the high-potential electrode.

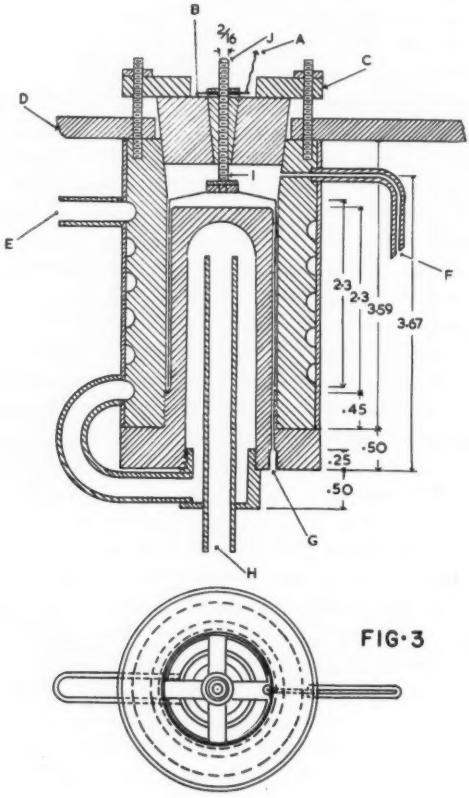

FIG·3

The two grounded cylinders are massive, the outer one (2.375 in. O.D.) having a helical water channel cut in its periphery, after which a brass sleeve has been shrunk over it. A brazed-in tubulature ($\frac{3}{8}$ in. O.D.) is provided at "E" to serve as the outlet for temperature-regulated water. The upper end of the bore is tapered 1: 10 to receive a tapered joint, while the lower end of the bore is threaded to receive the threaded shoulder formed on the innermost cylinder. The remaining portion, which forms the electrically-active surface, is brought to a high polish with rouge-laden chamois skin, after first being brought to the best possible finish by mechanical means. The inside diameter of the active portion of this outer cylinder is 1.399 in. or 3.553 cm.

The innermost cylinder is flanged at the bottom end and is provided with an externally threaded shoulder accurately and tightly fitting the internal thread in the bore of the outer member. Above this shoulder, the outside diameter is reduced to 1.281 in. (3.253 cm.) by polishing with rouge-laden chamois skin after first tooling to the best possible finish. The importance of the quality of finish on these parts, as on both inner and outer surfaces of the intermediate cylinder, cannot be overemphasized. The core of the inner cylinder has been bored roughly to form an internal "water-jacket", which is connected by $\frac{3}{8}$ in. O.D. tubing to the water passage encompassing the outer cylinder and provided with a central inlet $\frac{3}{8}$ in. O.D. as shown in Fig. 3. The fit of the two mating threads of the two cylinders is such that the outer member must be heated somewhat to enable them to be screwed tightly together.

After assembly, the solution inlet hole at "G", Fig. 3, is drilled into the bottom end of the recess between inner and outer cylinders, the lower end being enlarged and tapped with a fine thread as shown. A #78 drill is used for the upper portion of the hole which connects with the annulus in the cell; the shoulder occurring at the upper end of the threaded hole is finished with care to provide a seat for a small Teflon gasket. Finally, the outer member of the assembly is drilled and tapped at the top to accommodate the studs used to clamp the stopper in place and for the stainless-steel overflow exit (not less than $\frac{1}{16}$ in. I.D.) shown at "F" in Fig. 3. It has been found desirable to lag the exterior surface with friction tape to minimize heat exchange and condensation of water vapor.

The annular space between the outer and inner cylinders is 3 mm. wide, and into this is fitted the third cylinder which has an O.D. of 1.359 in. (3.453 cm.) and an I.D. of 1.320 in. (3.353 cm.). Here again great care has been taken to provide the best possible finish on both inside and outside surfaces. The 0.5 mm. wall is pierced by three 0.0625 in. holes spaced 120° apart and at a distance of 0.5 in. from the lower end (not shown in figure). These three holes accommodate small Teflon plugs which act as spacers to maintain the 0.5 mm. spacing between members, and also serve to damp out vibration of the intermediate cylinder. As is shown in the top view (Fig. 3) this hollow cylinder, which forms the insulated electrode, is supported at its upper end by a stainless-steel spider to which it is welded. A nut is welded to the hub of this spider to accommodate the hollow, threaded terminal "J", which is drilled laterally

at "I" just above the nut, to provide pressure release for air trapped in the upper part of the liquid chamber. Hole "I" is located just above the liquid level as determined by the overflow vent "F". The axial hole in "J" may be closed after filling by means of a screw cap (not shown in the figure).

The hollow terminal "J" passes through a tapered Teflon bushing which is pressed firmly into the Pyrex stopper "B". Nuts provided on "J" above and below the Teflon bushing serve both to position the insulated electrode at the correct height and to draw the bushing firmly downward into the tapered hole in the Pyrex stopper. The Pyrex stopper is made with an external taper of 1: 10, as shown in the figure, which accurately fits the taper in the bore of the outer stainless steel cylinder. A bakelite ring is provided to secure the high potential electrode in place by means of pressure on the rim of the Pyrex stopper and is locked in place by nuts run down on three threaded studs shown projecting upwards through the bottom of a shield-box (D, Figs. 3, 4, and 8), the lower end of these studs being threaded into the top end of the outer cylinder as before mentioned, two of these studs being shown in section in Fig. 3. Three machine screws (not shown) also pass through suitably positioned holes in the bottom of the cast aluminum shield box and are screwed into three threaded holes in the top of the outer cylinder, thus drawing the complete cell upward into intimate contact with the bottom of the box (D, Fig. 3).

The shield-box "D" with the cell so suspended from it is supported at the end carrying the cell by attachment securely against the front panel of the heterodyne oscillator, the other end resting firmly upon the top panel of the 733-N standard condenser. The height of the whole assembly of apparatus is adjusted to allow for ample space beneath the test cell to accommodate the filling device, water inlet, etc. As shown in Fig. 8, which illustrates the plan view of the shield-box with cover removed, the high potential terminals and connections are all very thoroughly shielded by this device when the cover is replaced. This view also shows the micrometer standard capacitor with its polystyrene insulated electrode projecting to the left inside the shield-box (just behind the terminals of the 722-N standard) and the micrometer head projecting to the right, outside the box.

Again considering the test cell, from the foregoing it is seen that the spacing between electrodes is quite small (0.5 mm.), which makes possible the high electrostatic capacity of *ca.* 220 $\mu\mu$f., while only requiring a relatively small volume of solution (*ca.* 14 ml.) to fill it to constant level as determined by the overflow vent (F, Fig. 3). The residual capacity as determined with pure benzene is *ca.* 3 $\mu\mu$f., and is due largely to the capacity-to-ground of terminal "J" through the composite insulator formed by the Teflon bushing and the Pyrex stopper "B".

Variation of dielectric constant with temperature is controlled by forced circulation of water from a constant-temperature bath equipped with heating and cooling facilities controlled by the thermoregulator which can be seen in Fig. 4, installed at the water outlet "E", Fig. 3. The close proximity of the

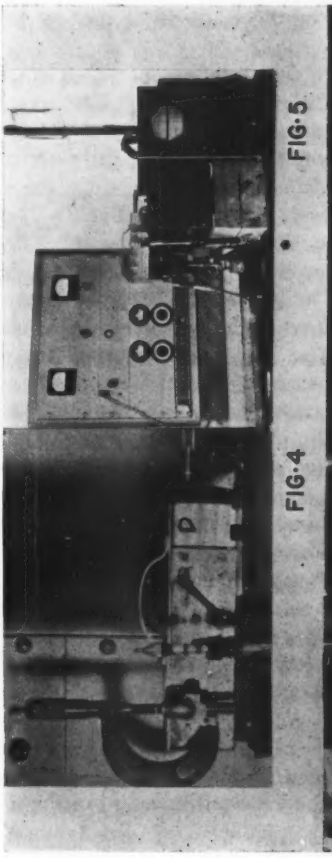

FIG. 4

FIG. 5

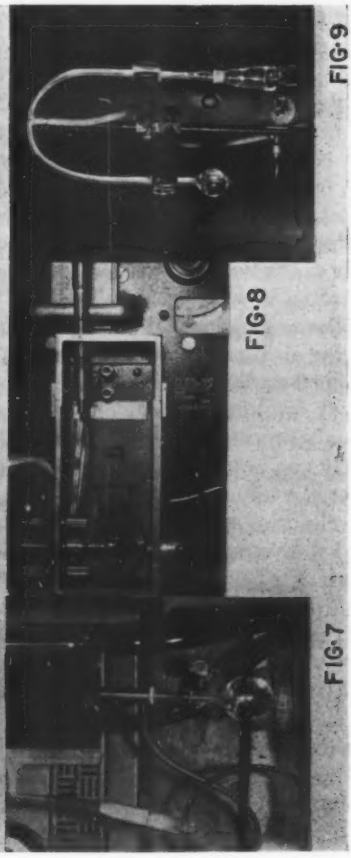

FIG. 8

FIG. 9

FIG. 7

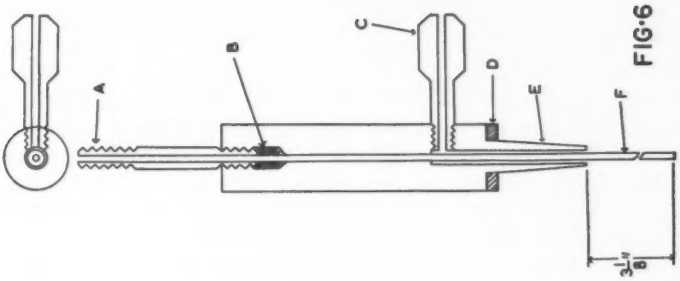

FIG. 6

thermoregulator to the cell ensures temperature regulation to within 0.05° as measured by a multijunction thermocouple introduced into the annular space within the cell. Rapid circulation of the water is needed to maintain this regulation.

The cell is filled by means of the device shown in Fig. 6, which is attached at "G", Fig. 3, by means of the threaded nipple "A", Fig. 6. The body of the adapter is drilled axially to a slip fit on the outside of the 0.035 in. O.D. stainless tubing (F, Fig. 6) which is allowed to project slightly above "A", (Fig. 6), and is swaged over to provide a tight seal against the Teflon gasket installed at the upper end of the threaded hole "G", (Fig. 3). The lower end of nipple "A" seals against the Teflon Packing "B", (Fig. 6). The lower extremity of the body of this adapter is provided with a taper to fit a $\frac{5}{12}$ outer member of an interchangeable TS joint, and is additionally provided with a plastic silicone gasket (D, Fig. 6) to ensure a tight seal when the cell is filled by applying air pressure at "C", Fig. 6. The air pressure so applied forces the liquid from the volumetric flask of 15 ml. capacity (which can be seen in Figs. 5 and 7) up into the test cell. The filling action is continued until a few drops of liquid fall from outlet tube "F", Fig. 3, into the side-arm test tube (equipped with a calcium chloride drying tube), also seen in Figs. 5 and 7. A clamp applied to the air pressure hose at "C", Fig. 6, satisfactorily maintains the liquid level during the capacitance determination. Release of the clamp allows the liquid to return to the volumetric flask.

After use, the cell may be cleaned by drawing chemically and optically pure solvent through it by the application of vacuum, followed by drying by passage of clean, dry air through the apparatus. It is extremely important in so doing that every precaution is taken to exclude particulate matter from the air stream. After cleaning and drying, the capacitance of the empty cell is measured.

If C_a is the value of capacitance determined for the empty cell (air dielectric), C_l is the capacitance for the liquid-filled cell (liquid dielectric), and C_r is the residual terminal capacitance of the cell, the dielectric constant of the solution is given by—

$$\epsilon = (C_l - C_r)/(C_a - C_r),$$

where ϵ is the dielectric constant of the liquid.

The 14 ml. volumetric flask from which the cell is filled also serves as a pycnometer. This flask is equipped with a capillary neck upon which are etched 11 calibrated marks. Densities may be determined to a precision of one part in 10^4 by filling the flask "N" with a solution prepared in the weighing flask "O", Fig. 9 through a stainless steel tubing (0.035 in. O.D.). This stainless steel tubing is housed in a glass capillary "U" tube equipped at one end with a 12/10 TS outer joint member. An air inlet tube joins the "U" tube at its center, through which molten polyethylene is introduced to seal off the air space between the hypodermic needle and the wall of the "U" tube in the leg leading to the pycnometer. When filled as described, the pycnometer is weighed (to 0.1 mgm.) and placed in a thermostat to determine the interpolated volume with a telescope.

The low residual capacity of the cell is due to the elimination of long connecting leads or cables made possible by mounting the cell from the under side of the cast aluminum shield box, as mentioned above and shown in Figs. 4, 5, and 8, and to the long insulation path through the stopper of the cell itself. From Fig. 8, it is seen that the connection between the high-potential electrode of the cell and the VFO terminal is very short and rigid.

The shield-box (8 in. × 3.25 in. × 2.12 in. with $\frac{1}{4}$ in. thick walls) encloses the insulated terminal of the VFO and is adequately grounded to the VFO panel by two ground terminals located on either side of the insulated terminal. It is seen that the right-hand end of the box rests upon the top panel of the General Radio #722-N standard capacitor and completely encloses its terminals, and also encloses the high potential parts of the micrometer capacitor. A ground connection in the form of a copper strip (0.18 in. wide × 0.015 in. thick) runs from both ground terminals on the VFO panel to the ground terminal on the 722-N standard and a similar strip joins the insulated, high-potential terminals of VFO, 722-N, and micrometer capacitor. The ground connection for the micrometer capacitor is made by the aluminum box itself. The use of these massive connections reduces the residual inductance in the capacitor circuits to a minimum, while the short (*ca.* 1 in.) rigid connection to the insulated electrode of the test cell together with the long dielectric path through the composite stopper maintains the residual capacity of the cell at a very low and constant value. Complete shielding of the connections is provided by the $\frac{1}{4}$ in. thick box lid (not shown) which is secured firmly in place while the apparatus is in use.

A standard 2 in. micrometer caliper has been altered to provide means for the precise determination of the dielectric constant of small pellets of organic substances. This device may be seen in Fig. 4. The alteration consists of securely attaching a standard coaxial elbow fitting at the position ordinarily occupied by the anvil of the micrometer caliper. The vertical arm of the elbow has been cut away externally to expose about $\frac{3}{32}$ in. of the polystyrene insulation and internally to remove the split conductor sleeve and replace it by a rod of Wood's metal. Into the open end of the horizontal arm of the coaxial elbow is screwed a brass replica of the coaxial fitting with which the assembly is fitted to the VFO. This fitting is necessary in order to prevent loss of polystyrene during heating and it also serves as a source of heat when it is warmed to 150°C. The anvil is now aligned with the micrometer stem by means of a tubular jig which fits closely enough to hold anvil and stem together and concentric. The brass replica and the coaxial fitting are now heated until the Wood's metal is molten and the polystyrene is plastic. Then the prolongation of the anvil is lowered into the molten Wood's metal by turning down the micrometer screw. This operation embeds the anvil in the soft plastic and expands the latter so that it fits tightly to the inside of the coaxial elbow. When the assembly is cool the anvil is parallel to and concentric with the 0.250 in. diameter micrometer stem. The horizontal arm of the elbow is now provided with a suitable fitting to provide connection to the coaxial socket (L, Fig. 8) installed in the aluminum shield-box, the external metal parts of these

fittings providing both mechanical support for and electrical grounding of the micrometer assembly. The central, insulated conductor of the coaxial socket is connected to the measuring circuit by a short lead terminating in a "banana plug", which plugs into the hollow end of the VFO terminal. The residual capacitance of the device is measured with the micrometer stem retracted to its limit.

An amalgam which is semisolid at room temperature is prepared by solution of 0.5 gm. of zinc dust in 8 gm. of boiling mercury. A small amount of this pasty metal is placed upon the insulated anvil and surmounted by one of a series of pellets 0.25 in. in diameter which are of previously-determined but varying thickness. On the top of the pellet is placed a small amount of the amalgam. The micrometer stem is now screwed down into light contact with the upper surface of the pellet. A closely-fitting sleeve (slightly chamfered internally at its lower end) on the micrometer stem is now brought down with care until it encircles pellet, stem, and anvil, thus accurately aligning the pellet with respect to the condenser plates. Firm pressure is now applied with judgment to avoid crushing the pellet, by means of the micrometer screw. The sleeve is then raised to its upper position on the micrometer stem (Fig. 4) and the excess of amalgam is thoroughly brushed away. The capacitance now is measured by adjustment of the micrometer standard to zero-beat, the reference point being the zero-beat obtained by determination of the residual capacitance as described above. The reading so obtained is $C_x = C_p + C_r$ where C_p is the capacity of the test fixture containing a pellet and C_r is the residual capacity of the test fixture. The pellet is now removed and the amalgam cleaned off. The micrometer stem is returned to the reading representing the thickness of the pellet and zero-beat is obtained by readjustment of the micrometer standard capacitator. This reading is $C_y = C_a + C_r$ where C_a is the air capacitance at this plate separation and C_r as before is the residual capacity. Then the dielectric constant of the pellet is

$$\epsilon = (C_x - C_r)/(C_y - C_r).$$

The density of the pellet is obtained by centrifugation in comparable media.

After a series of pellets of varying thicknesses have been measured in this way the values of ϵ_p are plotted against thickness in order to obtain an extrapolated value at zero thickness (ϵ_∞). The combined electronic and atomic molar polarization of the chemical substance is then

$$P_{e+a} = (\epsilon_\infty - 1)/(\epsilon_\infty + 2).M/d$$

where M is the molecular weight at density d. A typical extrapolation is shown in Fig. 10 for diphenyl mercury, ($d = 2.3$, $\epsilon_\infty = 2.91$). The polarization, P_{e+a}, of 58.9 is in reasonable agreement with the estimated value.

It is important that the pellets used in these determinations of solid dielectric constant be free of included air. To do so requires the application of considerable pressure under a hydraulic press, and to avoid swelling the die, it has been found necessary to use a high-tensile steel (Atlas SPS 245) for this purpose.

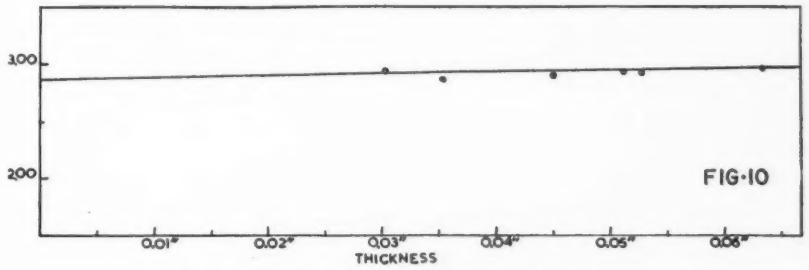

FIG. 10. Dielectric constant of diphenyl mercury.

After finish-machining, the 2 in. O.D. die is heat-treated to obtain maximum strength. Additionally, it is beneficial to form the pellets *in vacuo*. For this purpose a vacuum chamber has been constructed, utilizing a $4\frac{3}{8}$ in. O.D. extra-flexible bellows, #D-22834, obtainable from the Clifford Manufacturing Company.

REFERENCES

1. CHIEN, J.-Y. J. Chem. Educ. 24: 494. 1947.
2. FRANKLIN, C. S. Brit. Patent No. 335,526 and 369,575.
3. JELATIS, J. G. J. Appl. Phys. 19: 4–19. 1948.
4. PULLEN, K. A., JR. Proc. I.R.E. 34: 402. 1946.
5. R.C.A. Tube Handbook. Vol. 3–4. Data sheet CE 6934V. "5651 Voltage reference tube".
6. SZIKLAI, G. C. and SCHROEDER, A. C. Proc. I.R.E. 33: 701. 1945.

A COMPARISON OF THE FLOW OF HIGH POLYMERS IN THE CAVITY OF A MOONEY PLASTOMETER[1]

By D. S. Fensom

ABSTRACT

From idealized Mooney plasticity – time curves for Butyl and GR-S synthetic rubber the distinctive features of the various parts of the shearing curve are pointed out. Actual experimental curves are given for Butyl, GR-S, "Cold rubber", polyisobutylene, polybutadiene, polystyrene, and some natural rubber gum stocks. For polymers which were produced in emulsion, the degree of branching as indicated by the Huggins k' value seemed to be loosely correlated with the time to reach the primary peak in the Mooney flow curve. Cross linking and entanglement in structure as indicated by high gel content seemed to be correlated with secondary rise in shearing force shown during a long test. An hypothesis of flow in the cavity of the Mooney machine is advanced to explain these phenomena, supported by drawings of cross-sections of samples run in the machine. According to this hypothesis, some high polymers shear in a streamline fashion, others shear along certain slip planes and may even exhibit a mixing of parts which seems to be similar to turbulence in fluids.

INTRODUCTION

In 1951 a brief survey of the viscosity–time curves obtained during the shearing of GR-S and Butyl synthetic rubber samples in a Mooney plastometer was made (1). As a result, some views on the flow inside the cavity of this plastometer have been formed and the work described below is a continuation of the original study. Two comparisons have been attempted: the comparison of the flow curves of high polymers whose structure and properties were either measured or known, and the comparison of the actual rubber residues taken from the machine after shearing.

IDEALIZED MOONEY CURVES

When a sample of high polymer is sheared under standard conditions in a Mooney plastometer the strain on the shearing mechanism is measured and may be plotted against time (4). It has been the custom for the rubber industry to depend chiefly on the Mooney value (i.e. the measured strain) after four minutes' shearing, but in previous work it was suggested that all parts of the curve may reflect the structure of the sample (1).

Two very important types of synthetic rubber, Butyl and GR-S, were found to give two distinct types of Mooney curves. Idealized curves for these two rubber types are given in Figs. 1 and 2.

In Fig. 1, which is for Butyl rubber, a steady flow portion A′C′ or BC is shown, but the dotted-line curve A′C′ has the characteristic shape for samples which have been heavily "massed" (i.e. milled between heated rolls) and cooled but which have not been allowed to relax in the hot cavity of the machine for more than a second or two. The full line, ABC, is typical of a low viscosity

[1]*Manuscript received in original form September 7, 1954, and, as revised, February 4, 1955. Contribution from Ridley College, St. Catharines, Ontario. Paper read at High Polymer Forum, London, Ontario, November, 1953.*

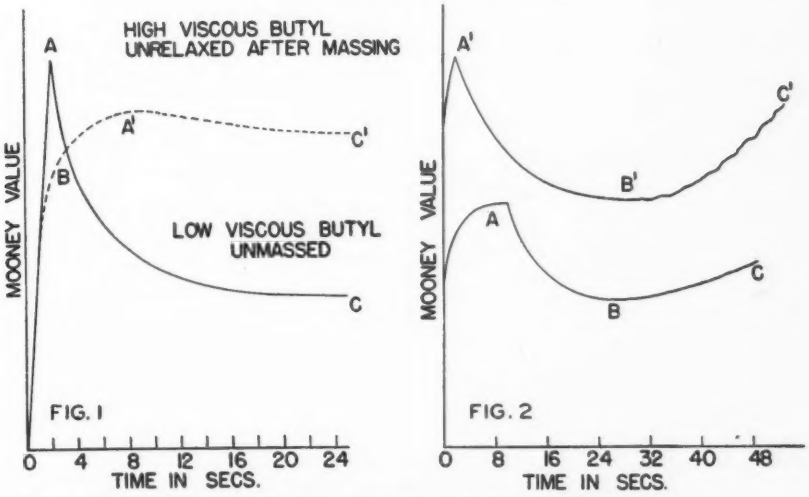

FIG. 1. Idealized Mooney plasticity – time curves for Butyl rubbers.
FIG. 2. Typical Mooney curves of unmassed butadiene–styrene copolymers containing about 23% bound styrene.

Butyl sample relaxed or "conditioned" for the normal period of one minute. The part of the curve 0A (or 0A′) was largely the result of rubber extension, while AC (or A′C′) was largely due to flow of rubber. When a high viscosity sample of Butyl rubber was tested, with the usual period of conditioning, the curve followed the shape 0ABA′C′.

In Fig. 2 the curves are shown of two typical GR-S rubbers, i.e. butadiene–styrene copolymers, which have not been massed prior to running, but which have been conditioned in the machine for one minute before shearing. The difference in shape of these curves may be seen in comparison with those of Fig. 1: the low and flattened part of the curve 0A and the secondary rise at C in about four minutes. The sample giving curve 0ABC would be lower in viscosity and gel content than that giving 0A′B′C′.

THE MOONEY CURVES OF VARIOUS HIGH POLYMER TYPES

Some ten distinctive types of high polymer relating to Butyl or GR-S synthetic rubber were run in a standard Mooney machine at 212°F. A standard rotor was used and the rotor speed was kept at 2 r.p.m. according to the requirements of one of the commonest tests carried out by this machine (4). Each high polymer was allowed to condition in the machine for one minute (unless stated to the contrary) and according to thermocouple measurements made in the sample mass inside the cavity, the high polymer temperature at the start of shear was within 5° of 212°F.

While there is no reason to think that the curves shown in Figs. 3–10 are the only ones which might be obtained for their polymer group, in most cases the main shape of the curve would seem to be characteristic of typical samples.

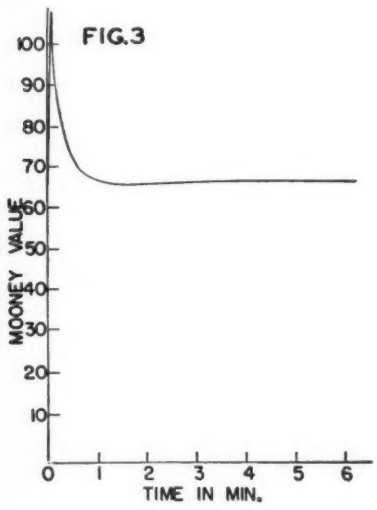

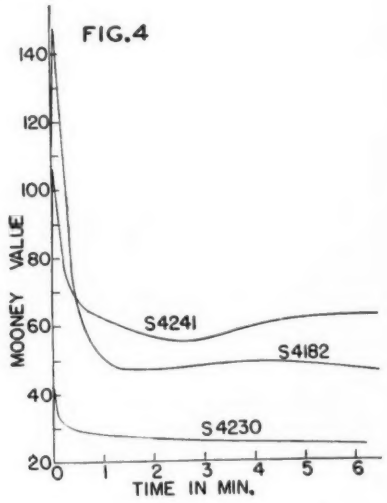

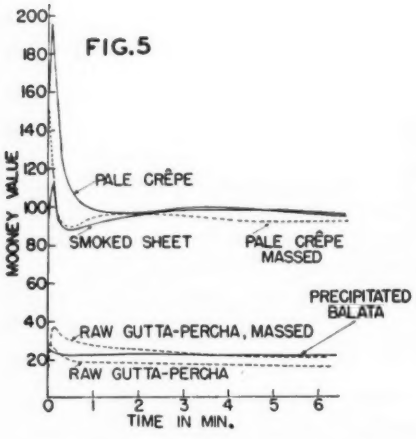

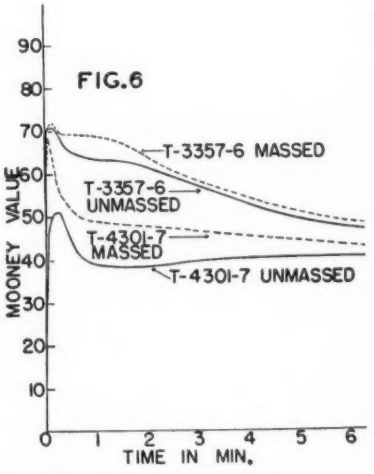

FIG. 3. Mooney curve of a sample of polystyrene run at 273°F.
FIG. 4. Mooney curves of samples of polyisobutylene run at 212°F.
FIG. 5. Mooney curves of Natural rubber samples run at 212°F.
FIG. 6. Mooney curves of samples of polybutadiene (polymerized at 122°F.) run at 212°F.

Where duplicate runs were made (not done in the case of polystyrene, the Natural rubbers, or "Special" rubbers) the curves lay within two Mooney points of each other at comparable times.

All samples were run between cellophane sheets to prevent the polymer from sticking to the rotor or platens.

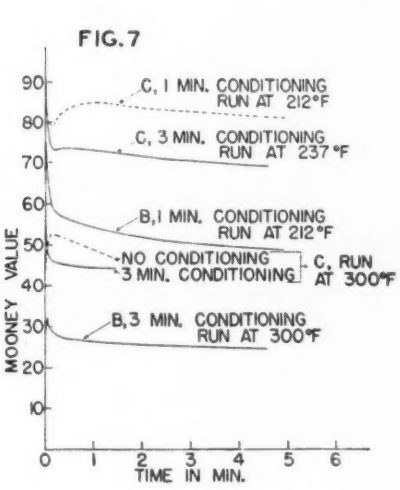

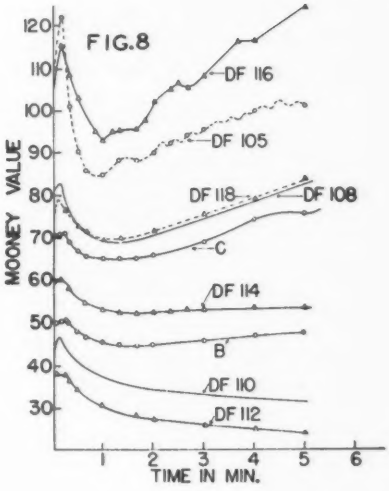

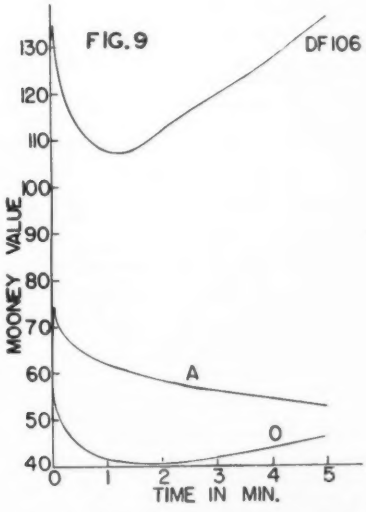

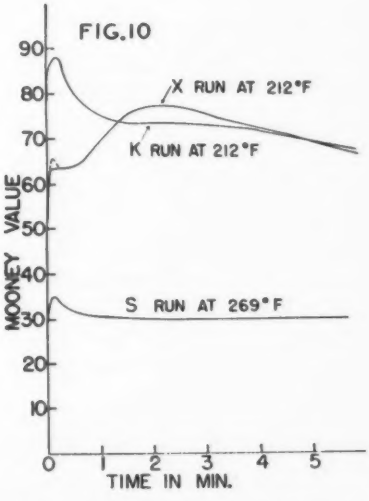

FIG. 7. Mooney curves of samples of Butyl rubber, run at various temperatures.

FIG. 8. Mooney curves of samples of butadiene–styrene copolymers (polymerized at 122°F. and with 23% bound styrene) run at 212°F. unmassed.

FIG. 9. Mooney curves of samples of butadiene–styrene copolymers (polymerized at 55°F. and with 23% bound styrene) run at 212°F. unmassed.

FIG. 10. Mooney curves of samples of miscellaneous synthetic rubbers polymerized at 122°F. and run at various temperatures. Sample X was a butadiene–styrene copolymer with 25% bound styrene and 0.3% divinyl benzene. Sample S was a butadiene–styrene copolymer with 85% bound styrene. Sample K was a butadiene–acrylonitrile copolymer with 32% bound acrylonitrile.

Some properties of the miscellaneous polymers are listed in Table I, the butadiene–styrene (or related) copolymers in Table II, and the Butyl samples selected as typical in Table III.

TABLE I

PROPERTIES OF POLYMERS

	Intrinsic viscosity $[\eta]$	Branching factor k'	Gel, %	Comments
Polystyrene	1.18	.33	—	Preheated to 280°F. before the Mooney run
Polyisobutylene				
S.4230	.92	.38	—	Conversion 51%
S.4241	2.51	.37	—	Conversion 52%; after Mooney run $[\eta] = 2.51$
S.4182	5.06	.39	—	Conversion 72%
Polybutadiene, polymerized in emulsion at 122°F.				
T-4301-7	2.03	.43	—	After Mooney run $[\eta] = 2.02$, $k' = .41$
T-3357-6	2.25	.39	—	After Mooney run $[\eta] = 2.19$, $k' = .35$

TABLE II

PROPERTIES OF BUTADIENE–STYRENE COPOLYMERS

	Intrinsic viscosity $[\eta]$	Branching factor k'	Gel, %	Comments
Polymerized in emulsion at 122°F., 23% bound styrene				
DF.112	1.50	.36	0.7	Pilot plant batch, 62% conversion
DF.110	1.82	.35	0.2	Pilot plant batch, 57% conversion
B	2.37	.42	1.2	Plant batch, 72% conversion; after Mooney run $[\eta] = 2.37$, $k' = .40$
DF.114	2.20	.34	1.0	Pilot plant batch, 59% conversion
C	>3	—	61.2	Plant batch, 73% conversion
DF.108	2.96	.35	14.5	Pilot plant batch, 59% conversion
DF.118	—	—	36	Pilot plant batch, 60% conversion
DF.105	—	—	58.6	Plant batch, 71% conversion
DF.116	—	—	47	Pilot plant batch, 59% conversion
Polymerized in emulsion at 55°F., 23% bound styrene				
O	3.89	.37	5.7	Supposed to be identical with DF.106 coagulated with 45 oil: 100 polymer. Analysis based on oil-free sample
A	2.17	.32	0.1	
DF.106	3.78	.36	40.8	Plant masterbatch, 70% conversion
Polymerized in emulsion at 122°F., miscellaneous types				
S	1.21	.34	10.0	85% bound styrene
X	—	—	78.2	25% bound styrene+0.3% divinyl benzene
K	—	—	39.7	32% acrylonitrile replacing all styrene

TABLE III

PROPERTIES OF BUTYL RUBBER SAMPLES CONTAINING ABOUT 8% ISOPRENE COPOLYMERIZED WITH ISOBUTYLENE

	Intrinsic viscosity $[\eta]$	Branching factor k'	Gel, %	Comments
B	1.10	.37	0.1	After Mooney run $[\eta] = 1.03$, $k' = .36$
C	1.30	.40	1.3	After Mooney run $[\eta] = 1.28$, $k' = .39$

Intrinsic viscosities, $[\eta]$, and the branching factor, k', were both found from measurements of dilute solution of polymer in toluene (2, 3). The solutions were filtered to remove gel and then run in an Ubbelohde viscometer at 25.0°C.±.02°. Concentrations were kept below 0.5 gm. per 100 ml. and k' was calculated from the slopes of the viscosity curve using the relation:

$$(\ln \eta_r)/c = [\eta] - \beta[\eta]^2 c$$

and

$$k' = (0.50 - \beta)$$

where η_r is the relative viscosity, c is concentration, and $\beta[\eta]^2$ is the slope of the curve.

The gel content of polymers was obtained by suspending a $\frac{1}{10}$ gm. sample of polymer within a 100 mesh stainless steel wire cage in toluene at room temperature for 48 hr. The cage and residue were dried at 100°C. for one hour before weighing.

THE COMPARISON OF ACTUAL MOONEY CURVES

(a) *Primary Peaks*

The outstanding feature of the Mooney curves of polystyrene and polyisobutylene, Figs. 3 and 4, was the extremely sharp primary peak reached within four seconds from the start of shear. The curves of these two types were similar in general shape to that of a typical low-viscosity Butyl rubber with a low branching factor (see Butyl B, Fig. 7) but very different in shape from the curves of polybutadiene (Fig. 6). The primary peak of the polybutadiene curves for unmassed samples was not at all sharp and was not reached until some 10–17 sec. after shearing was started.

A further set of Natural rubber samples was then run (Fig. 5). Raw pale crepe rubber, which is considered to be fairly pure polyisoprene polymerized without branches in a latex emulsion in the hevea tree, showed a sharp primary peak rather similar to polyisobutylene. This sample would probably have been rolled at least once. Smoked crepe, a less pure grade of latex dried under conditions which might be expected to lead to more cross linking, showed a broader peak than raw pale crepe. Balata gum, precipitated and purified, showed a sharp primary peak in spite of its low viscosity at 212°F., but the Gutta-percha sample, which contained some gums and resins other than pure rubber, showed again a flattened peak. These tests, though too few to be con-

clusive, suggested that the sharpness of the primary peak might be related to lack of branching in a polymer, or to some similar structural feature of the material, rather than to the process of manufacture.

(*b*) *Secondary Peaks*

It will be noticed from Figs. 1 and 2 that in addition to the primary peak a secondary rise may also appear in certain Mooney curves. In Butyl rubber samples this secondary rise occurred within one minute of the start of shearing and was dependent upon the temperature of the sample. Thus a sample which showed a pronounced secondary rise (Butyl C, Fig. 7) when run at 212°F. after one minute of conditioning showed less rise if the conditioning period were extended or if the temperature were raised. Low viscosity samples showed even less rise or none whatever.

With GR-S samples and related rubbers, the secondary rise was also noticeable. However, with these materials it was seldom noticeable until after one and one-half minutes of shearing and often did not attain its peak until some four or five minutes had elapsed. With these rubbers the secondary rise was hardly affected by temperature change or conditioning period, but was certainly increased by increasing molecular weight and increasing gel as Fig. 8 and Table II show.

THE COMPARISON OF PLUGS OF ACTUAL MOONEY SAMPLES

To determine the particular reasons for these flow peculiarities, several experiments were devised. Samples of GR-S and Butyl rubber were evacuated for 24 hr. at 100°C. at a pressure around 10 mm. mercury. Nitrogen was then admitted at atmospheric pressure and the samples were allowed to cool in its atmosphere before they were run in the Mooney machine. Since no appreciable change in the flow curve resulted, it was concluded that entrapped air played little part in influencing the shape of the flow curves.

A study of the decay of stress in the sample after shearing but while the sample was still in the machine was a little more useful. This indicated that no true structural effect occurred in Butyl rubbers to cause the secondary rise, but in GR-S samples a lasting change occurred in the sample during its shearing.

Greatest progress was made by examining the sample plugs from the machine after a definite period of shearing. To do this Messrs. Storey and Briggs of Polymer Corporation devised a method of placing a different color of rubber in each half of the shearing cavity. Polyisobutylene was impregnated with a small quantity of carbon black to give some color to it. However, the GR-S samples had to be colored with chemicals, since milling with carbon black would destroy the original structure on which the secondary rise seems to depend. After it had been run for the desired time the machine was stopped and heated to 300°F. in order to allow a fairly permanent relaxation of each sample to occur so that the sample would not distort unduly when it was removed from the die.

Drawings of the cross sections of these plugs are shown in Figs. 11 and 12.

It will be seen that the plugs of polyisobutylene indicate a stretching of the sample at first, followed by flow of a streamline nature which started at the

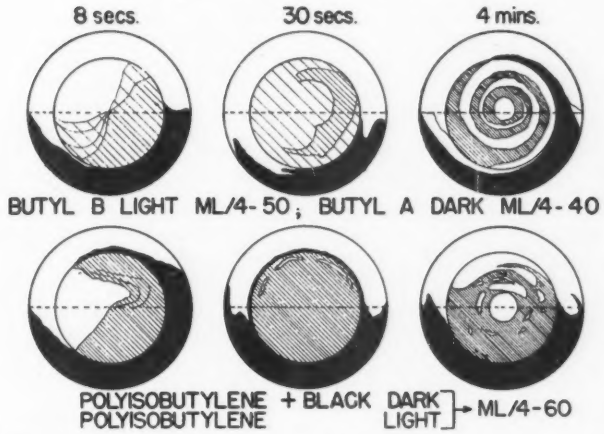

FIG. 11. Drawings of cross-sections of actual sample plugs from the Mooney machine: Butyl (low viscosity) and polyisobutylene after 8 sec., 30 sec., and 4 min. shearing (i.e. one quarter, one, and eight revolutions).

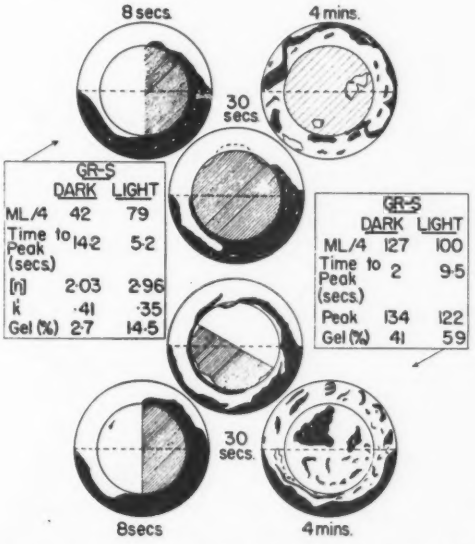

FIG. 12. Drawings of cross-sections of actual sample plugs from the Mooney machine: GR-S (i.e. butadiene–styrene copolymers with 23% bound styrene) of low and high viscosity after 8 sec., 30 sec., and 4 min. shearing.

outside of the rotor. As time went on the sample seemed to wind up around the axis of shear and the streamlines approached the center. After four minutes there was some indication of breakup in the flow units. The flow planes of low viscosity Butyl rubber were also streamline in their nature.

In the case of the plugs of GR-S rubber, extension was again visible, but to a much smaller extent than in Butyl or polyisobutylene. With the extension was definite evidence of slippage along certain slip planes at fixed distance from the center. This, apparently, was the cause of flatness in the primary peak which has been noted above. After about 30 sec. of shearing, the GR-S samples showed signs of a peculiar turbulence or nodulizing which became more and more apparent with time. This coincided with the period of "secondary rise".

DISCUSSION OF RESULTS

If these results may be taken as typical of the classes of rubber from which they are taken, it will be agreed that these synthetic rubbers fall into two classes: those which exhibit substantially a streamline type of flow after high extension in the Mooney chamber, and those which exhibit slip with the primary extension followed by granulation or "turbulence" in the main flow section. These two forms of flow may be used to explain most of the curves obtained during the survey of the various polymers.

Upon consideration of the primary peaks it is suggested that emulsion-produced polymers have lines of low resistance to shear running between the emulsion granules. If the polymer has been massed these granules will be broken open to some extent. Also, if the polymer is linear in structure it is suggested that there would be a greater tendency for granules to become uniformly interlinked by heat motion. With branched chains the granules would more probably retain their identity and hence one would expect a greater extension of slippage upon the original extension since the granules would only be intertangled by free ends of polymer chain. That some such correlation between branching and time to primary peak does occur is shown by Fig. 13 in which branching is measured by k' determinations from dilute solution viscosity in toluene.

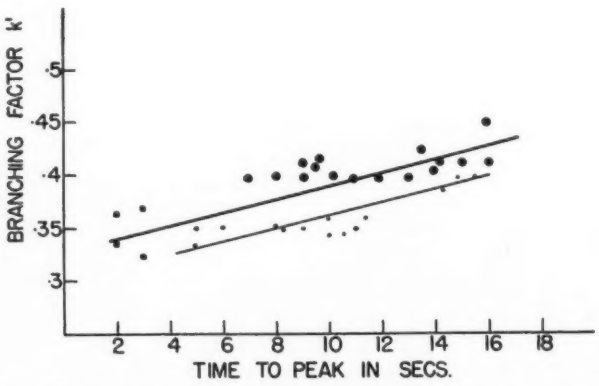

FIG. 13. The variation between the branching factor k' and the time to reach Mooney peak. The upper line is for plant samples, the lower line for pilot plant batches. All samples were butadiene–styrene copolymers with 23% bound styrene. The square points indicate samples polymerized at 55°F.; all others were polymerized at 122°F.

As flow continues these emulsion granules apparently tend to form larger aggregations which give the appearance of turbulence of flow. The turbulence is not in this case precisely the same as turbulence of ordinary liquids, and the Reynold's number as ordinarily used probably does not apply. However, the tendency of GR-S polymer to flow along certain slip planes will raise the relative velocity of different parts of the sample to high local values and increase the granular appearance which results. It is also suggested that increased branching or entanglement (looping of chains) will increase the apparent turbulence and so give a greater secondary rise to the shearing force. This is borne out by Fig. 8, in which the secondary rise clearly increases with the increase in molecular weight (and gel content) of the polymer.

ACKNOWLEDGMENT

This work was part of a research program assisted by the National Research Council of Canada and in co-operation with the Research and Development Division of Polymer Corporation Limited of Sarnia. Laboratory assistance was provided by G. T. MacKenzie. This help is most gratefully acknowledged.

REFERENCES

1. FENSOM, D. S. Rubber Age, N.Y. 73: 795. 1953.
2. HUGGINS, M. L. J. Am. Chem. Soc. 64: 2716. 1942.
3. MANSON, J. A. and CRAGG, L. H. Can. J. Chem. 30: 482. 1952.
4. TAYLOR, R. H., FIELDING, J. H., and MOONEY, M. Rubber Age, N.Y. 61: 567. 1947.

ON THE FRICTION OF RUBBER COVERED WHEELS ON ICE[1]

By C. D. Niven

ABSTRACT

The friction between a small rubber covered wheel and ice was examined. Amontons' linear relation between load and frictional force was found to hold at 20°F. and lower. There was a distinct indication that on wet ice soft rubber gripped better than harder rubber. However on wet ice and on ice just below the freezing temperature friction was so low that the squeezing down of the rubber under load vitiated results. The work suggested that a pneumatic tire must be used as a test sample if road conditions are to be duplicated.

INTRODUCTION

Serious accidents occur due to the slipping of rubber-tired wheels on ice. Little is known about the principles underlying this phenomenon. Rubber and ice both have exceptional friction qualities. Roth, Driscoll, and Holt (3) have studied the friction of rubber on steel and on some other surfaces, while both Thirion (6) and Schallamach (4) have experimented with rubber sliding on glass and Denny (1) has done some work on rubber sliding on wet glass. Pfalzner (2) examined in this laboratory the friction of flat samples of natural and synthetic rubbers sliding on ice but the behavior of rubber-tired wheels on ice has been largely overlooked by experimental physicists up to the present time.

Indeed much of our information on this point comes from those who have had winter driving experience and one of the frequently quoted of drivers' observations is that a heavy vehicle is apt to slip less than a light one but that once it has started slipping it will slip worse. An attempt which the writer made to verify this using flat samples of rubber indicated that sliding samples were unsatisfactory. Heavily loaded rubber samples would not slide smoothly on the turntable at any rate when it was turning slowly. Under such conditions the experiment demonstrated a fine example of the stick-slip motion and on one occasion when the temperature was low enough to freeze the melted surface almost as soon as the sample had passed over, an even pattern of ripples frozen on the surface of the track could be seen. Apart from the difficulty of making any good estimate of the drag value when a sample is jerking the balance violently, the measurement of friction on a ripple covered track was out of the question. Under warmer conditions, especially if the turntable was speeded up, the sample could be made to run fairly smoothly but close examination of the track revealed that under these circumstances there was moisture on it. The test then simply referred to the friction of ice at 32°F. and of course gave a nice demonstration of power consumed by the motor, which drove the turntable, ending up as heat energy melting ice.

It was clear that the use of a rolling sample was unavoidable and with this in view apparatus was designed for measuring the force parallel to the surface

[1]*Manuscript received January 5, 1955.*
Contribution from Division of Physics, National Research Council, Ottawa, Canada. Issued as N.R.C. No. 3576.

of the ice which the rubber exerted just at the moment when slipping occurred. The term rolling friction has been avoided because Tabor (5) has used this to describe the friction between two surfaces separated by a rolling body.

The use of a wheel in place of a flat sample introduced another difficulty. The wheel was covered with a $\frac{1}{4}$ in. layer of rubber and this squeezed down under heavy loading to form a flat on the circumference of the wheel. The result was that the wheel acted as a runner rather than as a roller and defeated to some extent the purpose of using the wheel at all. The rubber on the wheels was accordingly machined off to give a covering merely $\frac{1}{16}$ in. in thickness. This did not entirely stop the formation of a flat portion and far lighter loadings had to be used than were first intended. The work described below concerns loads up to only about six or eight kilograms on wheels $1\frac{5}{8}$ in. in diameter.

EXPERIMENTAL METHODS

The apparatus consisted essentially of a spindle on which were mounted the test wheel and a small drum as shown in Fig. 1. Around this drum was

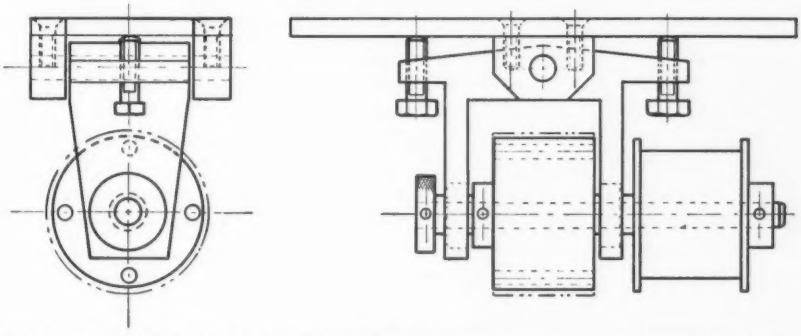

FIG. 1. Assembly drawing of mounting and spindle carrying rubber covered wheel and drum.

wrapped a string which was then passed over a pulley mounted on ball bearings. A weight pan was attached to the end of the string; the arrangement is shown diagrammatically in Fig. 2. The spindle carrying the wheel and drum turned on ball bearings in a bracket attached to the underside of the heavy arm on the turntable described in a previous communication. This arm was so heavy that special provision had to be made by means of an overhead pulley on ball bearings to reduce the weight.

The test was conducted as follows: After adjusting the loading which was to be put on the wheel, the string was wrapped around the drum about twice and the wheel put down on the ice surface. Weights were put on the pan and the wheel gently rolled back and forth on the ice. This was done by moving the arm in a horizontal direction: it was only necessary to turn the wheel through an angle of 15° or 20°. If it rolled and did not slide then more weight was added to the pan; if it slid and would not roll or if the weight pan fell to the padded stop, then too much weight was on the pan. The critical force was calculated from the value of the largest weight on the pan which would permit

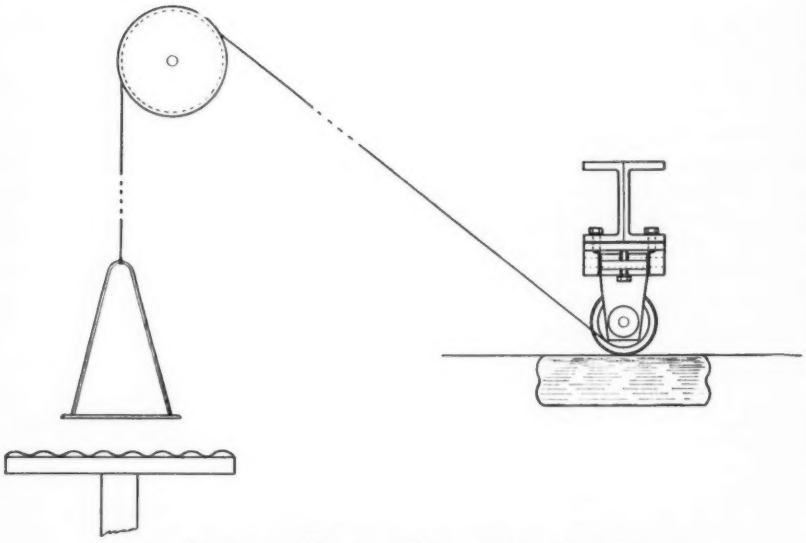

FIG. 2. Diagrammatic illustration of the experimental arrangements.

rolling. The turntable was turning during the machining of the flat ice surface but was still during the actual test.

The wheels used for the tests were brass wheels $1\frac{1}{2}$ in. in diameter and 1 in., $\frac{1}{2}$ in., and $\frac{1}{4}$ in. in width. These were covered with rubber which was then machined off to give a covering of $\frac{1}{16}$ in. A rubber of the normal hardness used for a tire tread was used, but in order to compare with this a softer rubber, a second $\frac{1}{2}$ in. wheel was provided and covered with a softer rubber. These four samples are referred to below in the charts showing the results as "one-inch hard", "half-inch hard", "quarter-inch hard", and "half-inch soft".

The National Research Council's Rubber Laboratory prepared the samples of rubber and have supplied details in this connection which are given in Table I. The hardness was measured on a Shore Durometer Type A.

TABLE I

Sample	Hard	Soft
Shore hardness value	65	50
Composition		
Polysar Krylene	100	100
Circosol 2 XH	5	5
Neozone D	1	1
Zinc oxide	5	5
Philblack O	50	20
Sulphur	1.75	1.75
Santocure	1	1
Preparation		
Cure one hour; raise to 310°F.; one hour at 310°F.		

Deciding the end point of the rolling motion and the starting point of the sliding motion was sometimes not easy because this was not precise at milder temperatures. At zero temperatures on the other hand it was fairly definite because after the limit of friction had been exceeded, the grip would suddenly let go and the pan would fall to the padded stop. When the apparatus behaved in this way repetition of the results was good. At mild temperatures, however, if the loading arm was moved in a horizontal direction, the wheel would slip through a small angle owing to the tension on the string, and then grip. When the arm was moved again the same thing would be repeated, with the result that it was very hard to decide whether the wheel was gripping or not at that particular string tension. On wet ice an extreme example of this turn-grip motion could be observed when a wheel would keep turning continuously at a very slow speed as though the surface were covered with a very viscous grease.

To complicate matters in the milder temperature range, once a wheel had started slipping, the conditions of test might change. The wheel would be moistened with the water melted during momentary slipping while the surface would have lost some of its grip. It was then desirable to move the turntable to get a new piece of ice and to use a dry part of the rubber wheel. The rubber wheel appeared to have a polishing action at these temperatures when it slipped—an observation which tallies with driving experience at a "stop" sign. Rolling rubber on the other hand does not polish but was observed to even roughen the surface when the turntable was made to revolve with the rubber wheel running freely. The two motions can be compared to drawing a knife along a piece of butter or lifting it off at right-angles to the surface.

The ice surface used for these tests had always stood overnight after being machined, because it was found that at mild temperatures machining even with a smoothing tool could increase the friction quite markedly. This increase gradually disappeared in the course of a few hours while the surface became obviously glossier. At zero temperatures on the other hand the effect of such machining was unimportant.

RESULTS

The results are shown in Figs. 3, 4, 5, and 6 where limiting frictional force at the surface of the ice is plotted against load. Each set of graphs refers to a particular wheel while the different graphs of a set correspond to different temperatures. Observations which have been repeated once, twice, or three times have respectively a small, medium, or large circle or marker around each. At lower temperatures a linear relation seems to be indicated: the curvature, if any, is away from the load axis.

At 30°F. the results are more complicated. The points are dotted over a large area giving a spread that is itself comparable with the smaller values. As a general rule a high frictional force value at low loading corresponds to high force values at higher loadings so that if each set of readings had been plotted independently the graphs would fan out from the origin. The spread is least for the half-inch soft sample and greatest for the quarter-inch hard sample

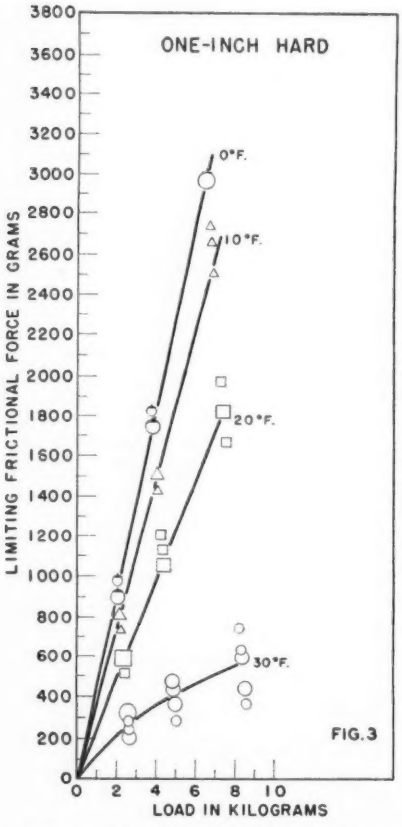

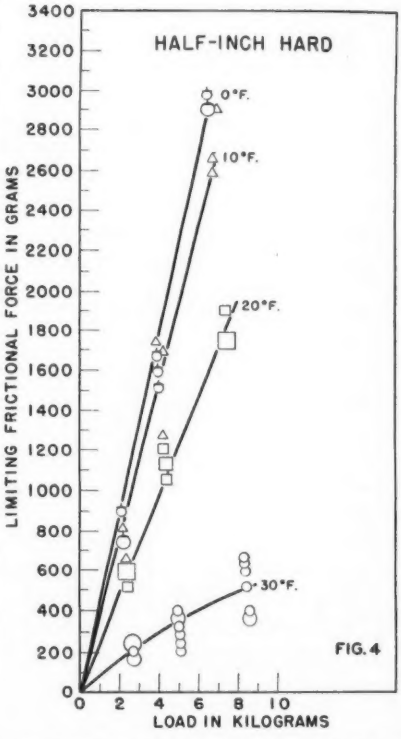

FIG. 3. Graphs showing limiting frictional force at various temperatures plotted against load for a brass wheel 1½ in. in diameter and 1 in. in width covered with $\frac{1}{16}$ in. layer of rubber of hardness 65 on Shore durometer.

FIG. 4. Graphs showing limiting frictional force at various temperatures plotted against load for a brass wheel 1½ in. in diameter and ½ in. width covered with $\frac{1}{16}$ in. layer of rubber of hardness 65 on Shore durometer.

with one very high point at the high loading. Generally speaking these graphs at 30°F. curve toward the load axis and so the curve which has been drawn on the chart to represent the average behavior of the wheel at 30°F. has also been drawn with a marked curvature towards the load axis.

Some measurements on wet ice were attempted but these presented difficulties. As far as could be judged the frictional force on hard wet ice was the same for all three loadings on the hard samples, but for the soft sample increase of friction accompanied increase of load. The width of the hard samples did not appear to be important, but what was of interest was that the soft sample had about double the friction of the hard sample under the 8.4 kgm. loading.

The curving of the graphs in the milder temperature range may possibly be a spurious effect due to the compression of the rubber and the question

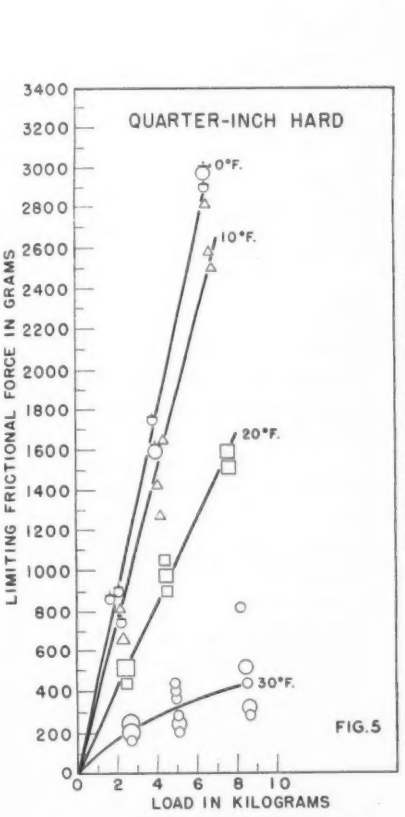

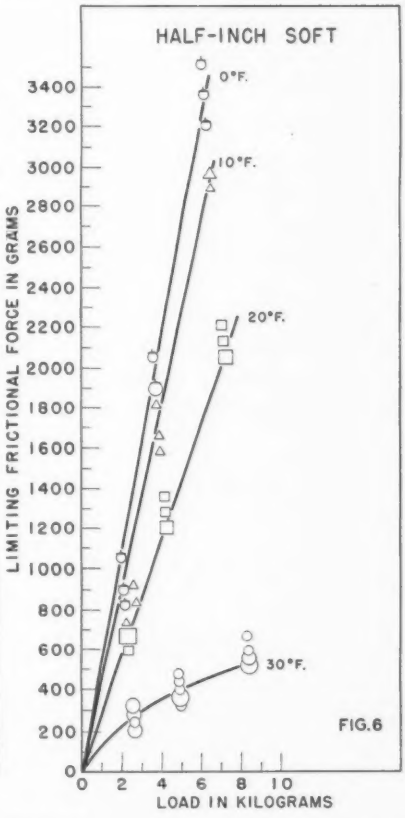

FIG. 5. Graphs showing limiting frictional force at various temperatures plotted against load for a brass wheel 1½ in. in diameter and ¼ in. in width covered with $\frac{1}{16}$ in. layer of rubber of hardness 65 on Shore durometer.

FIG. 6. Graphs showing limiting frictional force at various temperatures plotted against load for a brass wheel 1½ in. in diameter and ½ in. in width covered with $\frac{1}{16}$ in. layer of rubber of hardness 50 on Shore durometer.

arises as to whether a pneumatic tire would act in the same manner. The curvature at lower temperatures away from the load axis is not large enough to warrant the suggestion that Amontons' Law be violated in that region of temperature, and indeed it is of interest to note how closely many of the repeated points obey a linear relation. One may therefore conclude that Amontons' Law is obeyed at 20°F. or lower. In mild temperatures the heavier the load the less the grip in proportion.

The results failed to show that softness of rubber and width of tire are of great importance on cold dry ice: only a small advantage was found. It was on wet ice that the soft rubber showed up to real advantage.

Using the data given on Fig. 3, Fig. 7 has been constructed and shows how the frictional force at a particular loading increases with decrease of tempera-

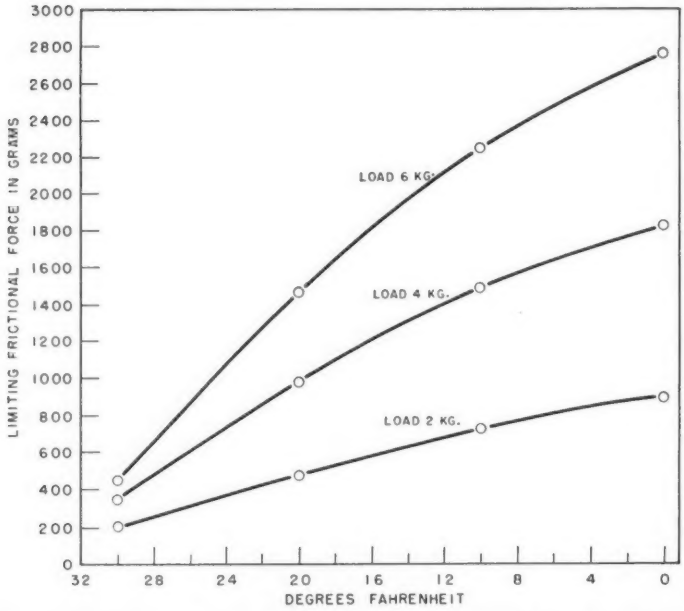

FIG. 7. Graphs constructed from data on Fig. 3 showing how limiting friction force at a particular loading varies with ice temperature.

ture. The curves are not linear and the increase in frictional force in the 30° to 20°F. range is about twice as large as it is in the 10° to 0°F. range.

The work has failed to prove that at high loadings the grip of a rubber wheel on ice is relatively better than at low loadings and has in fact indicated the reverse in mild winter temperatures; it is concluded that the experimental conditions described above do not duplicate road conditions sufficiently well, and that a pneumatic tire and a wheel of much larger radius are necessary as a test sample instead of a small rubber covered brass wheel.

ACKNOWLEDGMENTS

The author would like to express his thanks to the Director of the Division of Mechanical Engineering, N.R.C. for the hospitality of the Low Temperature Laboratory needed for this work and to Mr. T. R. Griffith of the Rubber Laboratory, Division of Applied Chemistry for his co-operation in providing the samples.

REFERENCES

1. DENNY, D. F. Proc. Phys. Soc. (London), B, 66: 721–727. 1953.
2. PFALZNER, P. M. Can. J. Research, F, 28: 468–487. 1950.
3. ROTH, F. L., DRISCOLL, R. L., and HOLT, W. L. J. Research Natl. Bur. Standards, 28: 439–462. 1942.
4. SCHALLAMACH, A. Proc. Phys. Soc. (London), B, 65: 657–661. 1952.
5. TABOR, D. Phil. Mag. 43: 1055–1059. 1952.
6. THIRION, P. Rev. gén. caoutchouc, 23: 101–106. 1946.

CALCULATED RADIATION CHARACTERISTICS OF SLOTS CUT IN METAL SHEETS[1]

By James R. Wait and R. E. Walpole

ABSTRACT

Calculated radiation patterns are presented for an axial slot cut in a thin elliptic cylinder of perfect conductivity. The radiation conductance of the slot is also computed and is seen to be an oscillating function of the width of the thin elliptic cylinder. The patterns and conductances for a slot on a semi-infinite sheet are also calculated.

INTRODUCTION

The radiative properties of slots cut in metal conducting surfaces are now extensively utilized in microwave radiating systems. It is often assumed, for purposes of design, that the metal surface can be regarded as infinite in extent and thus the radiation diffracted around the edges is neglected. This can be a serious source of error.

When the conducting surface is in the form of a sheet or a plate, it is reasonable to expect that an elliptic cylinder is a good representation if the eccentricity is large. It would then seem desirable to investigate the radiation characteristics for slots cut in such idealized surfaces as a step toward the more complete evaluation for surfaces of arbitrary shape and limited extent.

In a previous paper (10), a derivation was given for the electromagnetic field produced by an arbitrary slot cut in the surface of an elliptic cylinder of perfect conductivity and infinite length. The electric field tangential to the slot was assumed to be a prescribed function. When the results were specialized to the far zone region and to axial or transverse slots, agreement was obtained with the earlier results of Wong (11) who employed a different method. In the present paper calculated radiation patterns are presented for narrow axial slots on thin elliptic cylinders. For sake of completeness the corresponding patterns for a slot on a semi-infinite conducting plane sheet are also computed.

FIELD OF THE AXIAL SLOT

The perfectly conducting cylinder is taken to be of infinite length with major axis $2a$ and minor axis $2b$. If the cylinder axis is coincident with the z axis of a rectangular coordinate system (x, y, z), the surface of the cylinder is specified by

$$x^2/a^2+y^2/b^2 = 1. \tag{1}$$

As in the previous paper (10), it is convenient now to introduce elliptic cylinder coordinates (u, v, z) which are defined by the following transformation:

$$\begin{aligned} x &= d \cosh u \cos v, \\ y &= d \sinh u \sin v, \\ z &= z, \end{aligned} \tag{2}$$

[1]*Manuscript received January 17, 1955.*
Contribution from the Radio Physics Laboratory, Defence Research Board, Ottawa, Canada.

where $2d$ is the distance between the foci of the ellipse. The foci are located at the points $(x = \pm d, y = 0)$. The surfaces $u =$ constant represent a family of confocal cylinders of elliptic cross section. The semimajor and semiminor axes of the ellipse $u = u_0$ are given by

$$a = d \cosh u_0,$$
$$b = d \sinh u_0.$$

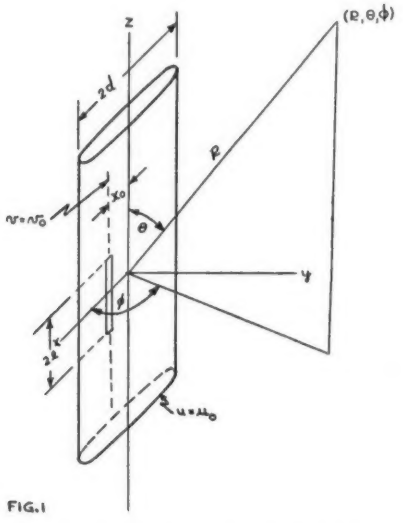

FIG. 1. Coordinate system for thin elliptic cylinder of width $2d$ with narrow axial slot.

A narrow rectangular slot is located on the cylinder at $v = v_0$ extending from $z = -l$ to $z = +l$ in the axial direction. As a result of the assumed small width of the slot, only the transverse voltage $V(z)$ along the slot contributes to the radiated fields. From previous analyses (10, 11) it then follows that, in terms of spherical coordinates (R, θ, ϕ), the electric field at large distances from the cylinder has only a significant ϕ component and is given by

$$[3] \qquad E_\phi = (2/\pi)^{\frac{1}{2}} \exp(-ikR + i\omega t) R^{-1} S(\theta)\, P(\theta, \phi)$$

where

$$[4] \qquad S(\theta) = \frac{k \sin \theta}{2} \int_{-l}^{+l} V(z') \exp(ik \cos \theta z')\, dz'$$

with $k = 2\pi/\text{wavelength}$, and $S(\theta)$ is the pattern of the slot if it were cut in an infinite plane conducting sheet. The factor $P(\theta, \phi)$ which accounts for diffraction by the elliptic cylinder, in the far zone (i.e. $kR \gg 1$), is given by the rather cumbersome expression:

$$[5] \qquad P(c, \phi) = \sum_{m=0}^{\infty} \frac{i^m Se,o_m\,(c, \cos v_0)\; Se,o_m(c, \cos \phi)}{N_m^{e,o}(c)[\partial He,o_m^{(2)}(c, \cosh u_0)/\partial u_0]}$$

where $c = kd \sin \theta$. The functions $Se_{,o_m}$, $He^{(2)}_{,o_m}$, and $N^{e,o}_m$ are the angular, radial, and normalization constants, respectively, of the Mathieu functions of order m. The double suffix e,o indicates that the summation takes place over both even and odd Mathieu functions.

It should be noted that the function $P(c, \phi)$ is independent of the voltage distribution $V(z)$ along the narrow axial slot. This function can be called the "elliptic-cylinder space factor" as it fully describes the effect of the finite width of the conducting surface on which the slot is located.

The function $P(c, \phi)$ when plotted as a function of ϕ characterizes the azimuthal radiation pattern for a fixed value of $c = kd \sin \theta$. Since in certain practical microwave radiating systems slots are cut in surfaces which can be approximated by elliptic cylinders, it is worth while to carry out computation of $P(c, \phi)$ for various values of c. To simplify the calculations, only the case of a very thin elliptic cylinder is considered. That is $b \ll a$ and therefore $\cosh u_0$ in equation [5] can be replaced by unity. The infinite series solution can now be simplified by making use of the following identities (5):

$$[6] \qquad [\partial He^{(2)}_m(c, \cosh u)/\partial u]_{u=0} = -i/Je_m(c, 1)$$

and

$$[7] \qquad \sum_{m=0}^{\infty} i^m Se_m(c, \cos v_0) Se_m(c, \cos \phi) Je_m(c, 1)/N^e_m(c) = (8\pi)^{-\frac{1}{2}} \exp(ic \cos v_0 \cos \phi).$$

The space factor for the thin elliptic cylinder is then written in the form:

$$[8] \qquad P(c, \phi) = i(8\pi)^{-\frac{1}{2}} \exp(ic \cos v_0 \cos \phi) + \sum_{m=0}^{\infty} \frac{i^m So_m(c, \cos v_0) So_m(c, \cos \phi)}{N^o_m(c) Ho^{(2)'}_m(c, 1)}$$

where

$$Ho^{(2)'}_m(c, 1) = [\partial Ho^{(2)}_m(c, \cosh u)/\partial u]_{u=0}.$$

The function $|P(c, \phi)|$ is then plotted as a function of ϕ in Figs. 2 to 6 for $c = kd \sin \theta$ taking values of 1, 2, 4, 6, and 8 with $v_0 = 90°$. These patterns are symmetrical about $v = 90°$ since the slot in this case is located at the center of the thin elliptic cylinder. It can be noted that the rear lobes become smaller and more numerous as the width $2d$ increases.

Computations were also carried out for the case where the axial slot is displaced from the center line by an amount $d/2$. The angular location of the slot is then at $v_0 = 60°$. The function $|P(c, \phi)|$ is shown plotted for this case in Figs. 7 and 8 for $kd \sin \theta = 2$ and 4 respectively. It is to be noted that the pattern is now asymmetrical and the maximum is tilted away from the broadside direction.

The patterns shown in Figs. 2 to 8 are generally applicable to any narrow axial slot on the elliptic cylinder. To completely describe the three-dimensional pattern, of course it is also necessary to specify $S(\theta)$ which depends on the functional form of $V(z)$. As an example, computations are carried out for the

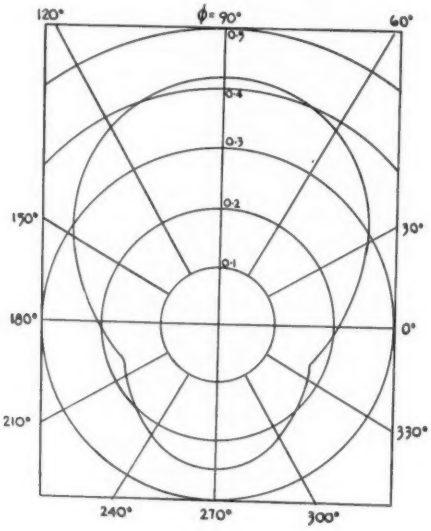

FIG. 2

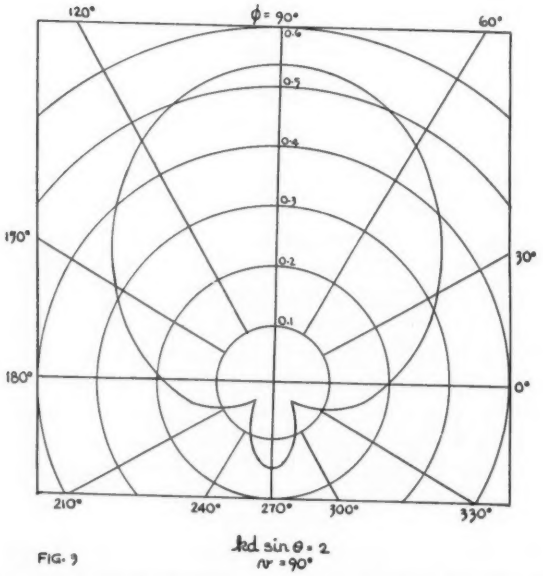

FIG. 3

FIG. 2. The azimuthal radiation pattern for the slot located at the center of the broad face of the thin elliptic cylinder with $2d \sin \theta = \lambda/\pi$.

FIG. 3. The azimuthal radiation pattern for the slot located at the center of the broad face of the thin elliptic cylinder with $2d \sin \theta = 2\lambda/\pi$. [For $v = 90°$ read $v_0 = 90°$.]

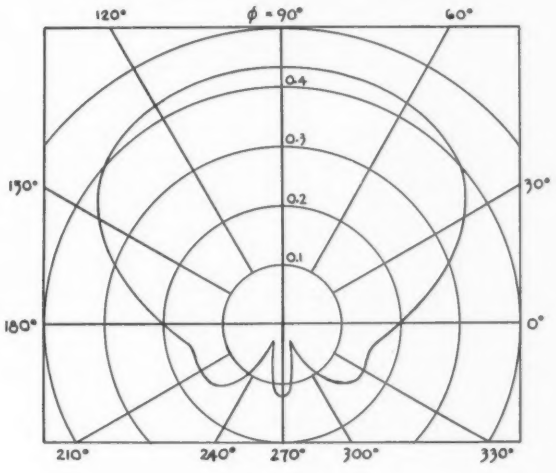

FIG. 4 $kd \sin\theta = 4$, $\psi_0 = 90°$

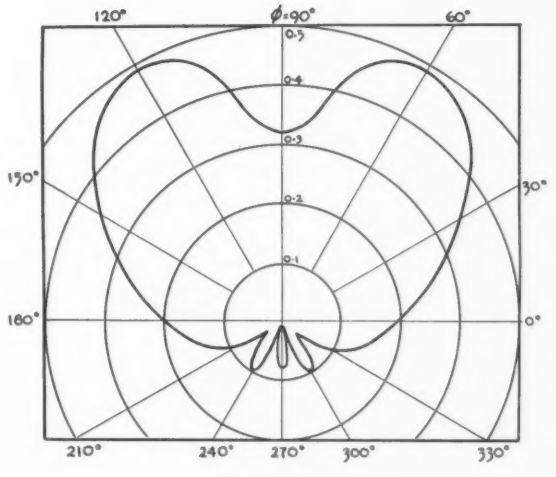

FIG. 5 $kd \sin\theta = 6$, $\psi_0 = 90°$

FIG. 4. The azimuthal radiation pattern for the slot located at the center of the broad face of the thin elliptic cylinder with $2d \sin\theta = 4\lambda/\pi$.

FIG. 5. The azimuthal radiation pattern for the slot located at the center of the broad face of the thin elliptic cylinder with $2d \sin\theta = 6\lambda/\pi$.

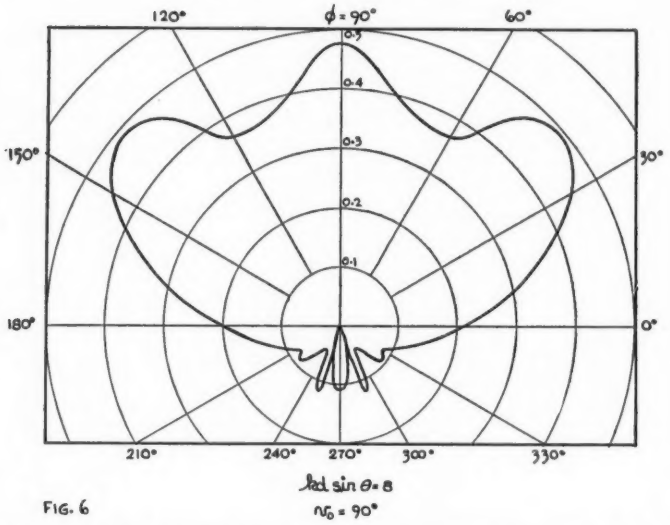

FIG. 6

FIG. 6. The azimuthal radiation pattern for the slot located at the center of the broad face of the thin elliptic cylinder with $2d \sin\theta = 8\lambda/\pi$.

principal elevation pattern (i.e. $\phi = 90°$) for the centrally located slot (i.e. $v_0 = 90°$). For convenience it is assumed that the voltage along the slot is sinusoidal such that

$$V(z) = V_0 \frac{\sin k(l - |z|)}{\sin kl} \tag{9}$$

where V_0 is the voltage at the center of the slot and consequently, for $2l = \lambda/2$,

$$S(\theta) = V_0 \frac{\cos(\frac{1}{2}\pi \cos\theta)}{\sin\theta}. \tag{10}$$

The principal elevation patterns for the case $kd = 2$ and 4 are then plotted in Figs. 9 and 10.

CONDUCTANCE OF THE AXIAL SLOT

It is of some interest to compute the radiation conductance of an axial slot on the thin elliptic cylinder. Again for convenience the slot is assumed to have a sinusoidal voltage distribution and a length equal to $\lambda/2$. The conductance G is defined in the usual way by calculating the power radiated P from the slot crossing an infinite sphere such that

$$G = 2P/V_0^2 \tag{11}$$

with

$$2P = \frac{1}{\eta_0} \int_0^{2\pi} \int_0^{\pi} |E_\phi|^2 R^2 \sin\theta \, d\theta \, d\phi \tag{12}$$

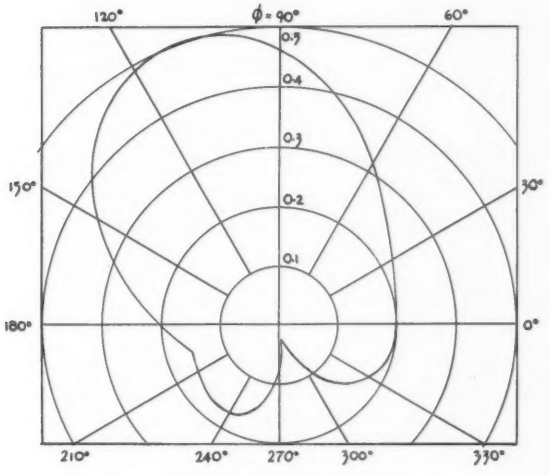

FIG. 7 $kd \sin\theta = 2$ $\theta_0 = 60°$

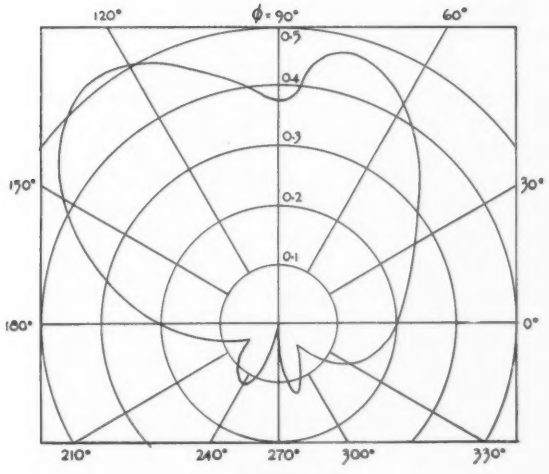

FIG. 8 $kd \sin\theta = 4$ $\theta_0 = 60°$

FIG. 7. The azimuthal radiation pattern for the slot offset by an amount $d/2$ from the center of the elliptic cylinder with $2d \sin\theta = 2\lambda/\pi$.

FIG. 8. The azimuthal radiation pattern for the slot offset by an amount $d/2$ from the center of the elliptic cylinder with $2d \sin\theta = 4\lambda/\pi$.

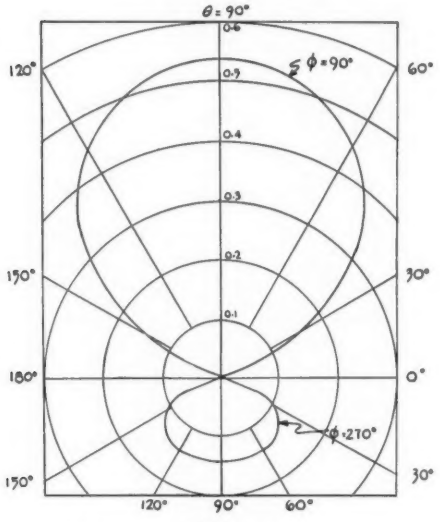

FIG. 9 $kd \sin\theta = 2$
$\sqrt{\varepsilon_0} = 90°$

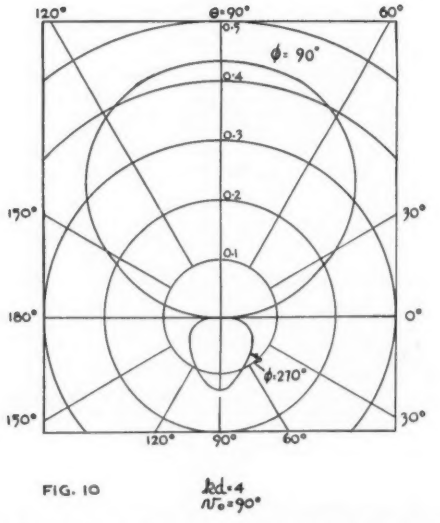

FIG. 10 $kd = 4$
$\sqrt{\varepsilon_0} = 90°$

FIG. 9. The principal elevation patterns for the slot on the thin elliptic cylinder for $2d = 2\lambda/\pi$.
FIG. 10. The principal elevation patterns for the slot on the thin elliptic cylinder for $2d = 4\lambda/\pi$.

and $\eta_0 = 120\pi$ ohms. Employing the orthogonality relation (5)

$$[13] \qquad \int_0^{2\pi} So_m(c, \cos\phi) So_n(c, \cos\phi) d\phi = \begin{matrix} 0 \text{ for } n \neq m, \\ N_m^o(c) \text{ for } n = m, \end{matrix}$$

it follows that

$$[14] \quad G = \frac{1}{\eta_0^2}\left[73.13 + 240 \int_0^{\pi} \frac{\cos^2(\frac{1}{2}\pi \cos\theta)}{\sin\theta} \sum_{m=1}^{\infty} \frac{[So_m(c, \cos v_0)]^2}{N_m^o(c)|Ho_m^{(2)'}(c, 1)|^2} d\theta\right].$$

It can be noted here that when c tends to zero corresponding to a vanishingly small elliptic cylinder, the summation term approaches zero and therefore

$$[15] \qquad \begin{aligned} G]_{kd\to 0} &= 73.13/\eta_0^2 \text{ mhos} \\ &= 0.517 \text{ millimhos.} \end{aligned}$$

It can be immediately recognized that the value 73.13 can be identified with the radiation resistance in ohms of the complementary half-wave wire antenna. This simple equation is a statement of Babinet's principle.

For large values of c it is not apparent what the limiting value of the infinite series should be. However, in the limiting case of very large kd, the elliptic cylinder is equivalent to an infinite plane conducting surface as far as the slot is concerned. Following the reasoning of Booker (1) and remembering that the slot radiates only on the one side of the sheet, it would be expected that

$$[16] \qquad \begin{aligned} G]_{kd\to\infty} &= 2 \times 73.13/\eta_0^2 \text{ mhos} \\ &= 1.033 \text{ millimhos.} \end{aligned}$$

The conductance G for intermediate values of kd is computed by a numerical integration of equation [14]. The result for the case of the centered half-wave slot (i.e. $v_0 = 90°$) is shown plotted in Fig. 11 for kd varying from 0 to 10. It is quite clear that the conductance is approaching the limiting value of 1.033 for the larger kd. The ripples in the curve can be interpreted as the effect of reflections of the primary field of the slot from the edges of the thin elliptic cylinder. In fact, it can be noted that the period of these ripples is very close to π.

It is worth while to compare these results with a corresponding calculation carried out previously (8) for the conductance of an axial slot on a circular conducting cylinder. In that case the conductance plotted as a function of the radius of the cylinder was a monotonically increasing function between the limiting values of 0.517 and 1.033 millimhos. Presumably the primary excitation of the slot is not appreciably reflected from the smooth curvature of the circular cylinder.

COMPARISON WITH SLOT ON KNIFE EDGE

It has probably occurred to the reader that the conducting elliptic cylinder with a vanishing minor axis is somewhat similar to a thin flat ribbon. With this in mind it would seem reasonable to expect an axial slot near the edge of a large ribbon or plate to be adequately represented by a semi-infinite, thin, perfectly conducting plane sheet or knife edge. It is worth while to investigate this problem in some detail.

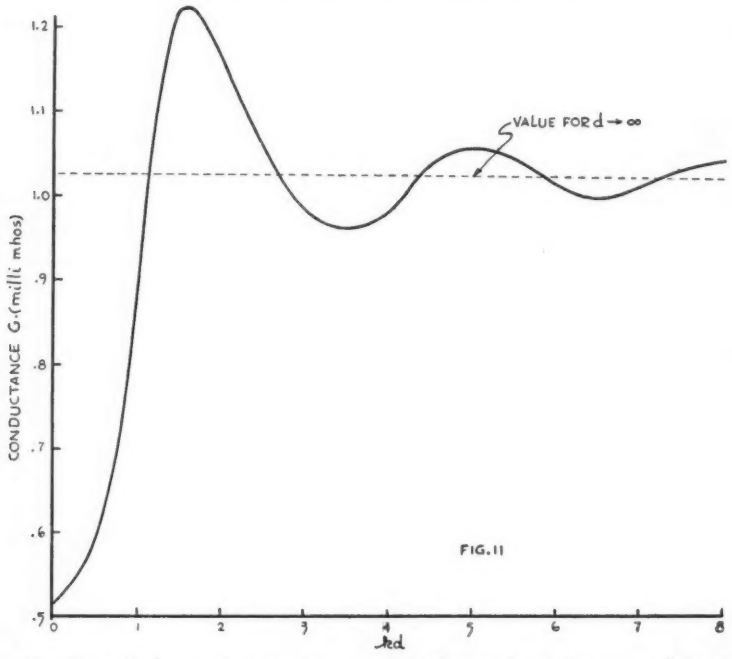

FIG. 11. The radiation conductance of a narrow half-wave slot at the center of the elliptic cylinder.

With reference to Fig. 12, the slot of length $2l$ is located on the perfectly conducting sheet defined by $\phi = 0$, at a distance ρ from the edge. As in the case of the thin elliptic cylinder the slot is assumed to be narrow and radiates

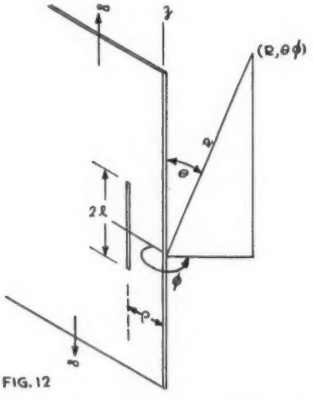

FIG. 12. Coordinate system for semi-infinite conducting plane or knife edge with narrow axial slot radiating from one side.

only on one side of the sheet. The radiation or far-zone field at (R, θ, ϕ) due to a specified transverse voltage $V(z)$ along the slot could be obtained rather indirectly from the formula for diffraction of a plane wave by a knife edge. In this case it would be necessary to generalize Sommerfeld's classical solution (7) to oblique incidence and then properly apply the reciprocity theorem. Such a procedure has been employed by Sinclair (6) and others in similar problems. Another approach is to treat the problem directly by constructing a suitable solution to the wave equation and ensuring that it satisfies the radiation conditions and reduces to the prescribed tangential electric field on the surface of the screen. This method was applied previously to an arbitrary slot on the surface of a cylindrically tipped wedge (9). The far-zone field was obtained by applying the saddle-point method to the infinite integrals in the general solution. Clearly the slot located on the sheet and parallel to the edge is a special case where the radius of the tip is zero and the wedge angle is 2π. This particular result can then be written down here immediately:

$$E_\phi = i(2\pi R)^{-1} \exp(-ikR + i\omega t)\, S(\theta)\, Q(g, \phi) \tag{17}$$

where $S(\theta)$ is defined by equation [4] and

$$Q(g, \phi) = \tfrac{1}{2} \sum_{m=0}^{\infty} \epsilon_m i^{m/2} \cos(m\phi/2) J_{m/2}(g) \tag{18}$$

where $g = k\rho \sin\theta$ and $\epsilon_0 = 1$, $\epsilon_m = 2$ for $m \neq 0$. Fortunately, infinite series of this type can be transformed to a closed form (4), so that

$$Q(g, \phi) = e^{ig\cos\phi} F[(2g)^{\frac{1}{2}} \cos(\phi/2)] \tag{19}$$

where $F(p)$ is a Fresnel integral defined by

$$F(p) = (i/\pi)^{\frac{1}{2}} \int_{-\infty}^{p} \exp(-it^2) dt. \tag{20}$$

The function $|Q(g, \phi)|$ which characterizes the azimuthal pattern is plotted as a function of ϕ in Figs. 13 to 18 for values of $g = k\rho \sin\theta$ of $\frac{1}{2}\pi$ to 5π.

It is rather interesting to compare these patterns with those for the thin elliptic cylinder or ribbon. As would be expected the patterns of the slot on the semi-infinite sheet are quite asymmetrical and there is no lobe structure in the geometrical shadow (i.e. $\phi > 180°$). There is a lobe structure, however, on the illuminated side (i.e. $\phi < 180°$) which becomes more complex as $k\rho \sin\theta$ increases. In fact it appears that the number of lobes is approximately equal to one-third the value of $k\rho \sin\theta$. In the case of the slot on the thin elliptic cylinder or ribbon, the number of lobes is approximately equal to $kd \sin\theta$ including the smaller rear lobes.

The conductance G of the $\lambda/2$ slot on the conducting screen is found in the manner described for the thin elliptic cylinder. Employing the orthogonality relation

$$\int_0^{2\pi} \cos(m\phi/2) \cos(n\phi/2) d\phi \quad \begin{matrix} = 0 \text{ if } m \neq n, \\ = 2\pi/\epsilon_m \text{ if } m = n, \end{matrix} \tag{21}$$

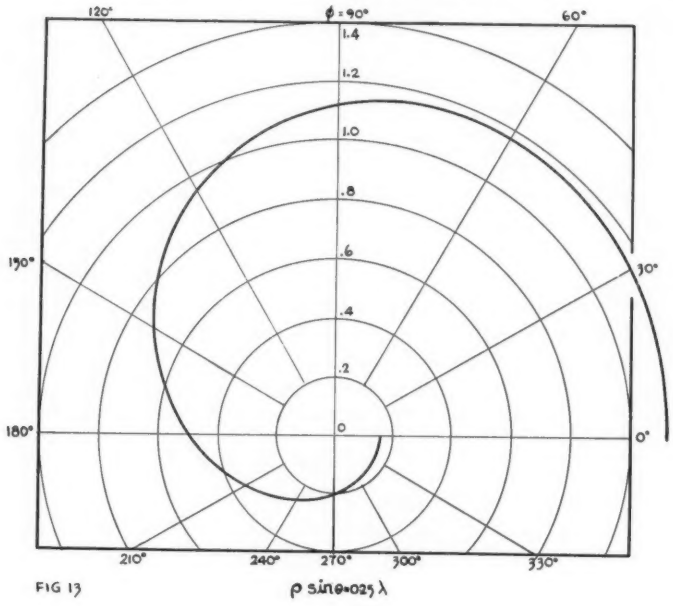

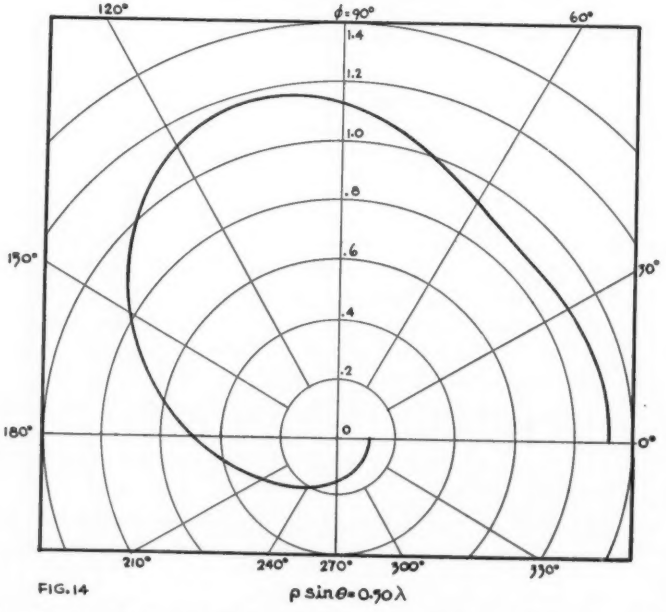

FIG. 13. The azimuthal radiation pattern for the slot on the knife edge for $\rho \sin \theta = 0.25\lambda$.
FIG. 14. The azimuthal radiation pattern for the slot on the knife edge for $\rho \sin \theta = 0.50\lambda$.

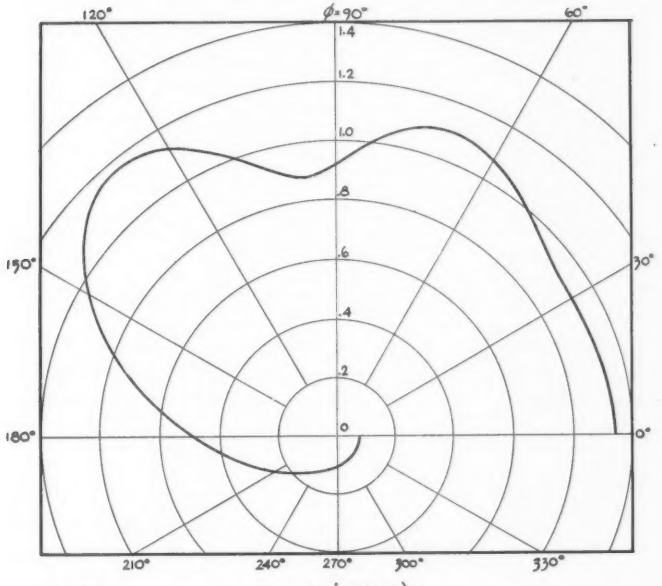

FIG. 15 $\rho \sin\theta = 1.0\lambda$

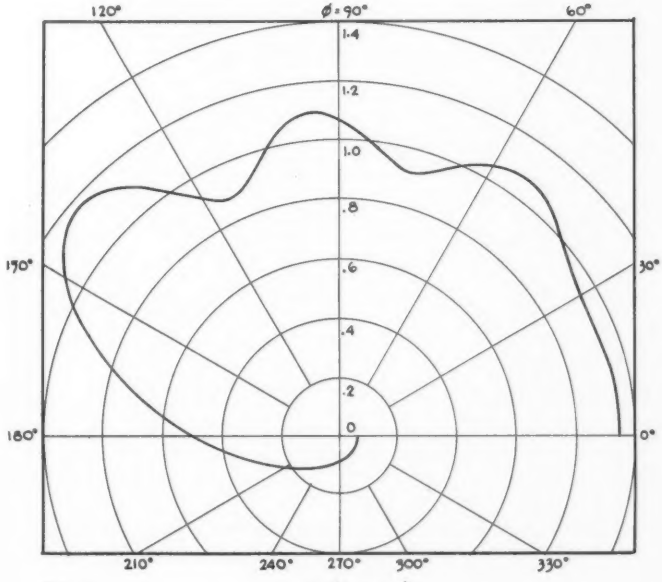

FIG. 16 $\rho \sin\theta = 1.5\lambda$

FIG. 15. The azimuthal radiation pattern for the slot on the knife edge for $\rho \sin\theta = 1.0\lambda$.
FIG. 16. The azimuthal radiation pattern for the slot on the knife edge for $\rho \sin\theta = 1.5\lambda$.

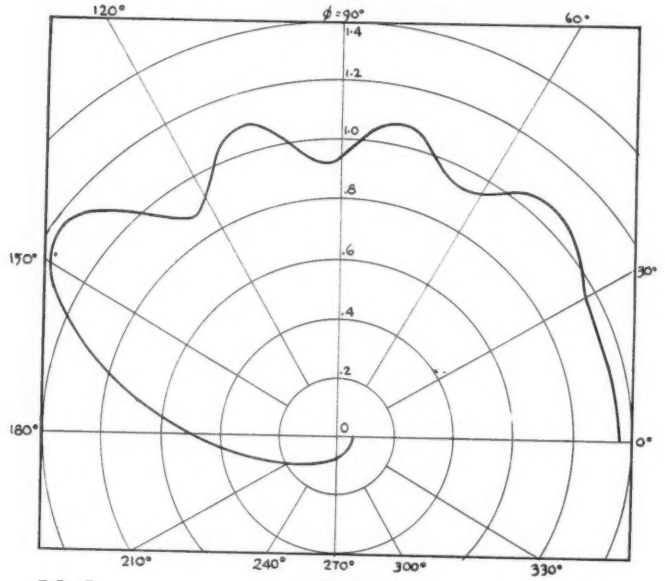

FIG. 17

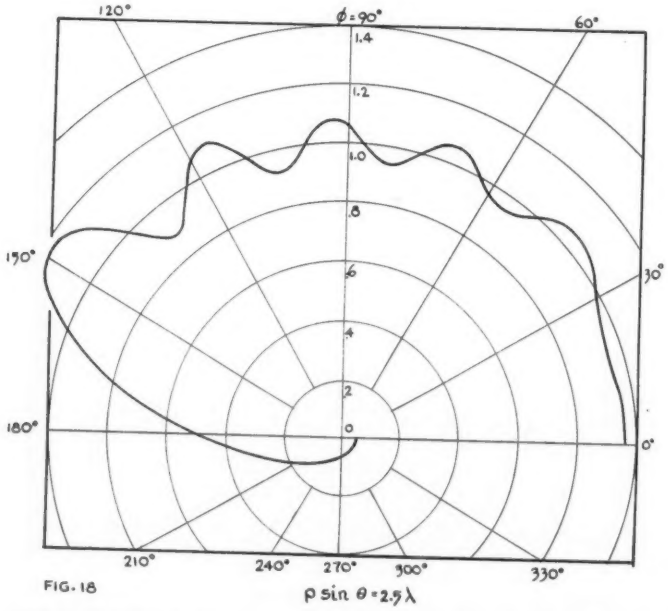

FIG. 18

FIG. 17. The azimuthal radiation pattern for the slot on the knife edge for $\rho \sin \theta = 2.0\lambda$.
FIG. 18. The azimuthal radiation pattern for the slot on the knife edge for $\rho \sin \theta = 2.5\lambda$.

it follows that

$$[22] \qquad G = \frac{60}{\eta_0^2} \int_0^{\pi} \frac{\cos^2(\frac{1}{2}\pi \cos\theta)}{\sin\theta} \sum_{m=0,1,2\ldots}^{\infty} \epsilon_m J_{m/2}^2(k\rho \sin\theta)\, d\theta.$$

The evaluation of the infinite series is somewhat simplified if it is noted that the summation over the even terms is expressible in closed form (2), that is,

$$[23] \qquad \sum_{m=0,2,4\ldots}^{\infty} J_{m/2}^2(x) = 1$$

and therefore

$$[24] \quad G = \frac{1}{\eta_0^2}\left[73.13 + 120 \int_0^{\pi} \frac{\cos^2(\frac{1}{2}\pi \cos\theta)}{\sin\theta} \sum_{m=1,3,5\ldots}^{\infty} J_{m/2}^2(k\rho \sin\theta) d\theta\right].$$

The limiting values of G for very small and very large values of $k\rho$ are 0.517 and 1.033 millimhos, respectively. Employing numerical integration for intermediate values of $k\rho$ the results are shown plotted in Fig. 19. Again the ripples

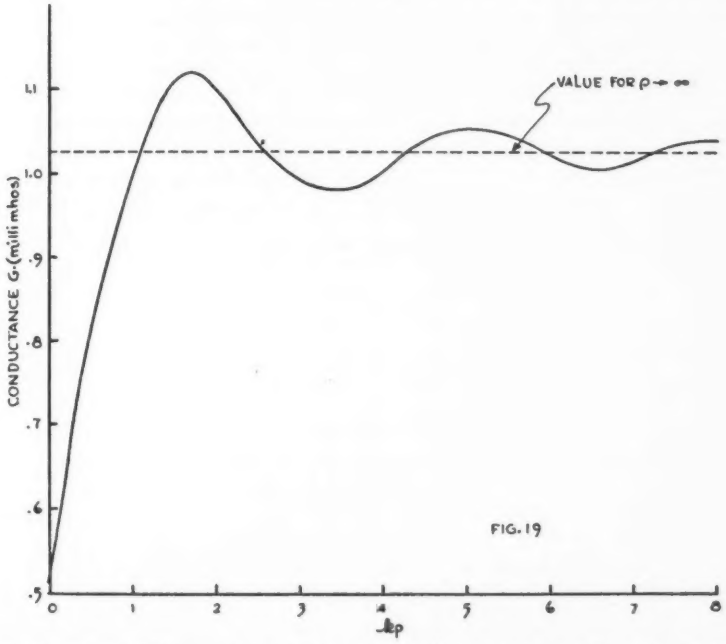

FIG. 19. The radiation conductance of a narrow half-wave slot parallel to and a distance ρ from the edge of a knife edge.

in the curve can be attributed to a reflection of the primary field of the slot with the edge of the sheet. The behavior of the function G in this case is very similar to that shown in Fig. 11 for the slot on the thin elliptic cylinder.

As a result of the geometrical similarity between a knife edge and vanishingly thin elliptic cylinder it is natural to expect a close connection between the

diffraction phenomena for the two cases. In fact this has already been demonstrated for the case of the conductance. To further illustrate the relation it is worth while to treat the thin elliptic cylinder as being equivalent to two knife edges. In other words, the diffraction from the slot by each edge will be assumed to be given by the formula appropriate for a semi-infinite knife edge. By superimposing these two components of the scattered fields, an approximate expression is obtained for the resultant field. The accuracy of the procedure can be expected to improve when the width of the thin elliptic cylinder becomes large.

Employing the same coordinate system (R, θ, ϕ) as was used for the far fields of the slot on the thin elliptic cylinder it follows that

$$E_\phi = i(2\pi R)^{-1} \exp(-ikR)\, S(\theta)\, T(g, \phi) \tag{25}$$

where

$$T(g, \phi) \cong \{F[(2g)^{\frac{1}{2}}\sin \tfrac{1}{2}\phi] + F[(2g)^{\frac{1}{2}}\cos \tfrac{1}{2}\phi] - 1\} \tag{26}$$

for $0 \leqslant \phi \leqslant 180°$ and

$$T(g, \phi) \cong \{F[-(2g)^{\frac{1}{2}}\sin \tfrac{1}{2}\phi] + F[+(2g)^{\frac{1}{2}}\cos \tfrac{1}{2}\phi]\} \tag{27}$$

for $180° < \phi \leqslant 360°$ with $g = kd \sin\theta$. The expressions given above for $T(g, \phi)$ must be considered semiempirical as no rigorous mathematical justification can be given for them. It should be noted that there is a discontinuity in $T(g, \phi)$ at $\phi = 180°$ and $360°$ which of course does not exist in reality. It is, however, of the order of $g^{-3/2}$ and is not of any practical consequence for larger values of kd. As an example, the function $T(g, \phi)$ is plotted in Fig. 20 for $g = 6$.

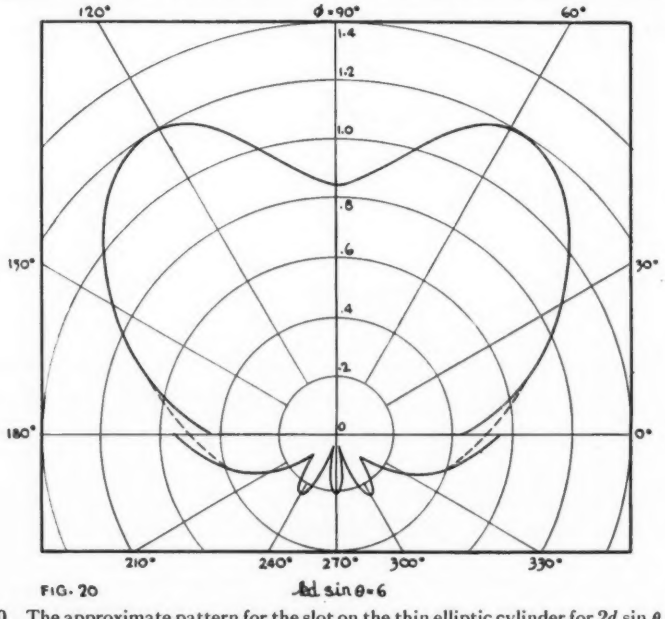

FIG. 20. The approximate pattern for the slot on the thin elliptic cylinder for $2d \sin\theta = 6\lambda/\pi$. The dashed sections of the curve are interpolated.

This pattern can be compared with the more exact calculated pattern in Fig. 5. The general shape of the pattern is the same. The agreement is somewhat poorer for smaller values of g. It is not possible to estimate the accuracy of this approximate procedure for much larger values of g, since the numerical work involved in evaluating the rigorous series solution in equation [14] is prohibitive. It can be expected, however, that for $g > 10$ the interaction between the two knife edges would be negligible. Recent experimental work of Frood (3) confirms this viewpoint.

CONCLUDING REMARKS

In any practical arrangement for slots on metal sheets, the dimensions are finite in the longitudinal direction as well as the lateral direction. It can be expected, however, that only the edges of the sheet parallel to the slot will appreciably effect the pattern and the conductance. For example, if a slot is cut in the center of a rectangular metal plate the primary radiation of the slot is predominantly in the broadside direction so that diffraction or scattering by the ends of the plate is small compared to the contribution from the parallel sides. In fact, recent experimental tests by Frood (3) indicate that if the length of the plate is equal to or greater than the total width, the pattern is within a few per cent of the corresponding theoretical pattern for a plate of infinite length.

Another important practical consideration is the method of feeding the slot and its effect on the pattern. In all cases discussed here, the slot is assumed to radiate only on one side of the sheet. In a practical scheme this requires that the slot is fed by a waveguide which itself is necessarily located on the rear side of the sheet. The theory neglects the diffraction by any obstacle such as waveguide assemblies behind the sheet. Further experimental work indicates that it is not a serious source of error as long as the width of the sheet is at least twice as wide as the broad dimension of the guide.

ACKNOWLEDGMENT

We would like to express thanks to Miss M. O'Grady and Mr. W. A. Pope, who assisted with the computations; and to Dr. J. Y. Wong for his helpful comments.

REFERENCES

1. Booker, H. G. J. Inst. Elec. Engrs. (London), Pt. III, A, 93: 620–628. 1946.
2. Erdélyi, A., Magnus, W., Oberhettinger, F., and Tricomi, F. G. Higher transcendental functions. Vol. 2. McGraw-Hill Book Company, Inc., New York. 1953. p. 100.
3. Frood, D. H. and Wait, J. R. An investigation of slot radiators cut in rectangular metal plates. Radio Phys. Lab. Project Rept. 19–0–11. 1 April, 1955.
4. Morse, P. M. and Feshbach, H. Methods of theoretical physics. Pt. II. McGraw-Hill Book Company, Inc., New York. 1953. p. 1386.
5. Morse, P. M. and Feshbach, H. Methods of theoretical physics. Pt. II. McGraw-Hill Book Company, Inc., New York. 1953. p. 1571.
6. Sinclair, G. Proc. Inst. Radio Engrs. 36: 1487–1492. 1948; 39: 660–668. 1951.
7. Sommerfeld, A. N. Math. Ann. 45: 263–280. 1894.
8. Wait, J. R., Pope, W. A., and O'Grady, M. Radiation characteristics of axial slots on a conducting cylinder. Radio Phys. Lab. Project Rept. 19–0–10. 15 November, 1954.
9. Wait, J. R. and Kahana, S. H. Can. J. Phys. 32: 714–722. 1954.
10. Wait, J. R. Field produced by an arbitrary slot on an elliptic cylinder. Radio Phys. Lab. Project Rept. 19–0–8. 15 June, 1954. J. Appl. Phys. In press. 1955.
11. Wong, J. Y. Proc. Inst. Radio Engrs. 41: 1172–1177. 1953.

A NEW TYPE OF IMPACT MACHINE FOR EVALUATING SENSITIVENESS OF EXPLOSIVES[1]

By P. E. Braid[2] and R. C. Langille[3]

ABSTRACT

An explosive charge and a number of small steel balls are oscillated in a steel cylinder which is closed except for a small opening which communicates with a manometer. Minute amounts of explosive situated at the points of contact during collisions may detonate, and pressure changes occur as a result of the accumulation of gaseous products of decomposition. Relative rates of increase of pressure at a fixed frequency of oscillation form a convenient basis for making comparisons of explosive materials. Values of sensitiveness of well-known explosives tested in this apparatus are in an order which corresponds with that expected as a result of practical experience. The machine was developed with the object of producing a statistical evaluation of explosibility and at the same time of eliminating much of the time and labor usually involved in such procedures.

INTRODUCTION

In the usual methods of determining the impact sensitiveness of explosives the sample is subjected to the blow from a falling weight (1, 4, 5, 6, 8). Apparatus design varies considerably, and the sensitiveness of one explosive relative to that of another is often very dependent on the geometry of the machine (2). The situation is further complicated in that noise, smoke, odor, and other signs of decomposition are usually all accepted as criteria of explosion or nonexplosion. These factors, however, are often weighted differently by different operators and for different explosives. In the Rotter impact machine used at Woolwich, England, the dependence on the operator's interpretation of such criteria is overcome by recording the volume of gas evolved in each trial. This principle is an essential feature of the present machine.

The sensitiveness of one explosive relative to that of another, in the case of measurements with most falling-weight machines, is expressed in terms of the "50% height", i.e., the height of fall of the weight for which explosions occur in 50% of the trials, since this is the most convenient height to use for such machines. Actually, comparison at a low percentage height is more useful for evaluating the danger of handling explosives since it approaches more nearly the "zero % height", or maximum shock which never results in an explosion. Although the preferability of the latter region is recognized, the difficulty in making reliable comparisons between a known and an unknown explosive on falling-weight machines is much greater in this than in the 50% height region. The number of trials made in such comparisons is necessarily restricted by the tedious and time-consuming nature of the procedure. In the device described here, however, the equivalent of a very large number of

[1]*Manuscript received in original form July 20, 1954, and, as revised, February 21, 1955. Contribution from the Department of Chemistry, University of Toronto, Toronto, Ontario.*
[2]*Occupational Health Laboratory, Department of National Health and Welfare, Ottawa, Ontario.*
[3]*Defence Research Telecommunications Establishment (Radio Physics Laboratory), Ottawa, Ontario.*

trials at a low percentage height may be achieved with very much less labor and uncertainty. The machine thus claims to provide, for an equivalent amount of time and labor, a much better statistical evaluation of the relative explosibility of two materials than is possible with the conventional machines.

A sample of explosive and a number of steel balls are shaken in a steel cylinder capped at both ends. The pressure due to gaseous products of explosion is recorded, the rate of shaking being variable. Explosives have been compared on the basis of the rate of gas evolution for a given rate of shaking, and also the rate of shaking for a given rate of gas evolution.

APPARATUS AND PROCEDURE

The apparatus is illustrated in Figs. 1 and 2. Two identical gas-tight cylinders are mounted side by side on an oscillating platform and connected to a differential mercury manometer J. A second manometer H is used to adjust

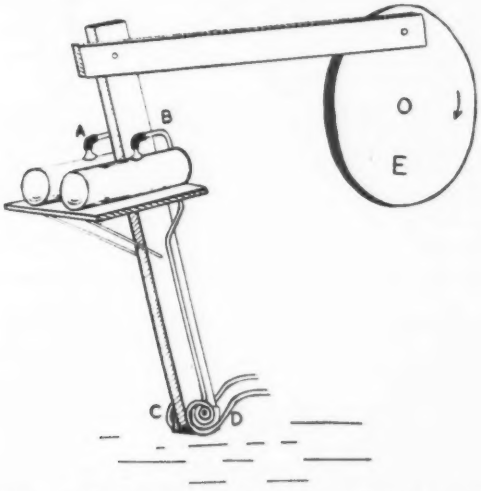

FIG. 1. Arrangement of cylinders on oscillating platform. Tubes A and B connect, through spirals C and D, to the manometers shown in Fig. 2. The flywheel E is driven by a 2 h.p. electric motor.

the initial (absolute) pressure. The system is connected to a vacuum pump and nitrogen source as shown. Since the tests are made in the presence of nitrogen at near-atmospheric pressure, room temperature fluctuations and the heating effect of the impacts of the balls cause large pressure changes which must be eliminated by compensation. This is achieved by the use of the two identical cylinders mounted close together.

The construction of the cylinders is shown in Fig. 3. The walls are stainless steel and the ends hardened tool steel disks. Each cylinder contains 120 steel ball bearings ¼ in. in diameter. These balls were roughened by shaking for

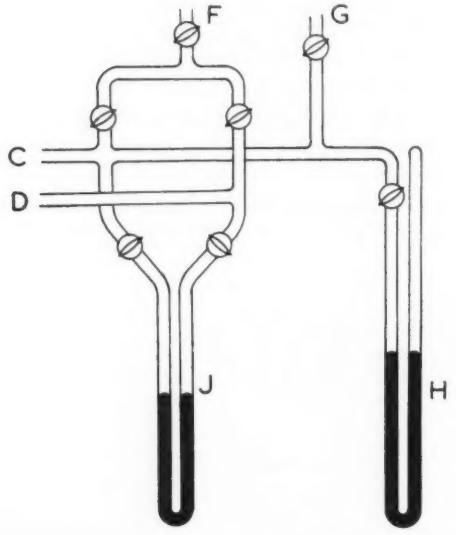

FIG. 2. The manometer system which is connected at C and D with the cylinders shown in Fig. 1. Nitrogen is introduced at F, the system being evacuated through G. J and H are the differential and absolute manometers, respectively.

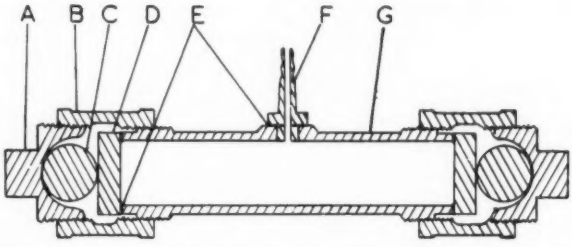

FIG. 3. Sectional view of a cylinder showing pipe-plug A, pipe-coupling B, ball bearing C, hardened steel and cap D, rubber gaskets E, outlet to manometers F, and main tube G.

12 hr. with abrasive powder in a ball mill. The agent used was an aluminum oxide abrasive passing a 150 mesh sieve and being retained on 200 mesh. As a consequence of this roughening treatment each ball acquires, during the first few cycles of shaking in the presence of an explosive, a thin coating of the explosive material. Localized explosions occur in the coatings as a result of ball-to-ball and ball-to-wall impacts, the coating being maintained by the excess of explosive material which is present.

In testing an explosive a 0.5 gm. sample is placed in one cylinder and 0.5 gm. of powdered sodium chloride in the other. After addition of the balls, the cylinders are capped, secured to the oscillating platform, and connected to the manometer. The whole system is then evacuated and filled with nitrogen

to slightly below atmospheric pressure. The platform is set in motion, a rate of shaking being chosen which is sufficiently rapid to give a measurable reading on the manometer within a reasonable time, e.g., at least 0.1 mm. in 10 min. In this case three readings would be made in a 30-min. trial, to improve the precision and check constancy of rate of evolution of gas. In the reported trials the time of shaking varied from 10 to 30 min. depending on the explosive. Three rates of shaking were employed: 120, 160, and 200 cycles per minute. For a given rate of shaking the rate of gas evolution becomes constant after a minute or two. Since pressure changes in the inert atmosphere in the cylinders are cancelled out by the use of two cylinders, the pressure difference indicated by manometer J (Fig. 2) is due only to the gaseous products of decomposition which are generated. Such pressure differences have been corrected to a standard temperature of 25° where necessary, although in most cases the correction was small.

Cleaning of the apparatus is accomplished by disconnecting the pipes from the platform and removing the end caps. The pipes are swabbed wih a cloth soaked with a suitable solvent (e.g., acetone) and dried in an oven for a few minutes. The end caps are treated similarly. The balls, after washing, are subjected to a few minutes' treatment with abrasive in the ball mill. It was found convenient to have a supply of extra balls on hand.

EXPERIMENTAL RESULTS

A typical differential pressure – time graph for an explosive at two different rates of shaking is shown in Fig. 4. The rate of differential pressure increase, d/dt (ΔP), is seen to have a constant value, and values for a series of explosives are given in Table I. Two methods were considered for expressing relative sensitiveness from the data.

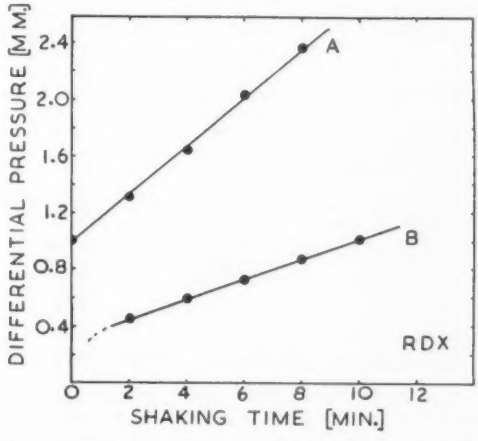

FIG. 4. Typical time–pressure curves for an explosive. For curve A the shaking rate was 200 cycles/min.; for curve B, 160 cycles/min.

TABLE I

RATES OF DIFFERENTIAL PRESSURE INCREASE OF TYPICAL EXPLOSIVES

Explosive	Rate of differential pressure increase, d/dt (ΔP), mm./min.			Chemical nature of explosive
	120 cycles/min.	160 cycles/min.	200 cycles/min.	
NENO		0.138	0.520	Di (nitroxyethyl) dinitro-oxamide
EDNA		0.133	0.225	Ethylenedinitramine
Fivolite		0.256	2.38	Tetra (nitroxymethyl) nitroxycyclopentane
Fivonite		0.133	0.565	Tetra (nitroxymethyl) cyclopentanone
Picric acid		0.025	0.038	Trinitrophenol
Tetryl		0.031	0.175	Methylpicrylnitramine
RDX		0.071	0.189	Cyclotrimethylene-trinitramine
PETN	0.105	1.32	2.13	Pentaerythritol tetranitrate
TNT		0.020	0.046	Trinitrotoluene
RDX/TNT		0.036	0.074	RDX 60%: TNT 40%
RDX/TNT		0.025	0.069	RDX 55%: TNT 45%
DINA		0.117	0.403	Di (nitroxyethyl) nitramine
NOG	0.745			Nitrosoguanidine

Method I.—Values of d/dt (ΔP) were compared at a constant rate of shaking. Figures of sensitiveness obtained in this way are given in Table II, the values being expressed in terms of that of RDX[4]. In Table II the explosives are listed in order of increasing sensitiveness (i.e., of increasing values of d/dt (ΔP)) based on the 160 cycles/min. shaking rate. It is seen that for the 200

TABLE II

SENSITIVENESS OF EXPLOSIVES REFERRED TO RDX AS STANDARD*

METHOD I

Explosive	d/dt (ΔP) explosive/d/dt (ΔP) RDX*	
	160 cycles/min.	200 cycles/min.
TNT	0.28	0.24
Picric acid	0.35	0.20
RDX/TNT (55/45)	0.35	0.37
Tetryl	0.44	0.93
RDX/TNT (60/40)	0.51	0.39
RDX	1.00	1.00
DINA	1.65	2.14
EDNA	1.87	1.19
Fivonite	1.87	2.99
NENO	1.94	2.75
Fivolite	3.61	12.6
PETN	18.6	10.7
NOG	7.12 (PETN = 1) at 120 cycles/min.	

**The figures of sensitiveness listed here, based on relative rate of evolution of gas, are not directly comparable with those derived from falling-weight tests. The latter usually represent ratios of heights of fall of the weight.*

[4]*Such direct comparisons without volume correction for each explosive are justified only because the common explosives all give the same volume (800–1000 cc./gm.) of gases upon explosion.*

cycles/min. rate there would be minor changes in the order. This situation arises with falling-weight machines when two different explosives are compared at two different percentage heights, owing to differences in the sigmoid curves (3, 9) for the explosives.

Method II.—Rates of shaking necessary to give a specified rate of gas evolution are compared. This method has the advantage of being more in line with those employed with falling-weight machines since it corresponds to comparing heights of fall for a specified percentage of explosions. Figures of sensitiveness of a few explosives, obtained by this method, are given in Table III. From linear plots of d/dt (ΔP) vs. rate of shaking values for the explosives in question the rates corresponding to an arbitrarily chosen value for d/dt (ΔP) of 0.2 mm./min. were obtained. A pressure difference of 0.2 mm./min. represents the explosion of 0.1 to 0.2% of the 0.5 gm. charge.

DISCUSSION OF RESULTS

It may be seen from an examination of Table III that the relative sensitiveness values of a series of five explosives obtained by method II are in the same order as that given by method I.

TABLE III

SENSITIVENESS OF EXPLOSIVES REFERRED TO RDX AS STANDARD

METHOD II

Explosive	Rate of shaking (cycles/min.) for d/dt (ΔP) = 0.2 mm./min.	Figure of sensitiveness (RDX = 1)
NOG	98	2.1
PETN	126	1.7
NENO	165	1.2
DINA	171	1.2
RDX	204	1.0

Unfortunately the data recorded here were obtained with the idea of applying method I only, and are not suitable for the compilation of a complete set of sensitiveness values by method II.

In the first two columns of Table IV a series of explosives are listed in order of increasing sensitiveness, as derived by method I at shaking rates of 160 and 200 cycles/min., respectively. In the next four columns are listed similar series as derived by means of tests on four conventional falling-weight machines. Of the series of explosives listed for each machine four well-known explosives, TNT, tetryl, RDX, and PETN, are underlined. The order of increasing sensitiveness for these materials is the same in each column of the table (except that in two cases adjacent members are indicated as equal in sensitiveness) and moreover this order is in agreement with that expected as a result of practical experience in the handling of these materials. The position

of the remaining explosives on the scale of sensitiveness varies from one machine to the next, possibly reflecting, among other things, a greater degree of dependence on the physical conditions of the test. The inclusion of these materials in the table may serve to give some idea of the difficulties associated with the determination of impact sensitiveness values. However, experience suggests that in the first two columns of Table IV the positions of picric acid, the two RDX/TNT mixtures, DINA, and NENO are in reasonable relation to those of the underlined group. The authors are less well acquainted with the remaining materials.

TABLE IV

RELATIVE IMPACT SENSITIVENESS OF EXPLOSIVES*; COMPARATIVE TABLE

New machine 160 cycles/min. rate	New machine 200 cycles/min. rate	Falling-weight machines			
		Machine (1)	Machine (2)	Machine (3)	Machine (4)
TNT	Picric acid	TNT	TNT	TNT	TNT
Picric acid	TNT	Fivonite	EDNA	Tetryl	Picric acid
RDX/TNT 55/45	RDX/TNT 55/45				
Tetryl	RDX/TNT 60/40	Tetryl	DINA	RDX	RDX/TNT 60/40
RDX/TNT 60/40	Tetryl	DINA	NENO	NENO	EDNA
RDX	RDX	Fivolite	Picric acid	PETN	Tetryl
DINA	EDNA	RDX	Tetryl		NENO
EDNA	DINA	NENO	RDX		DINA
Fivonite	NENO		RDX/TNT 60/40		RDX
NENO	Fivonite	PETN	PETN		PETN
Fivolite	PETN				
PETN	Fivolite				

**The explosives are listed in order of increasing sensitiveness from top to bottom of each column, except for members of bracketed groups, which are equal in sensitiveness.*

Falling-weight machines: (1) Formerly located in the University of Toronto, Department of Chemistry. Sensitiveness values were obtained by the authors and others.

(2) Located at Ottawa, Ontario, and operated by Department of Mines personnel.

(3) Located at Beloeil, Quebec, and operated by Canadian Industries Limited personnel.

(4) The values in this column were supplied by a referee in his criticism of the paper. Although the actual machine is not known the conditions of test are undoubtedly comparable for all explosives listed for that machine. This is true for machines (1), (2), and (3). However, conditions of test (size of weight, area of striking surface, etc.) vary from one machine to the next.

In replicated trials with several of the explosives tested, the values of d/dt (ΔP) showed a maximum deviation of $\pm 25\%$. Applied in terms of method I to the determination of relative sensitiveness of these explosives this means that for a single trial on each of the common explosives, RDX, TNT, tetryl, picric acid, DINA, and PETN, there could be inversions in the indicated relative sensitiveness of the three similar explosives, TNT, picric acid, and

tetryl. However, the indicated sensitiveness of this group would always be less than that of the remaining three materials, and the sensitiveness of these would always be in the order PETN > DINA > RDX. This degree of precision, attained by making trials at only one rate of shaking for each explosive tested, compares very favorably with results obtained from falling-weight machines in which each explosive is subjected to something of the order of twenty trials. However, by means of the present machine, an explosive may be tested at two rates of shaking in only a few minutes more than the time required for testing at one shaking rate. The information thus gained adds considerably to the knowledge of the explosive (6, 7). Thus, if TNT, picric acid, and tetryl are each tested only once but at two rates of shaking, and the values of d/dt (ΔP) are plotted as in method II, the pronounced similarity of the sensitiveness of TNT and picric acid as well as the relatively higher sensitiveness of tetryl are apparent.

CONCLUSIONS

A machine of design radically different from that heretofore employed in determining the impact sensitiveness of explosives is described. The values of relative sensitiveness of such well-known explosives as TNT, RDX, tetryl, and PETN, as determined by means of this machine, are in agreement with those derived by numerous tests with conventional machines and corroborated by practical experience. Values for some less well-known explosives are also given. For an equivalent expenditure of time and effort this machine will provide values of sensitiveness of explosives with greater precision than will the usual falling-weight machines.

ACKNOWLEDGMENTS

The authors wish to express their indebtedness to the late Dr. F. B. Kenrick, former head of the Department of Chemistry, University of Toronto, who conceived the working principle of the present machine and who took an active interest in its development even after his retirement. They also wish to express their sincere appreciation of the interest of Dr. G. F. Wright of the Department of Chemistry and of Dr. A. R. Gordon, Head of the Department, in the University of Toronto. Miss I. Janecek read the manuscript and made a number of helpful suggestions. This research was financed by a wartime grant from the National Research Council.

REFERENCES

1. Barnett, E. de B. Explosives. Baillière, Tindall & Cox, Ltd., London. 1919. pp. 208–211.
2. Copp, J. L., Napier, S. E., Nash, T., Powell, W. J., Skelly, H., Ubbelohde, A. R., and Woodward, P. Trans. Roy. Soc. (London), A, 241: 197–296. 1948.
3. Muraour, H. Mém. artillerie franç. 12: 559. 1933.
4. Rideal, E. K. and Robertson, A. J. B. Proc. Roy. Soc. (London), A, 195: 135–150. 1948.
5. Robertson, Sir R. J. Chem. Soc. 119 (No. 1): 1–29. 1921.
6. Urbanski, T. Z. ges. Schiess-u. Sprengstoffw. 33: 41–44. 1938.
7. Urbanski, T. Z. ges. Schiess-u. Sprengstoffw. 33: 62–65. 1938.
8. Urbanski, T. and Pietrzyk, C. Z. ges. Schiess-u. Sprengstoffw. 34: 206. 1939.
9. Wright, G. F. Organic chemistry, an advanced treatise. Vol. IV. *Edited by* H. Gilman. John Wiley & Sons, Inc., New York. 1953. p. 963.